1974

Measurement of transient critical heat flux by fluid modeling

Tien-Dun Shih
Iowa State University

Measurement of transient critical heat flux by fluid modeling

by

Tien-Dun Shih

A Dissertation Submitted to the
Graduate Faculty in Partial Fulfillment of
The Requirements for the Degree of
DOCTOR OF PHILOSOPHY

Department: Chemical Engineering and Nuclear Engineering
Major: Nuclear Engineering

Approved:

Signature was redacted for privacy.

In Charge of Major Work

Signature was redacted for privacy.

For the Major Department

Signature was redacted for privacy.

For the Graduate College

Iowa State University
Ames, Iowa

1974

TABLE OF CONTENTS

NOMENCLATURE

Roman Letters

A_{x-s}	Flow area	ft^2
C_p	Specific heat	$Btu/lb-^oF$
CHF	Critical heat flux	$Btu/hr-ft^2$
D	Hydraulic equivalent diameter = 4 x flow area/wetted perimeter	ft
D_{he}	Heated equivalent diameter = 4 x flow area/heated perimeter	ft
F	Parameter scale	---
G	Mass flux	$lb/hr-ft^2$
h	Enthalpy	Btu/lb
h_f	Enthalpy of saturated liquid	Btu/lb
h_{in}	Enthalpy of liquid at inlet	Btu/lb
ΔH_{in}	Inlet subcooling ($= h_f - h_{in}$)	Btu/lb
I	Current	Ampere
J	Mechanical equivalent of heat	$(ft-lb_f)/Btu$
L	Length	ft
P	Pressure	psia (lb_f/in^2)
P_H	Heated perimeter	ft
Q	Volume flux	$ft^3/hr-ft^2$

q	Heat flow	Btu/hr
T	Temperature	^{o}F
t	Time	sec
V	Velocity	ft/sec
$\bar{V}$	Voltage	volt
v	Specific volume	ft^3/lb
W	Mass flow	lb/hr
Z	Axial Coordinate length	ft

Greek Letters

α	Distortion factor	---
Δ	Difference of two quantities	---
δ	Prediction factor	---
λ	Latent heat of evaporation	Btu/lb
μ	Viscosity	lb/hr-ft
σ	Surface tension	lb/hr^2
ϕ	Heat flux	$Btu/hr-ft^2$
ρ	Density	lb/ft^3
χ	Quality	---

Subscripts

c	Critical quantity
F	Freon
f	Force unit
fg	Phase change between liquid and vapor
l	Liquid phase

m	Model
o	Initial value
p	Prototype
sat	Saturation
v	Vapor phase
W	Water

Note:

$$\text{Error (\%) of } \phi_{cm} = \frac{\phi_{cm} - \phi_{cp}}{\phi_{cp}} \times 100$$

$$\text{Error (\%) of } t_{measured} = \frac{t_{measured} - t_{calculated}}{t_{calculated}} \times 100$$

$$\text{rms error (\%) of } \phi_{cm} = \sqrt{\frac{\Sigma\ (\text{Error of } \phi_{cm})^2}{\text{No. of data points}}}$$

I. INTRODUCTION

Boiling under either natural or forced circulation has been recognized as one of the most effective mechanisms for the transfer of heat. One important application of the boiling heat transfer is in water cooled nuclear reactors where water is used as a neutron moderator as well as coolant of fuel rods.

When the heating surface of a boiling system is exposed to forced convective cooling and the temperature of the surface is increased gradually, the amount of heat absorbed by the flow can be found from the boiling curve, shown schematically in Figure 1. Initially, up to point B heat will be transferred by single phase forced convection only. After point B, heat will be transferred either by nucleate boiling or by forced convective evaporation until the critical heat flux (CHF) is reached at D. Between D and E partial film boiling will take place until it reaches the Leidenfrost point E. Beyond the Leidenfrost point no liquid can wet the wall and heat is transferred by stable film boiling only.

For heating surfaces such as the fuel rods of nuclear reactors where heat flux rather than surface temperature is under control a different path will be followed. During heating the heat flux follows curve ABCD but as soon as the critical heat flux is reached the surface temperature will

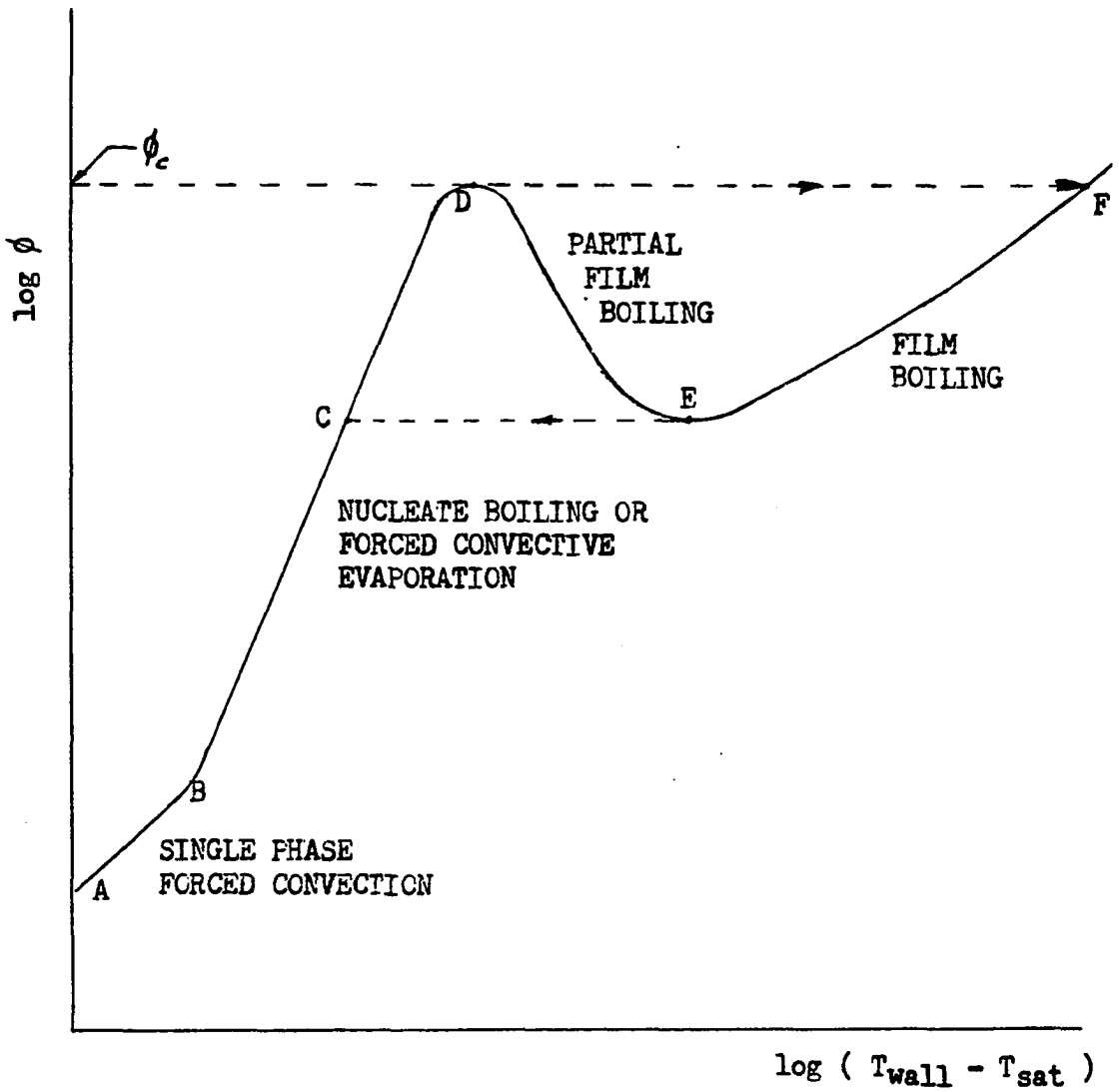

Figure 1. Regimes in boiling heat transfer

increase rapidly from point D to point F. If the heat flux is then reduced to point E, a sudden reduction in temperature, following path E-C will take place.

A major performance limit in light water reactors is thus set by the point D where CHF occurs, since beyond this there is a local determiration in heat transfer performance, that is, a sudden decrease in heat transfer coefficient. With a heat flux controlled surface, a sudden increase in surface temperature results, and this can lead to mechanical failure. The thermal and hydraulic limits associated with this CHF condition therefore create an important design limitation in nuclear reactors. A number of terms have been used to name the condition at point D such as critical heat flux (CHF), burnout, dryout, boiling crisis and departure from nucleate boiling (DNB). Although they are used in the literature interchangeably, they do have slightly different meanings. Tong (34) and Groeneveld (18) have detailed definitions for these terms.

In a power reactor there is a strong economic incentive to keep the margin between operating heat flux and CHF as small as possible, consistent with adequate allowance for possible variations and transients; so there is a need to be able to predict as reliably as possible the conditions which lead to the onset of CHF. Unfortunately the thermal and hydraulic conditions associated with the onset of CHF

are so complex that no adequate theory as yet exists for predicting when or under what condition it will occur.

Consequently the prediction of CHF conditions is dependent on empirical correlations. Tests on CHF conditions for a given nuclear fuel element are usually performed at out-of-pile facilities using similar test section geometries. Heat generation in the fuel rod is simulated by high heat flux electrical heater equipped with burnout detectors. These experiments are generally very costly, requiring large, high power, high pressure facilities. In order to reduce the cost of such experiments, many studies have been made to scale down the power and pressure of such loops.

One convenient method is to use a different fluid to model CHF conditions of high pressure water. The most widely used modeling fluids are Freons.[1] Freons are selected because of their low latent heats of evaporation compared with water, resulting in a reduced power for a given flow quality. Also, because the critical pressures are much lower, the simulating pressure is only a fraction of the corresponding water pressure. The required experimental facilities are therefore simpler and much less expensive.

Many investigations have been reported on the modeling

---

[1]Freon is the trade name of E. I. Du Pont Inc. for a series of fluorocarbons. Other trade names are Arcton, Racon and Isceon.

technique for CHF at steady state operating conditions (i.e., CHF occurs at constant pressure, flow rate and inlet temperature). These include:

Fluid - Freon-11, Freon-12, Freon-21, Freon-22, Freon-113, Freon-114 and CO_2.

Geometry - Round tubes, annuli and rod bundles.

Heated length - From 25 in. to 12 ft.

Pressure range - From atmospheric pressure to the pressure equivalent to 2400 psia in water system.

A number of photographic studies on the physical mechanism of CHF in Freon systems have also been done in recent years.

On the contrary, model studies on the occurrence of CHF during transient conditions (i.e., CHF occurs during flow coastdown or depressurization) have not been reported in the literature. It is obvious that if CHF does occur in a reactor, it is most likely to occur during transient conditions.

The main purpose of this work was to develop and test a fluid modeling technique for the study of transient CHF. The technique was developed from steady state CHF relationship. Tests were performed in a 36-in. single rod annular

test section. Freon-11 was used as modeling fluid. Simulated transients in a boiling water reactors included a recirculation valve closure and opening as well as recirculation pump seizure, depressurization and loss-of-coolant accidents.

II. REVIEW OF LITERATURE

Although single-phase fluid modeling has been used since last century, two phase modeling, especially for the nuclear reactor technology, is a more recent practice.

In 1961, the Societé Nationale d'Etude et de Construction de Moteurs d'Aviation (SNECMA) (29) reported an early attempt to use Freon to simulate both the hydrodynamic and thermal behavior of boiling water reactor systems. No comparisons with water systems or correlations were attempted. Barnett (5, 6) was the first one to report systematic analysis of modeling the water CHF behavior with fluorocarbon fluid. By the use of dimensional analysis, he took into account only the number of parameters in a given set which would be compatible with the degree of freedom available for experimentation.

In later investigations, Barnett and Wood (7) developed a set of 14 parametric combinations. Through the comparisons of water and Freon-12 data, one of the 14 combinations was shown to be substantially consistent with the experimental evidence. Their work presented only limited success but laid the ground work for the more direct empirical techniques that followed.

Since then a great amount of effort has been devoted to the development of CHF correlations through the fluid

modeling technique. Stevens and Kirby (31) constructed a graphical correlation with quality and a complex function of flow and geometry. They found that both water and Freon data would fall on the same curve if the water function was multiplied by a constant factor, k, namely,

$$\left[GD^{0.25}\left(\frac{D}{L}\right)^{0.59}\right]_{Freon} = k\left[GD^{0.25}\left(\frac{D}{L}\right)^{0.59}\right]_{Water} \quad (1)$$

and k = 0.658.

The correlation was developed for Freon-12 in round tubes at an equivalent water pressure of 1000 psia, but Stevens and Macbeth (32) indicated later that the correlation was also good for complex geometries.

Staub (30) modified the Stevens and Kirby's graphical correlation by introducing a boiling boundary concept to replace the total heating length, L, by the boiling length. His suggestion showed better results in correlating water and Freon data.

Bouré (8) proposed a modified dimensional analysis technique, which he claimed would include all the parametric effects of boiling heat transfer. Groups of dimensionless terms were amended by correction factors. These correction factors were then used to modify the scaling of the parameters between model and prototype systems.

Dix (13) made a modeling effort by the use of an existing water CHF correlation to develop a flow rate scale relation which included geometrical size. He reported the following functional form

$$k \equiv \frac{G_F}{G_W} = C_t(1.00 - 0.09\ G_W x 10^{-6})(1.04 - 0.05\ \frac{L}{D} x 10^{-2})$$

$$x\ (1.41 - 0.02\ \frac{\rho_l}{\rho_v}) \quad . \qquad (2)$$

The constant C_t was determined by comparing all of the Freon data to a common reference.

Coffield (12) extended the application of CHF modeling to subcooled liquid conditions. His results showed that the fluid modeling technique was successful for subcooled CHF conditions.

Ahmad (1) developed a general correlation by classical dimensional analysis and compensated distortion model theory suggested by Murphy (24). The generality of the correlation was demonstrated to apply to other fluids (e.g., potassium, water, Freon, carbon dioxide) over a wide range of pressures.

In reference 20 Polomik proposed a preliminary correlation for CHF in the annular flow regime by using heat balance relationship and dimensional analysis. Liquid entrainment was assumed to have a controlling influence on CHF occurrence.

Recent efforts in steady state CHF modeling have extended to more complex geometries. In references 2 and 22 a series of tests on Freon-12 models of a 72-in. annular test section and a 9-ft., 18-element bundle geometry have been reported. Results were used to determine the coefficients of Ahmad's correlation.

Motley et al. (23) conducted tests on an 8-ft., 16-element bundle Freon-11 model. Subcooled CHF data were obtained with cosine heat flux shape heating elements and were reported to agree with the correlation w-3 (35) within ± 23 percent.

In contrast to the extensive studies of the steady state CHF in both out-of-pile water facilities and Freon model systems, only a few investigations (11, 20, 28, 36) on transient CHF in water facilities have been reported. In these investigations, it was normally assumed that the transient prediction of CHF could be accomplished through the use of steady state CHF correlations.

Lahey et al. (21) developed an analytical technique, based on the method of characteristics (17) to predict the transient void fraction and the onset of CHF. The analysis resulted in the development of the computer codes, MAYU and MAYU-2 which permitted the solution of general transient cases numerically. In comparison with the experimental results from many different test geometries the codes

showed successful predictions for various transient conditions. In the same report, experiments on a heated tube with circulating Freon-114 were performed to test the exit void fraction under transient conditions. The experimental results were used to check the computer's predictions.

Up to today, no attempt of fluid modeling study has been reported for the prediction of transient CHF.

The effort of this work is to experimentally test the validity of predicting the onset time of transient CHF by fluid modeling technique.

III. ANALYSIS

A. Steady State CHF Analysis

According to Murphy (24), a general theory of model design may be developed by a simple extension of the general type equation which is derived by using dimensional analysis.

The first step in the analysis is to determine the pertinent variables and this step is by far the most important, since the validity of the result depends upon the correctness with which the pertinent factors are selected. Although there is no general rule for selecting these pertinent variables, Rohsenow and Choi (26) suggest that they can usually be found by logic or intuition developed from previous experiences with problems of a similar nature, but there is no way to ensure that all essential quantities have been included.

For the analysis of the problem of CHF, a functional form may be generally formulated as:

$$CHF = F \text{ (System Parameters, Geometry, Fluid Properties)} \tag{3}$$

From the experiences of previous analytical and experimental investigations on boiling heat transfer and burnout phenomena, some parametric effects are considered to have significant influences on the occurrence of CHF. The

characteristics which cause these effects are to be included in Equation 3 as pertinent variables, and Equation 3 becomes

$$\phi_c = F(G, \Delta H; L, D; \lambda, \rho_l, \rho_v, \mu_l, \sigma) \quad (4)$$

One important variable, namely system pressure, is not included in Equation 4. Since at any given pressure for any fluid there is a unique value of the density ratio ρ_l/ρ_v evaluated at equilibrium saturation conditions, this ratio can be used to represent pressure. The density ratio is chosen instead of pressure because for any two fluids it is possible to select pressures which give the same magnitude of this group for both fluids. Figure 2 shows a range of corresponding pressures for Freon-11 and for water which satisfies the density ratio condition. The linear relationship can be represented by the equation

$$P_F = 0.1728\ P_W - 9.5 \text{ (psia)} \quad (5)$$

The general type equation is formed by grouping the ten variables in Equation 4 into a set of dimensionless terms, called Pi-terms (or π-terms), through the use of the Buckingham's Pi Theorem (9). The Theorem states that the number of dimensionless and independent quantities sufficient to express a relationship among the variables in any phenomenon is equal to the number of quantities involved

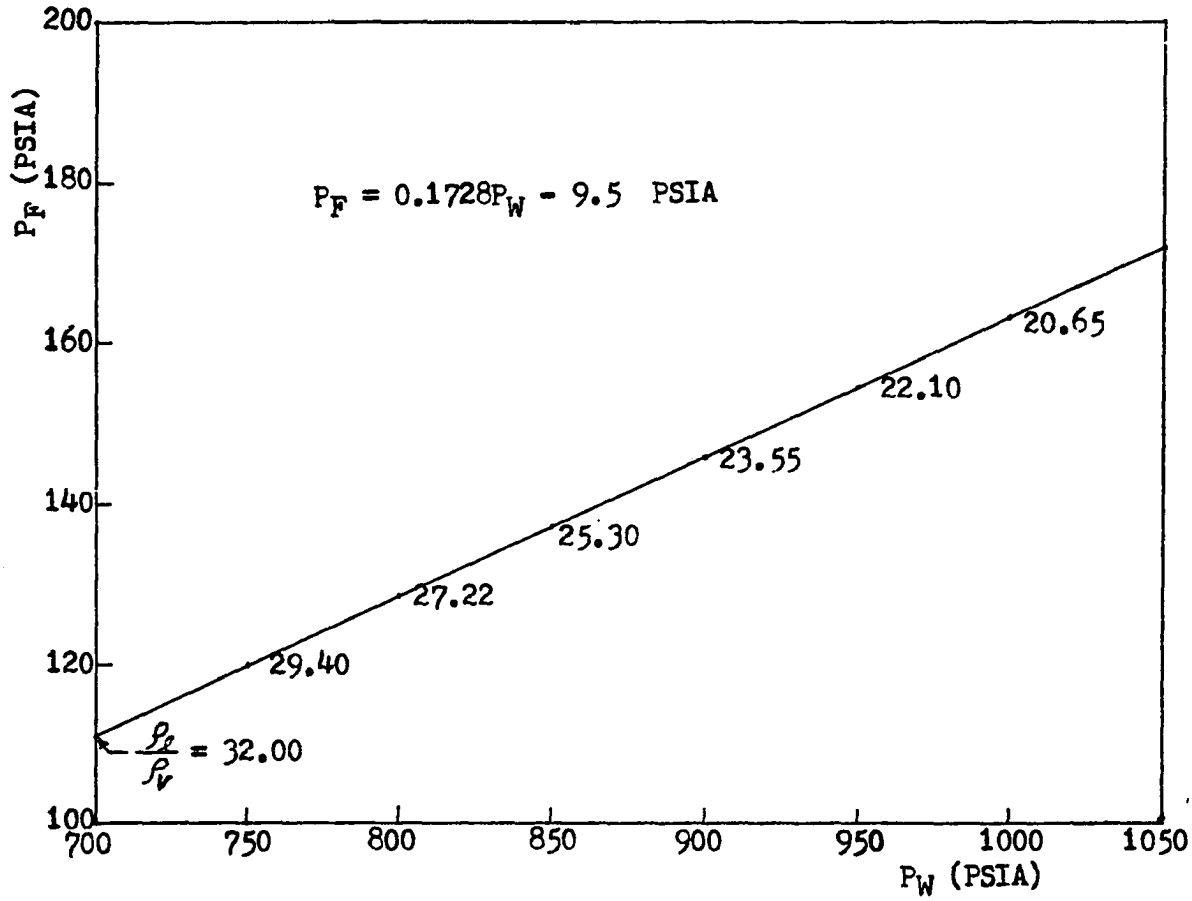

Figure 2. Relationship between saturation pressures for water and Freon-11 at the same values of ρ_l/ρ_v

minus the number of independent dimensions in which those quantities may be measured.

Table 1 is the list of 10 pertinent variables and their basic dimensions. From this table the basic independent dimensions for the present problem are M, L, T and H. According to Murphy (24), H may be considered to be independent of the other three dimensions if transformation of thermal energy to mechanical is not involved in the phenomenon. Since in the burnout experiments the transfer between two forms of energy is negligible in comparison with the power from the heater, H can be considered as an independent dimension. The same consideration has been adopted by Ahmad (1), Bouré (8) and Coffield (12).

The number of π-terms which is sufficient to express a relationship among the variables and therefore constitutes the general type equation is

$$10 - 4 = 6$$

There are an infinite number of sets of π-terms which may be derived from Equation 4, the only restrictions are that they must be dimensionless and independent. It should be noted, however, that with the aid of some well chosen examples some sets of π-terms are more useful in practice than others.

Due to this consideration one possible set of six

Table 1. List of pertinent variables

No.	Symbol	Description	Unit	Basic Dimension
1	ϕ_c	Critical heat flux	Btu/hr-ft^2	$HT^{-1}L^{-2}$
2	G	Mass flux	lb/hr-ft^2	$MT^{-1}L^{-2}$
3	ΔH	Inlet subcooling	Btu/lb	HM^{-1}
4	L	Length	ft	L
5	D	Equivalent diameter	ft	L
6	λ	Latent heat of evaporation	Btu/lb	HM^{-1}
7	ρ_l	Liquid density	lb/ft^3	ML^{-3}
8	ρ_v	Vapor density	lb/ft^3	ML^{-3}
9	μ_l	Liquid viscosity	lb/hr-ft	$MT^{-1}L^{-1}$
10	σ	Surface tension	lb/hr^2	MT^{-2}

π-terms is determined to be

$$\pi_1 = \frac{\phi_c}{G\lambda}$$

$$\pi_2 = \frac{GD}{\mu_1}$$

$$\pi_3 = \frac{L}{D} \qquad (6)$$

$$\pi_4 = \frac{\rho_1}{\rho_v}$$

$$\pi_5 = \frac{\Delta H}{\lambda}$$

$$\pi_6 = \frac{\mu_1^2}{\sigma \rho_1 D}$$

The general equation is then formulated as

$$\pi_1 = f(\pi_2, \pi_3, \pi_4, \pi_5, \pi_6) \qquad (7)$$

π_1, π_2 and π_6 are the classical numbers named as boiling number, Reynolds number and Weber-Reynolds number. The significance of these numbers has been well recognized. The rest of them are formed as the ratios of geometrical dimensions and fluid properties.

Equation 7 is to be used for developing the theory of model design. It is entirely general and hence the equation holds true for both the prototype (water system) and the

model (Freon system) as long as the same pertinent variables are involved. Therefore

$$\pi_{1p} = f(\pi_{2p}, \pi_{3p}, \pi_{4p}, \pi_{5p}, \pi_{6p})$$

and (8)

$$\pi_{1m} = f(\pi_{2m}, \pi_{3m}, \pi_{4m}, \pi_{5m}, \pi_{6m})$$

Now, if the model is designed and operated so that

$$\begin{aligned} \pi_{2m} &= \pi_{2p} \\ \pi_{3m} &= \pi_{3p} \\ \pi_{4m} &= \pi_{4p} \\ \pi_{5m} &= \pi_{5p} \\ \pi_{6m} &= \pi_{6p} \end{aligned} \tag{9}$$

it follows that

$$f(\pi_{2p},\pi_{3p},\pi_{4p},\pi_{5p},\pi_{6p}) = f(\pi_{2m},\pi_{3m},\pi_{4m},\pi_{5m},\pi_{6m}) \tag{10a}$$

or

$$\pi_{1p} = \pi_{1m} \tag{10b}$$

Equation 9 and 10b are called the design conditions and prediction equation respectively, and the model which satisfies Equation 9 and hence Equation 10b is called a

true model.

For the fluid modeling of CHF, a true model is impracticable, since π_6 contains fluid properties and there is no way to satisfy the design condition which matches π_6 in both water and Freon systems. An alternative way is to construct a distorted model. This is a model in which one or more design conditions are violated sufficiently to require correction of the prediction equation. Nevertheless, if the degree of distortion can be properly controlled or evaluated by a distortion factor α, so that $\pi_{6m} = \alpha\pi_{6p}$ then the prediction equation can be modified by a prediction factor δ, so that $\pi_{1p} = \delta\pi_{1m}$.

The prediction factor δ, is generally a function of α and may, in addition, be a function of the π-terms. To evaluate δ may be difficult if the system is complex. Murphy (24) further suggests that it is also possible to adjust the distortion factors in such a manner that the prediction factor becomes unity. The model, designed under this concept so that some distortions are to be adjusted to compensate the distorted effects produced by others, is called a compensated distortion model.

The objective of the present research is to develop and construct a compensated distortion model to predict the steady state and transient CHF in the prototype.

To establish the design conditions it is important to

decide which π-terms are to be distorted.

A detailed examination of Equation 9 reveals that π_6 is the term that cannot be matched and therefore a distortion factor has to be introduced. The factor is a function of pressure, since the saturated fluid properties contained in π_6 are functions of pressure.

π_5 can be controlled by the adjustment of the flow inlet temperature. Since the purpose of steady state tests is to provide the pressure dependent parameter scales for both flow transient and depressurization transient tests, two different design conditions of π_5 will be operated. One operates with exactly matched π_5 in both systems to provide parameter scales for flow transient tests. The other operates with distorted π_5 to provide parameter scales for depressurization transient tests, since in this case, only the initial inlet temperature can be controlled and π_5 cannot be matched during the transient.

π_4 is the density ratio and is unique for a given pressure. The condition of equal magnitude of π_4 may determine the operating pressure in the model system.

π_3 is the ratio of geometrical dimensions. A model can be designed and constructed to have geometrical similarity to the prototype.

Therefore, π_{3m} and π_{4m} are designed to have the same values as those in the prototype. The term which is to be

distorted purposely to compensate the other distortions is π_2, the Reynolds number. Since the Reynolds number contains mass flow rate which can be adjusted easily and effectively, the distortion of this group can be properly controlled.

The design conditions then can be written as

$$\begin{aligned} \pi_{2m} &= \alpha_2 \pi_{2p} \\ \pi_{3m} &= \pi_{3p} \\ \pi_{4m} &= \pi_{4p} \\ \pi_{5m} &= \alpha_5 \pi_{5p} \\ \pi_{6m} &= \alpha_6 \pi_{6p} \end{aligned} \tag{11}$$

α_6 is a function of pressure and is fixed when the operating pressure is fixed. In one set of experiments which π_5 is not distorted, α_5 is equal to one, in the other set, α_5 is also a function of pressure. α_2 is a floating adjustable distortion factor, when it is carefully controlled the prediction equation then becomes

$$\pi_{1p} = \pi_{1m} \tag{12}$$

The task now is to determine the distortion factor α_2 so that the prediction factor may become unity. The determination is done experimentally as outlined in the following procedure.

Experiments are conducted for observing the changes of π_{1m} with π_{2m} only. π_{3m} through π_{6m} are held constant during the tests by keeping the system pressure and inlet temperature constant. Data of CHFs at various Gs are converted into π_{1m} and π_{2m} and plotted on a log-log paper. Water data at the corresponding conditions are also plotted on the same log-log paper. A number of ratios of π_{2m} to π_{2p} are measured at the same values of π_1. α_2 is then determined to be the average value of the ratios. There is, however, major difficulty in this method since no adequate water data are available in the world for the evaluation of α_2s. The requirement of identical physical size, density ratio and inlet conditions has eliminated a considerable amount of the published water CHF data.

One alternative resolution adopted in this work is to employ a well established CHF correlation which represents a good fit to a number of water data at various conditions. The correlation was developed by Janssen and Kervinen (19) for an annular test section and is still being used for design (4).

The correlation states:

$$\left\{\begin{matrix}\text{Total}\\ \text{heat flux}\\ \text{at burnout}\end{matrix}\right\} = f(P_0\text{-}P)\left[\left\{\begin{matrix}\text{Pool boiling}\\ \text{burnout heat}\\ \text{flux at}\\ \text{1000 psia}\end{matrix}\right\} + \left\{\begin{matrix}\text{Add. flux due to}\\ \text{forced convection}\\ \text{at 1000 psia}\end{matrix}\right\} + \left\{\begin{matrix}\text{Adjustment in flux}\\ \text{depending on quality,}\\ \text{flow, hydraulic}\\ \text{diameter}\end{matrix}\right\}\right]$$

The final form is

$$\frac{\phi_c}{10^6} = \frac{\left[1 + 0.16\left(\frac{1000-P}{400}\right) - 0.04\left(\frac{1000-P}{400}\right)^2\right]}{1 - 0.008\ B\left(\frac{G}{10^6}\right)^{0.8}} \cdot \left[0.0172\ B\left(\frac{G}{10^6}\right)^{0.8}\right.$$

$$- \left\{0.3175\left(\frac{G}{10^6}\right)^{-2} - 1.8534\left(\frac{G}{10^6}\right)^{-1}\right\}$$

$$- \left\{2.4 + 3.2D + 0.83D\left(\frac{G}{10^6}\right)\right\} \cdot \left\{X - 0.0629\left(\frac{G}{10^6}\right)^{-2}\right.$$

$$\left. + 0.3429\left(\frac{G}{10^6}\right)^{-1} - 0.2494 + 0.0020\left(\frac{G}{10^6}\right)^{2}\right\}\Big] \qquad (13)$$

where

$$B = \left(\frac{D_2}{D_1}\right)^{0.5} (D_2 - D_1)^{-0.2}$$

D_2, D_1 in feet, representing I.D. of the shroud and O.D. of the heater

D in inches.

The ranges of the parameters are

Hydraulic diameter	:	0.25 to 0.875 in.
Pressure	:	600 to 1450 psia
Flow	:	0.14×10^6 to 6.2×10^6 lb/hr-ft^2
Quality	:	-0.12 to 0.45%
Heat flux	:	$\phi_c > 0.35 \times 10^6$ Btu/hr-ft^2

The correlation therefore stands for the prototype water system and is used to compare the Freon data at equivalent conditions for the determination of α_2s.

B. Transient CHF Analysis

One safety aspect of the thermal and hydraulic design of light water nuclear reactors is the requirement that each fuel rod be operated at some safe margin below the CHF. The margin is measured by the value of "critical heat flux ratio" (CHFR $\equiv \frac{\text{CHF}}{\text{operating heat flux}}$), and a safety factor is defined as "Minimum Critical Heat Flux Ratio" (MCHFR $\equiv$ min. of $\frac{\text{CHF}}{\text{operating heat flux}}$). For example, for Brown Ferry reactor (BWR) (33), MCHFR is equal to 1.9 and for Point Beach reactor (PWR) (38), MCHFR is 1.3.

In the normal operation, the heat fluxes of fuel rods are far below CHF. If a reactor is subjected to abnormal operations, however, CHFR may drop down to a value equal to

or below 1.0, and result in the occurrence of undesirable CHF.

Two types of transients which simulate typical BWR design basis accidents are under investigation. One is a flow transient, the other is a depressurization transient.

The time ranges of all transients up to the onset of CHF are in the order of seconds. It is assumed that under such types of transient, a general relationship of Equation 7 still holds true except all π-terms are, in general, functions of time and the relationship is formulated as

$$\pi_1(t) = f_t(\pi_2(t), \pi_3(t), \pi_4(t), \pi_5(t), \pi_6(t)) \qquad (14)$$

at each fixed time Equation 14 is the same as Equation 7. A simplified three-dimensional graphic explanation of Equation 14 is shown in Figure 3 assuming $\pi_3(t)$ through $\pi_6(t)$ are constant. If the functional relationship is found at each discrete time, it is assumed that the functional relationship in the continuous time spectrum is the smooth surface passed through those discrete curves.

The transient analysis therefore is based on the results from the steady state analysis.

1. Flow transient

A transient might occur when the circulation pumps lose their power or reduce their function suddenly and result in deficient cooling of fuel rods.

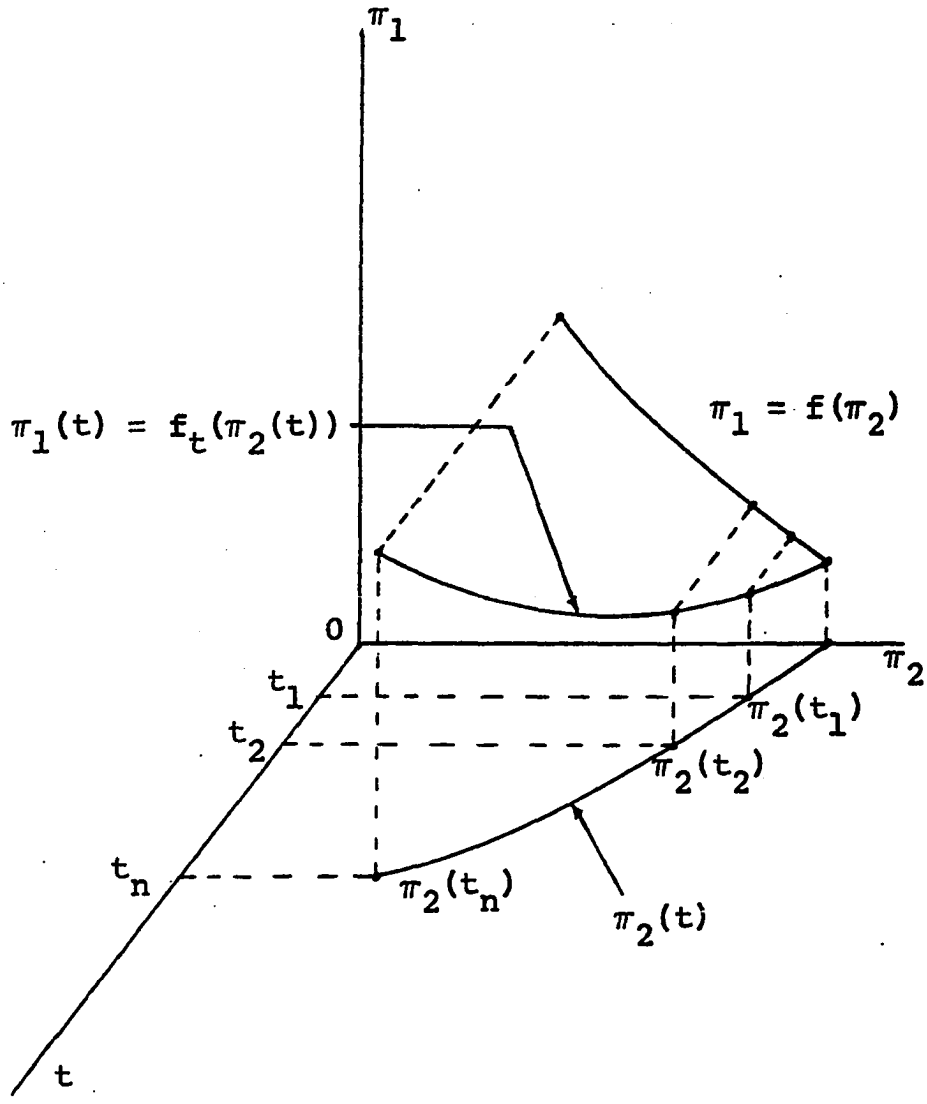

Figure 3. Graphical representation of $\pi_1(t) = f(\pi_2(t))$

Two assumptions are usually made (20, 28) for such flow coastdown cases.

1. System pressures are only slightly disturbed and therefore not subjected to change with time.
2. Since CHF always occurs within a few seconds, the inlet temperature will remain constant in time.

It should be noted that the assumptions are not necessarily true for long transient periods.

A compensated distortion model is designed and operated under the conditions derived from Equation 14. Since the system pressure is assumed to hold constant in time, the distortion factors and some of the π-terms are also constant in time. The design conditions are then listed as follows:

$$\pi_{2m}(t) = \pi_{2m}(t) = \alpha_2\pi_{2p}(t) = \alpha_2(t)\pi_{2p}(t)$$

$$\pi_{3m}(t) = \pi_{3m} = \pi_{3p} = \pi_{3p}(t)$$

$$\pi_{4m}(t) = \pi_{4m} = \pi_{4p} = \pi_{4p}(t) \qquad (15)$$

$$\pi_{5m}(t) = \pi_{5m} = \pi_{5p} = \pi_{5p}(t)$$

$$\pi_{6m}(t) = \pi_{6m} = \alpha_6\pi_{6p} = \alpha_6(t)\pi_{6p}(t)$$

Here $\alpha_5(t) = \alpha_5 = 1$ and α_6 is a fixed value calculated from the fluid property ratios of water and Freon. α_2 is not a function of time and its value is determined from the first set of steady state CHF data to compensate the other

distortion.

If a model satisfies these design conditions then the prediction equation

$$\pi_{1p}(t) = \pi_{1m}(t) \tag{16}$$

most hold true.

Equation 16 simply means that the trajectory of $\pi_{1p}(t)$ must be the same as that of $\pi_{1m}(t)$. This therefore implies that the onset time of CHF must be the same in both systems.

2. Depressurization transient

This type of transient could occur for example as the result of a break in the primary coolant pipe causing the decrease of system pressure. It frequently is associated with the loss of coolant from the system and hence also yields a flow decay transient.

The design and operating conditions for the model are derived from Equation 14 and are written as in the following:

$$\begin{aligned}
&\pi_{2m}(t) = \alpha_2(t)\,\pi_{2p}(t) \\
\pi_{3m}(t) = \pi_{3m} &= \pi_{3p} = \pi_{3p}(t) \\
&\pi_{4m}(t) = \pi_{4p}(t) \\
&\pi_{5m}(t) = \alpha_5(t)\,\pi_{5p}(t)
\end{aligned} \tag{17}$$

$$\pi_{6m}(t) = \alpha_6(t)\ \pi_{6p}(t)$$

All terms except π_3 are functions of time during depressurization transient since they are functions of system pressure. If the pressure decay history can be controlled or followed the design conditions can be fulfilled.

Since π_4 represents the system pressure, the condition $\pi_{4m}(t) = \pi_{4p}(t)$ thus confine a pressure decay pattern in the model corresponding to that in the prototype. Since the prototype system in this work is actually represented by a computer code, the condition can be easily met.

The second assumption in the flow transient case also applied in the present case, that is, the inlet temperature will not change during the transient period. π_5, the ratio of inlet subcooling to latent heat of evaporation, however, will change when the system begins to depressurize. The trajectory of $\pi_5(t)$ depends on the initial value and the pressure history only. There is no way for the trajectory $\pi_{5m}(t)$ to match $\pi_{5p}(t)$ since the pressure decay pattern is determined by the previous condition, i.e., $\pi_{4m}(t) = \pi_{4p}(t)$. But $\pi_{5m}(t)$ will be adjusted as close to $\pi_{5p}(t)$ as possible. The loci of $\pi_{5m}(t)$ and $\pi_{5p}(t)$ are actually selected beforehand, and are shown in Figure 4 where the variations of π_{5m} and π_{5p} with pressure were calculated under the assumption of constant inlet temperatures. Due to this

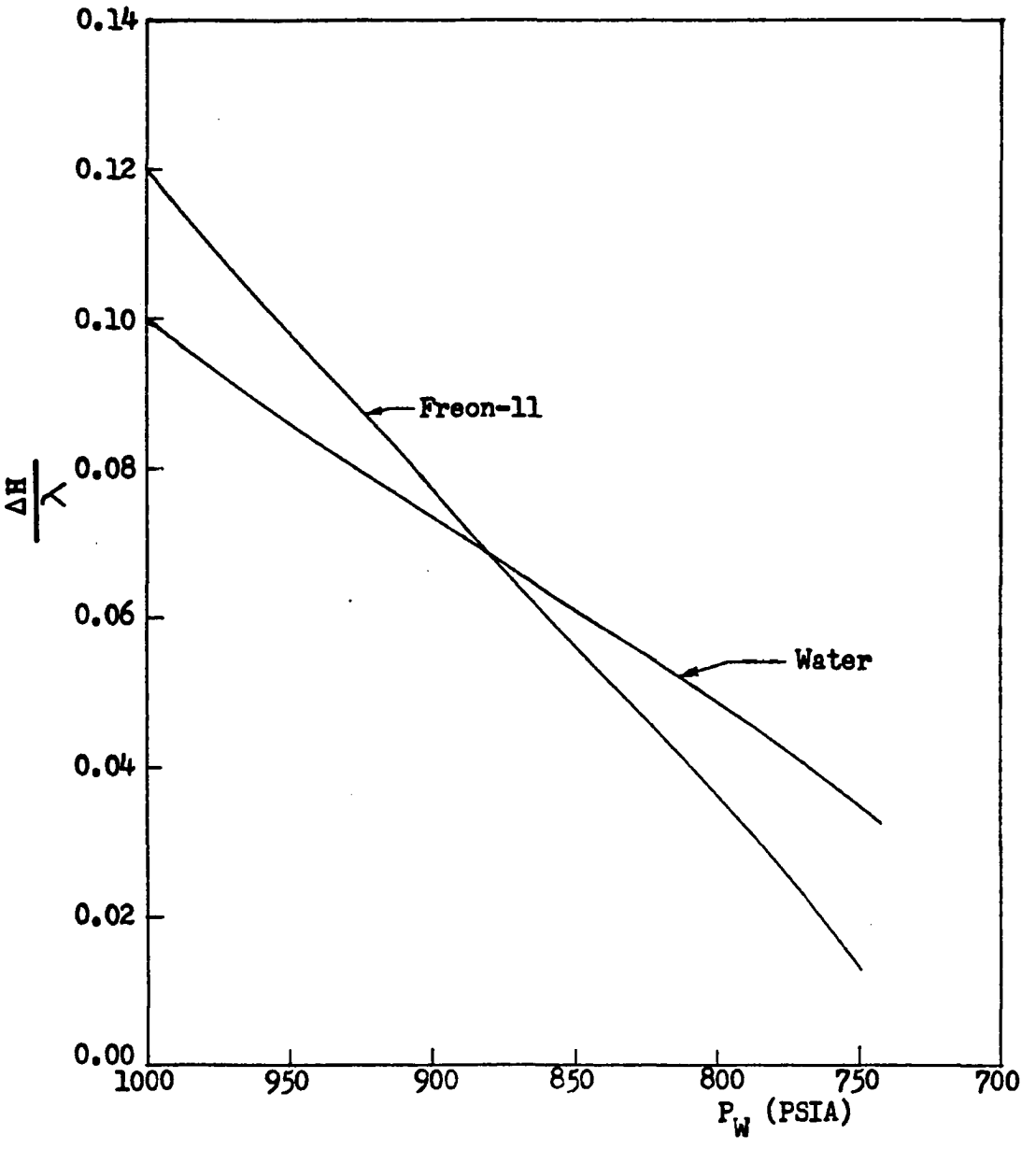

Figure 4. Variations of $\Delta H/\lambda)_W$ and $\Delta H/\lambda)_F$ with equivalent water pressures

uncontrollable effect, a distortion factor $\alpha_5(t)$ must be introduced.

Again the property group π_6 has to be distorted. The distortion factor is a function of time.

The most important factor is $\alpha_2(t)$. It is designed to compensate the other distortions and is a function of time. The values of $\alpha_2(t)$ are determined from the discrete α_2s at different pressures in the second set of steady state tests. Since all thermodynamic properties vary smoothly with pressure it is assumed that α_2 also changes with pressure smoothly. Therefore $\alpha_2(t)$ is determined to be the curve which fits smoothly to the discrete values of α_2s.

If a model satisfies the conditions listed in Equation 17 the prediction by the model can be established through the equation

$$\pi_{1p}(t) = \pi_{1m}(t) \tag{18}$$

The onset time of CHF can thus be predicted from the model.

3. MAYU-2 code

The transient data from the postulated prototype system were generated from the MAYU-2 computer code. It has been reported in references 21 and 28 that the code presents good analytical agreement with the results from

various experiments in water systems.

Based on the method of characteristics, MAYU-2 calculates mass flux and quality as functions of space and time numerically from the one-dimensional two-phase conservation equations

$$\frac{D\rho}{Dt} = -\rho \frac{\partial V}{\partial Z} \qquad \text{(Continuity equation)}$$

$$\rho \frac{Dh}{Dt} = \phi\left(\frac{P_H}{A_{x-s}}\right) + \frac{\partial P}{\partial t} \qquad \text{(Energy equation)}$$

$$\left.\begin{aligned} h &= h_f + \chi\lambda \\ \rho &= \frac{1}{v_f + \chi v_{fg}} \end{aligned}\right\} \qquad \text{(Equations of state)}$$

Four basic assumptions are made for the subsequent derivation:

1. The boiling two-phase flow is homogeneous (i.e., "no slip").
2. The kinetic and potential energy terms in the energy equation are neglected.
3. The pressure is uniform along the test section (i.e., assume $\frac{\partial P}{\partial Z} = 0$).
4. Subcooled boiling is neglected.

Some detail features of MAYU-2 code are described in Appendix D.

IV. EXPERIMENTAL APPARATUS

A. Test Section

The test section (Figure 5) consisted of a central heater and a concentric unheated shroud. The central heater was constructed from commercially available 0.625-in. O.D. by 0.02-in. wall thickness Type 304 stainless steel tubing. The total heated length was 36 in.

Nichrome wire was selected as heating material because of its low temperature coefficient of resistance (14). A 65-foot number 18 Nichrome wire was wound into a coil uniformly spaced with 0.32-in. O.D. and was located at the center of the heater sheath to ensure the uniform surface heat flux. The coil was supported by compactly swaged magnesium oxide (MgO) powder with two ends spot-welded to two 10-in. stainless steel rods which were used as electrodes. MgO powder was used as supporter as well as electrical insulation material of the heating coil. It is good heat conducting nonmetallic solid and it has also been reported (10) that the temperature response of the stainless steel clad heater with MgO powder was very close to the response of the actual uranium oxide (UO_2) fuel rod in power transient.

Two ungrounded Iron-constantan thermocouples were embedded in the inside wall of the heater near the outlet

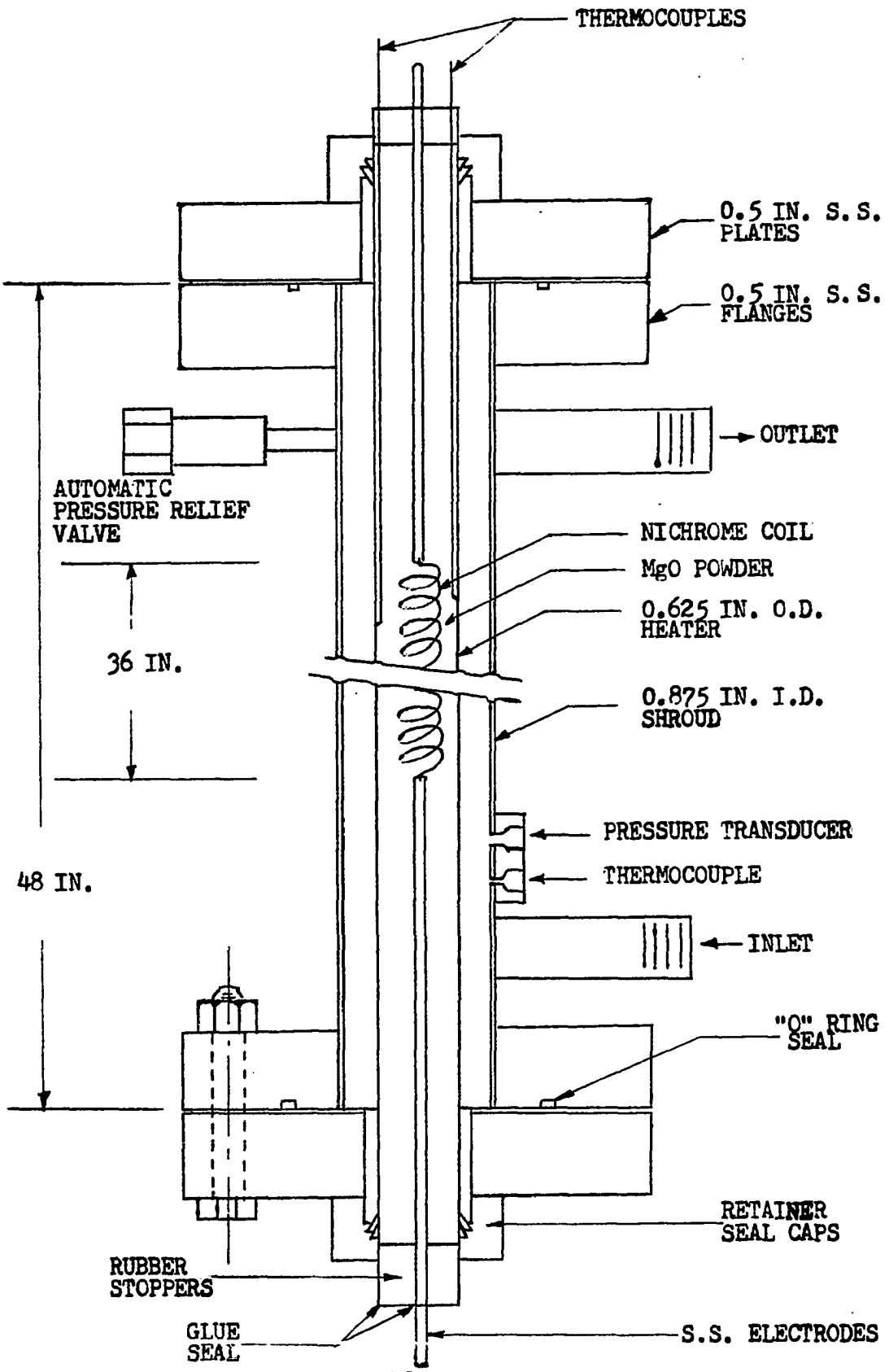

Figure 5. Test section assembly

of the heated end.

The shroud (Figure 6) was constructed from a 0.875-in. O.D. by 0.0625-in. wall thickness Type 304 seamless stainless steel tubing with two flanges welded at both ends. The material, thickness and physical dimensions were designed to meet the criteria in the Section VIII of ASME pressure vessel code. The number of bolts and bolt loads were calculated according to Shigley (27). The seal against high pressure was accomplished by the "O" ring in the groove between the flange and stainless steel plate and the retainer seal cap, which also held the heater concentrically in the shroud.

An adjustable automatic pressure relief valve was installed at the upper end of the test section for safety purposes. After the construction was completed the whole test section assembly was pretested hydraustatically to one and a half times the maximum operating pressure. The test was to check the mechanical seals and ensure the safety during high pressure operation.

The test section, after being installed in the loop, was insulated from its environment by 0.5 in. thick asbestos sheet. Heat balance test (Appendix B) showed that the heat loss during operation was less than 4 percent of the power input.

Power to the heater was supplied by a two-gang Variac

Figure 6. View of test section without asbestos insulation

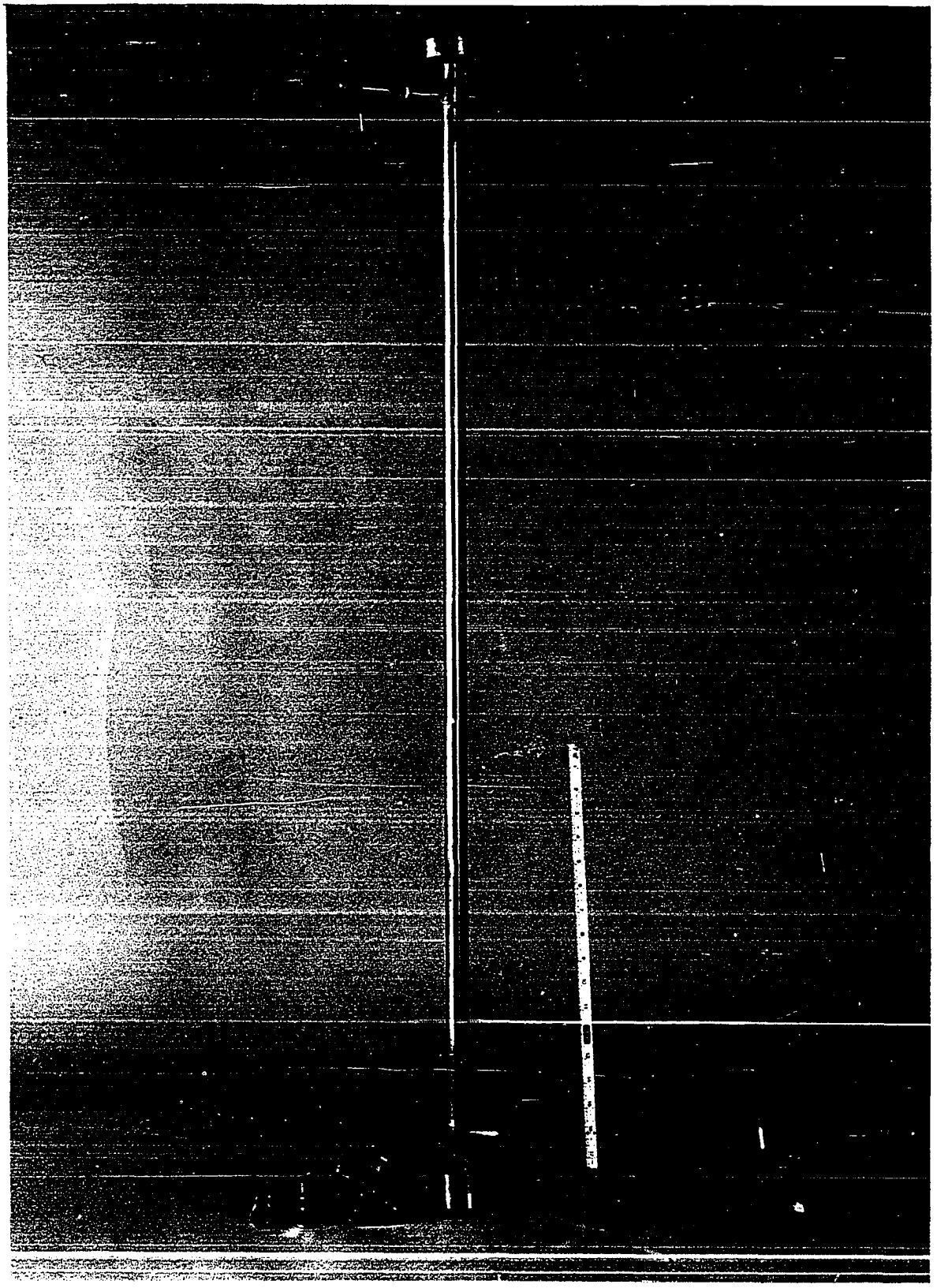

transformer manufactured by Superior Electric Co., and was rated at 28-amp., 500-volt when the input was from a 208-volt power source.

B. Freon Loop

A schematic of the closed flow Freon loop is shown in Figure 7.

The loop was constructed of 5/8 in. copper tubing with high-strength 95-5 solder used to sweat all joints. The working fluid was Freon-11 (CCl_3F) manufactured by E. I. Du Pont de Nemours and Company.

A 5-gallon steel tank was provided for the storage of Freon. The tank was equipped with a copper-constantan thermocouple for sensing the fluid temperature and an automatic pressure relief valve for releasing the pressure when it exceeded the preset safe limit. The whole system was kept pressurized by filling the gas to the Buna N gas bag in the storage tank.

Freon flow entered a pump from the storage tank. The Model 142-F pump manufactured by Thomas Pump Company is a two-stage turbine regenerative pump with bronze impellers, stainless steel shaft, and cast iron suction-discharge covers. It was rated at 5 gpm of Freon at 100°F and 300-foot head. Mechanical seals were provided to minimize the leakage of Freon which has low surface tension and excellent

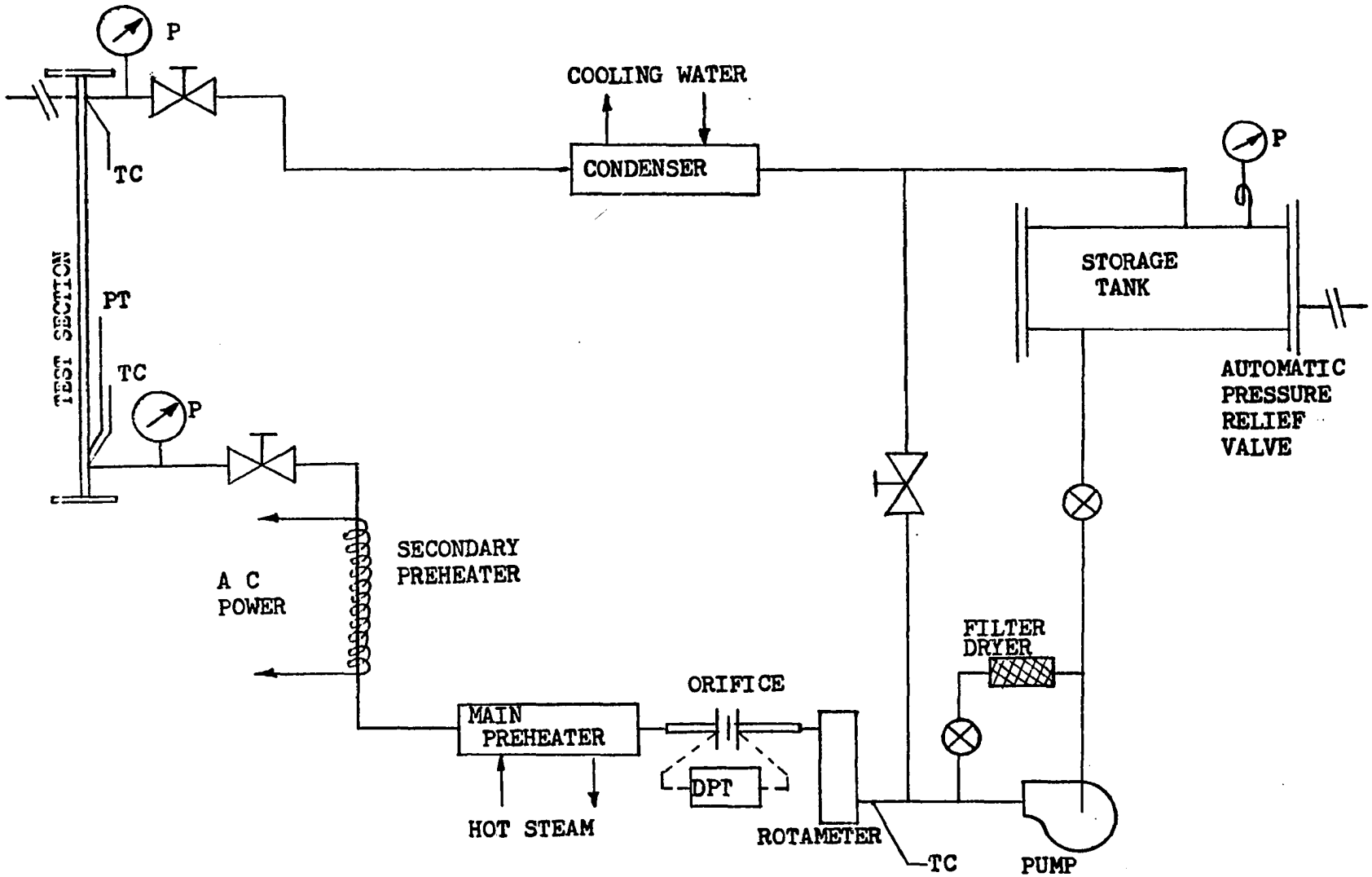

Figure 7. Schematic diagram of the Freon loop

wetting characteristics (25). Coupled with the pump was a 2-HP, 3-phase, 230/460-volt, 1750 RPM drip proof motor. A three-gang Variac transformer was used to raise the line voltage from 208 to 230 volts.

A vertical rotameter by Fischer and Porter Company served to monitor the steady state flow rate over the scale of 0-2.2 gpm water. The scale was easily convertible to Freon-11 flow rates by the manufacturer's specifications. Another horizontal orifice flow rate meter was used to measure the flow rate during transient tests. The time dependent flow rates were monitored by the pressure drop across the orifice.

After the flow rate meters, the Freon entered two preheaters served as the control of inlet condition of the flow. The main preheater was a heat exchanger and used hot steam as heat source. The second preheater was provided by a Nichrome heating coil wound externally to the copper tubing and served for fine adjustment of inlet temperature.

Freon flow after the test section was a mixture of liquid and vapor. The two phase flow then was cooled by entering a condenser. The condenser was a counter flow heat exchanger, and city water supply was used as coolant. After the condenser the Freon flowed into the storage tank again and completed a closed cycle.

One bypass line of the flow from the outlet of the pump back to the storage tank was provided. Since changes of the flow rates entering the test section were desirable, this bypass line allowed the pump to operate at a constant flow rate. Another bypass line from the discharge side to the suction side of the pump was provided. It was equipped with a Sporlan Catch-All filter dryer in the flow path to clean up and dehydrate part of the Freon flow continuously.

Two globe valves were installed near the inlet (upstream) and the outlet (downstream) of the test section, one needle valve was installed in the bypass line from the pump to the storage tank. These three throttling valves served to control the flow rate and pressure in the test section. Other valves were ball valves with Teflon seats to minimize the leakage of Freon.

C. Instrumentation

Burnout was detected by two ungrounded Iron-constantan thermocouples embedded in the heater. The thermocouple wires were buried in a 0.04-in. O.D. Type 304 stainless steel sheath with magnesium oxide powder for insulation.

During the experiment, the temperature signals were continuously sent into a Type M Dynograph Direct Writing Strip Chart Recorder manufactured by Beckman Instruments, Inc. Critical heat flux was defined experimentally as the

heat flux which caused the surface temperature of the heater to rise rapidly.

Temperatures at other points in the system were monitored by copper-constantan thermocouples in the 0.0625-in. O.D. Type 304 stainless steel sheaths and Emfs generated from the thermocouples were read by a potentiometer. A switch was provided to read the temperatures at different points as quickly as possible. The inlet temperature signal was also transferred continuously into the Type M Dynograph to permit observation of any possible changes during the experiment.

Transient flow rates were monitored by a CIC model 6100 differential pressure transducer, manufactured by the Computer Instrument Corporation. The two legs (high pressure and low pressure) of the transducer were attached to the two sides (upstream and downstream) of the orifice by brass compression fittings. Signals were also sent into the Type M Dynograph recorder.

Two Heise-Bourdon-tube pressure gauges located near the inlet and near the outlet of the test section were used to indicate the static pressure of the test section, while transient pressure was signaled by a Model 601A quartz pressure transducer manufactured by Kistler Instrument Corporation. Signals produced from the transducer were transmitted through a low-noise cable to a Model 568

universal electrostatic charge amplifier also manufactured by Kistler Instrument Corporation. After the charge amplifier, the signals entered a Brush Recorder Mark II manufactured by Brush Instruments and were recorded on strip chart paper.

Power to the heater was indicated by the current from an ammeter with a range of 0-25 amperes and the output voltage of the Variac transformer. An A-C rectifier associated with a voltage divider was made to convert the A-C voltages into D-C signals and input them to the Brush Recorder.

V. EXPERIMENTAL PROCEDURE

Before startup, the power source voltage was measured, all channels of the recorders were calibrated, cooling water to the condenser was turned on.

The experiment could then be started. The steady state experiments were carried out by the following steps:

1. The pump was turned on to circulate the Freon for about 10 minutes.
2. The system was adjusted to the operating pressure and desirable flow rate by the gas bag and the throttling valves.
3. The main preheater was turned on to bring the inlet temperature up to the approximate preset value.
4. The secondary preheater was turned on to adjust the inlet temperature to the exact preset value.
5. The power to the heater was turned on and raised to about 75% of the burnout power.
6. The system pressure, flow rate and inlet temperature were readjusted to correct the disturbances.
7. The heater power was gradually increased at small steps.
8. Steps 6 and 7 were repeated until CHF was reached.
9. The heater power was cut back about 5% and then increased at slow rate until CHF occurred again.
10. The power, flow rate, pressure and inlet temperature

were read and recorded.

11. The system parameter(s) were changed and the same procedure was repeated for another CHF test.

For transient tests, the procedure was carried out to step 6. Pressure, power and flow rate were then set at the calculated initial values. Transient conditions were established by varying the opening of the controlling valves or changing the output voltage of the power supply. All time dependent signals were sent into the strip chart recorders. After a sign of CHF was observed, the system was brought back to the nucleate boiling condition for preparing another run.

VI. RESULTS AND DISCUSSION

The results of the steady state and transient tests are presented in this chapter. Data from the steady state measurements of CHF are used for determining α_2s at different pressures. These values will be needed for the scaling of mass fluxes and CHFs in transient tests.

A. Steady State CHF

Experiments were run with mass fluxes ranging from 0.25 to 0.58 x 10^6 lb/hr-ft^2 at system pressures of 129, 137, 146, 154 and 163 psia. The equivalent mass fluxes in prototype ranged from 0.36 to 1.0 x 10^6 lb/hr-ft^2 and the equivalent pressures were at 800, 850, 900, 950, and 1000 psia respectively.

All data were converted into British units and are listed in Table A-1. Values from Table A-1 were further grouped into $\pi_1(\phi_c/G\lambda)$ and $\pi_2(GD/\mu_1)$, and are presented in a log-log plot with π_1 as a function of π_2. These are shown in Figures 8 through 12. Data points were fitted by a least square straight line programmed by the use of a computer. Water data, calculated from Equation 13 at equivalent conditions are also presented in the corresponding figures for the evaluation of the distortion factor α_2s and the results have shown that the Janssen and Kervinen's correlation represents nearly straight lines within the range of interest.

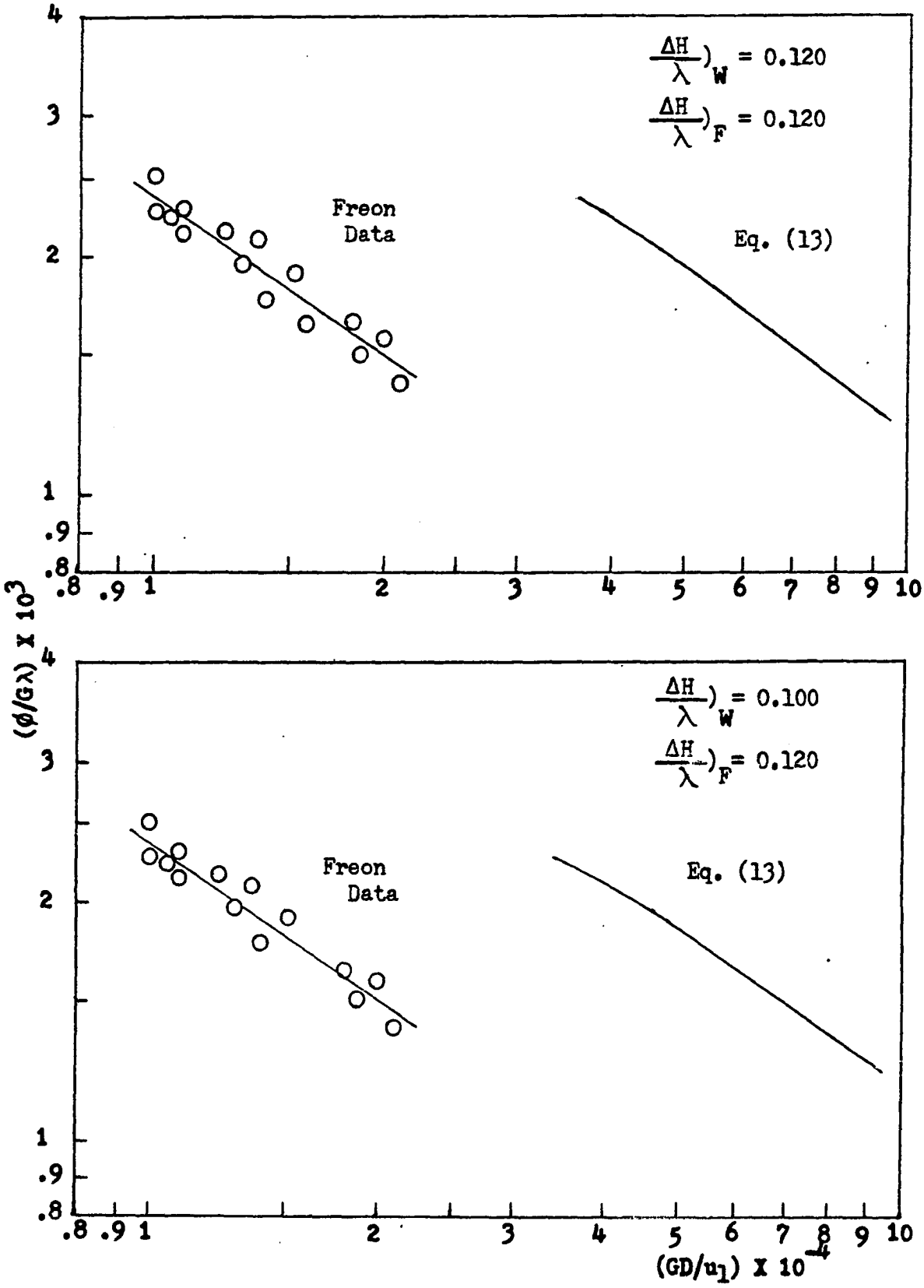

Figure 8. Results of π_1 versus π_2 for $\rho_l/\rho_v = 20.65$

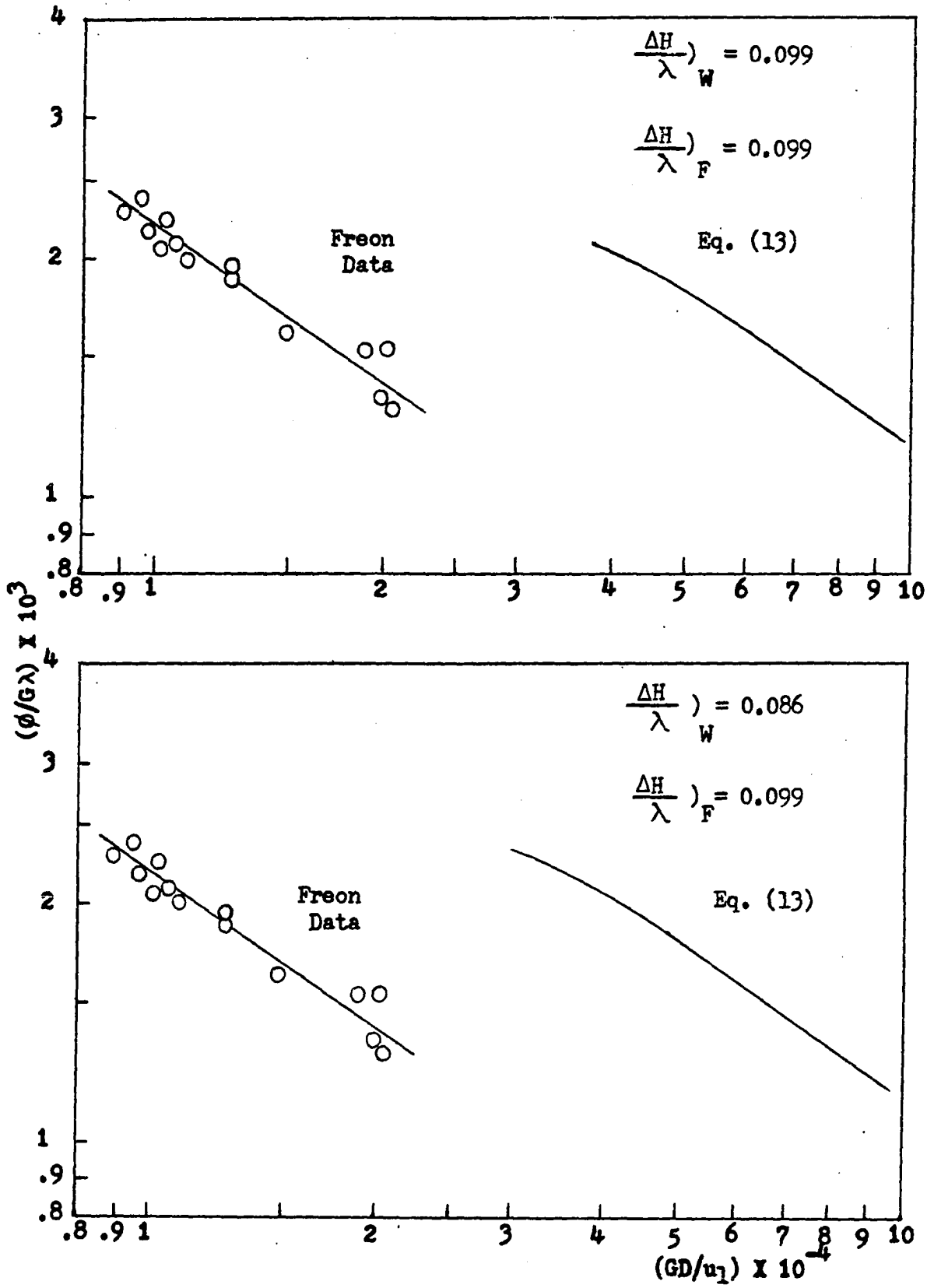

Figure 9. Results of π_1 versus π_2 for $\rho_l/\rho_v = 22.10$

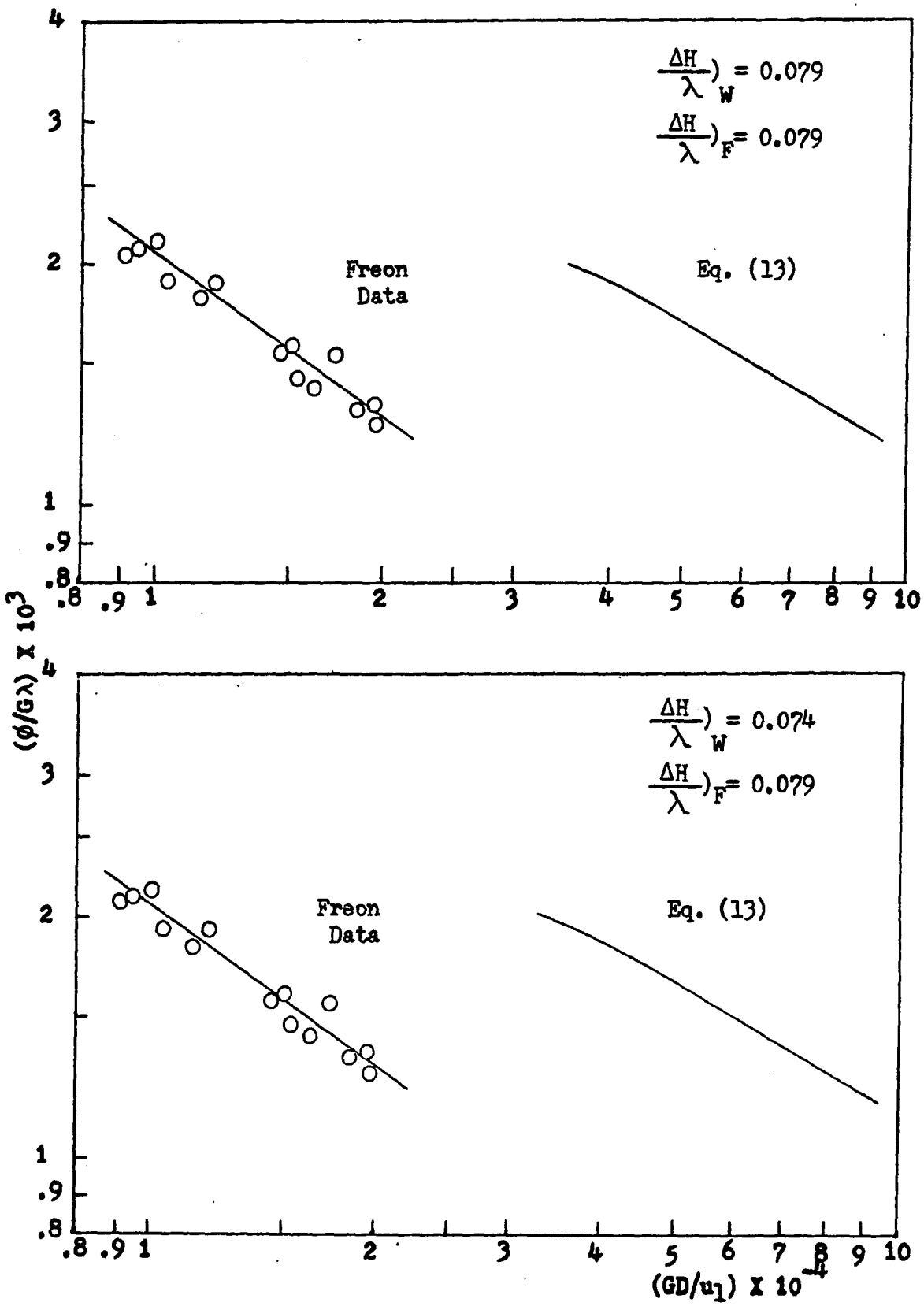

Figure 10. Results of π_1 versus π_2 for ρ_l/ρ_v = 23.55

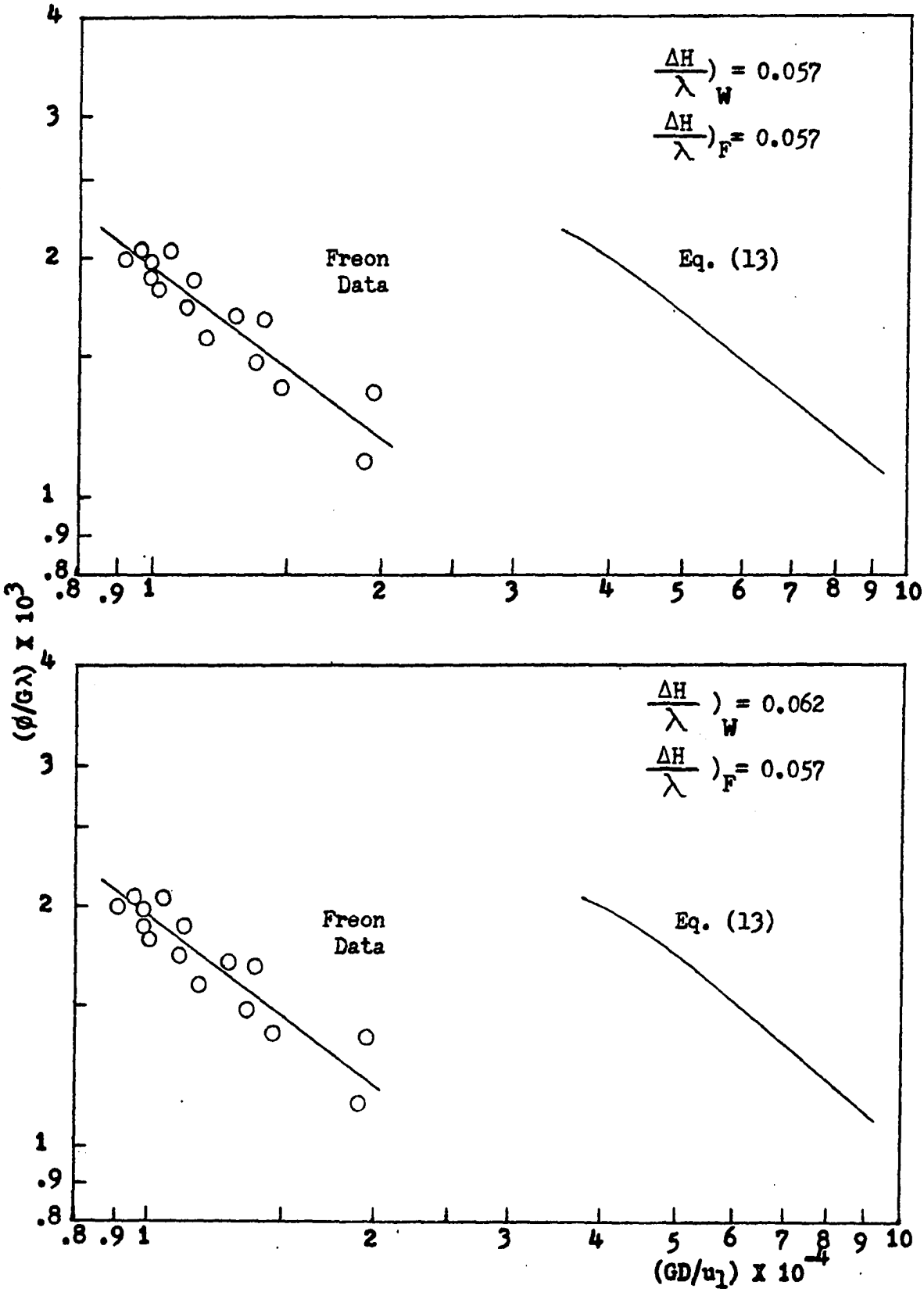

Figure 11. Results of π_1 versus π_2 for $\rho_l/\rho_v = 25.30$

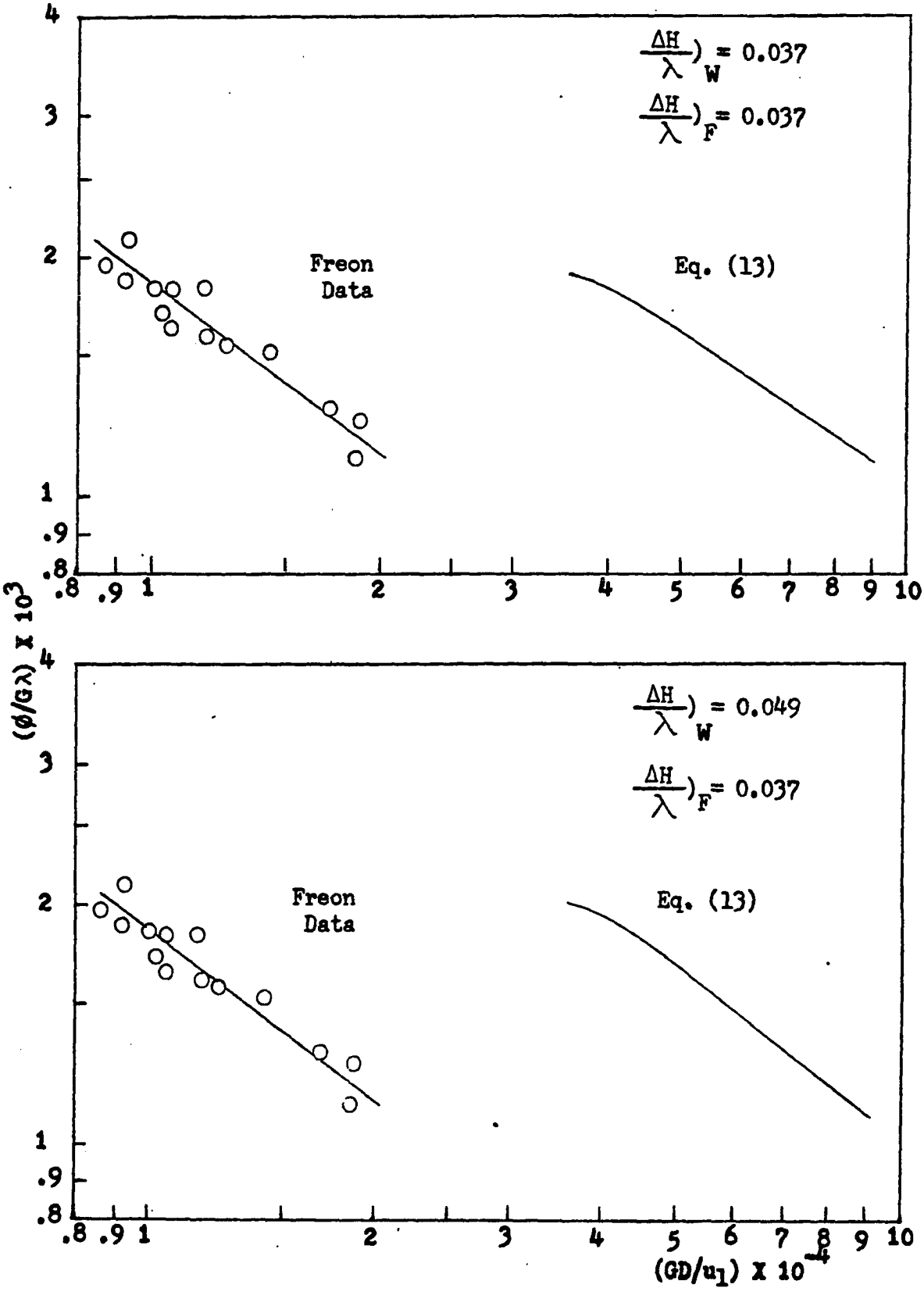

Figure 12. Results of π_1 versus π_2 for $\rho_l/\rho_v = 27.22$

Figure 8 shows the comparisons of the experimental data with two different prototype data calculated from Equation 13 with two different values of π_5. Figures 9 through 12 give similar comparisons. The distortion factors, α_2s, determined from the first set (upper figures) are to be used in flow transient tests, while that from the second set (lower figures) are to be used in depressurization transients.

The flow rate scale, $F_G(F_G = G_W/G_F)$ was then evaluated through the design condition, $\pi_{2m} = \alpha_2 \pi_{2p}$ and the CHF scale, $F_\phi(F_\phi = \phi_{cW}/\phi_{cF})$ was evaluated through the prediction equation $\pi_{1p} = \pi_{1m}$.

Values of α_2, F_G and F_ϕ are listed in Tables 2 and 3.

Figure 13 shows the plots of F_G, obtained from the first set of data, versus equivalent water pressures. Equation 2 was plotted to provide qualitative comparison. The equation was developed from round tube CHF data with Freon-114 as working fluid, and it was employed by Motley et al. (23) to calculate the flow rate scales in their 16-rod bundle CHF tests. The comparison revealed good agreement in not only the trend of the pressure effect on F_Gs but also the numerical values when C_T in Equation 2 was chosen to be 0.731.

F_G evaluated from the comparisons of the lower set of figures and its variation with pressure fitted by a smooth curve is shown in Figure 14. Based on the curve in Figure

Table 2. Distortion factors and parameter scales from the first set of data

Water Pressure psia	$\frac{\rho_l}{\rho_v}$	α_2	$F_G = \frac{G_W}{G_F}$	$F_\phi = \frac{\phi_{cW}}{\phi_{cF}}$
1000	20.65	0.279	1.47	16.00
950	22.10	0.267	1.54	16.86
900	23.55	0.260	1.58	17.36
850	25.30	0.245	1.66	18.26
800	27.22	0.242	1.68	18.55

Table 3. Distortion factors and parameter scales from the second set of data

Water Pressure psia	$\frac{\rho_l}{\rho_v}$	α_2	$F_G = \frac{G_W}{G_F}$	$F_\phi = \frac{\phi_{cW}}{\phi_{cF}}$
1000	20.65	0.286	1.44	15.53
950	22.10	0.278	1.47	16.28
900	23.55	0.263	1.56	17.14
850	25.30	0.241	1.68	18.08
800	27.22	0.238	1.70	19.15

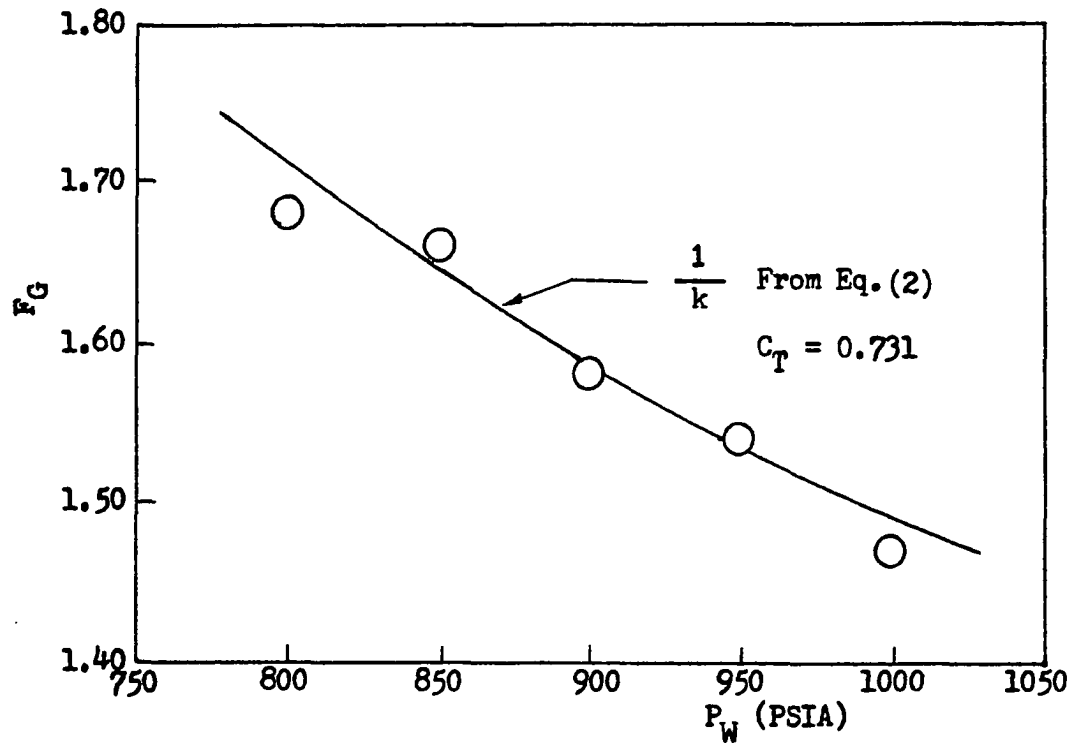

Figure 13. The effect of pressure on F_G with undistorted π_5, and the calculated results from Equation 2

14, the variation of F_{ϕ} with pressure was evaluated and plotted in Figure 15. The trend of their increasing magnitudes with decreasing pressures also agrees with the observations of Coffield (12), Dix (13) and Motley et al. (23). Figures 14 and 15 are the two graphical correlations established for the scaling in depressurization transient tests.

The predictions of steady state and CHF from the compensated distortion model were compared with the calculated water data at equivalent conditions. The results of 72 data points are shown in Figures 16 and 17. More than 97% of the total data are within the deviation of $\pm$ 15%. The successful prediction by the proposed model gives strong support for the extension of the scaling technique to transient tests. The rms error in Figure 16 is 6.24% and is 6.95% in Figure 17. The larger rms error in Figure 17 is not unexpected, since π_5s are not exactly matched in the evaluation of α_2s.

B. Transient CHF

Two different types of transient were run. All data were read from the recorders. The correction of the time lags introduced by measuring instruments is important and must be taken into account in the output data processing.

The response times of the Type M Dynograph and the Brush recorder were reported in their manuals to be less

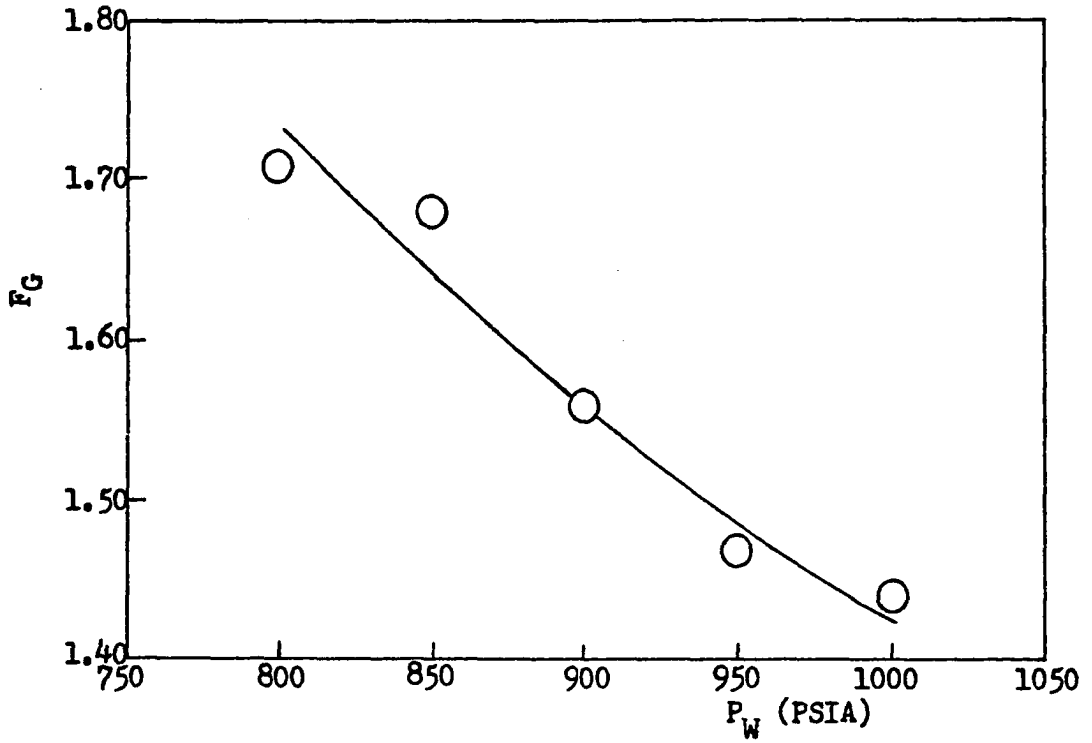

Figure 14. The effect of pressure on F_G with distorted π_5

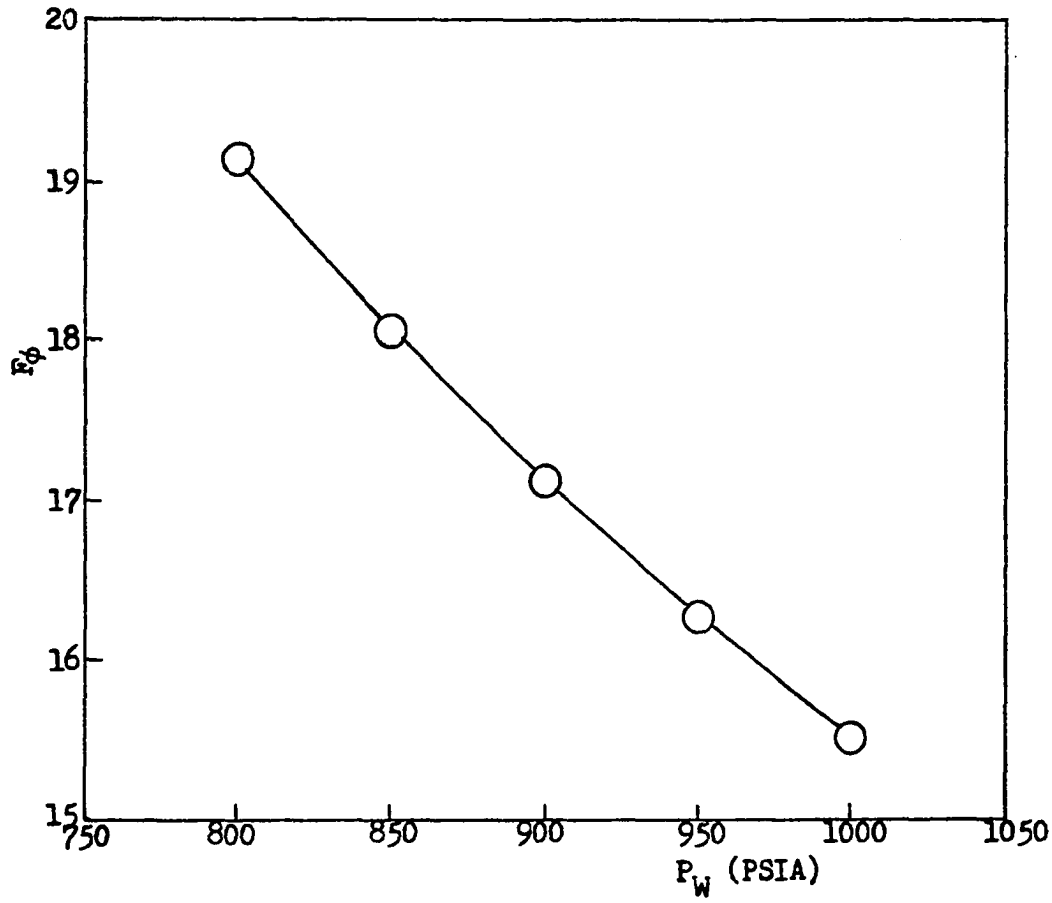

Figure 15. The effect of pressure on F_ϕ with distorted π_5. F_ϕs were evaluated from the prediction equation and the fitted curve in Figure 14

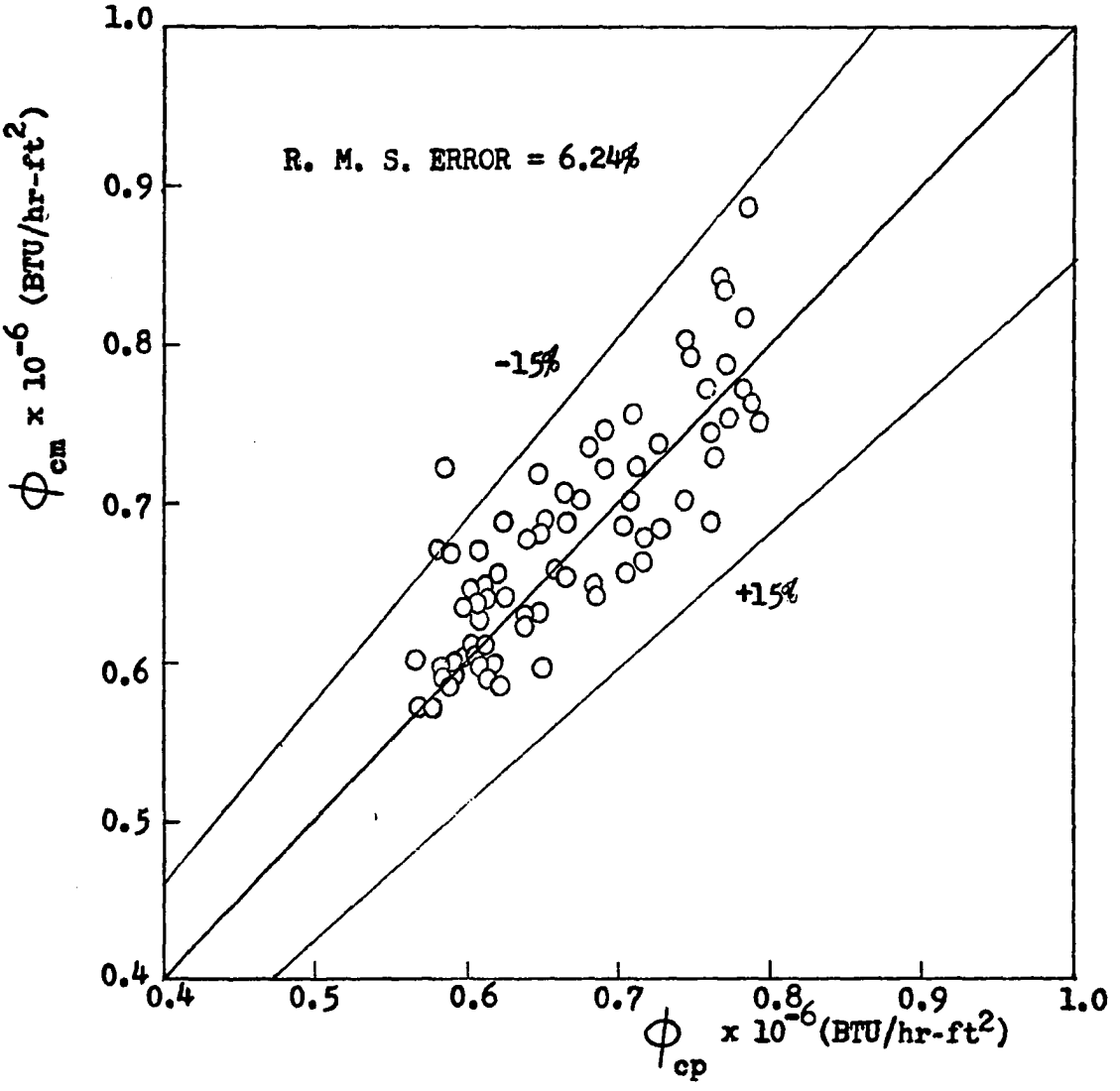

Figure 16. Comparison between prediction of Freon data and Equation 13 with undistorted π_5

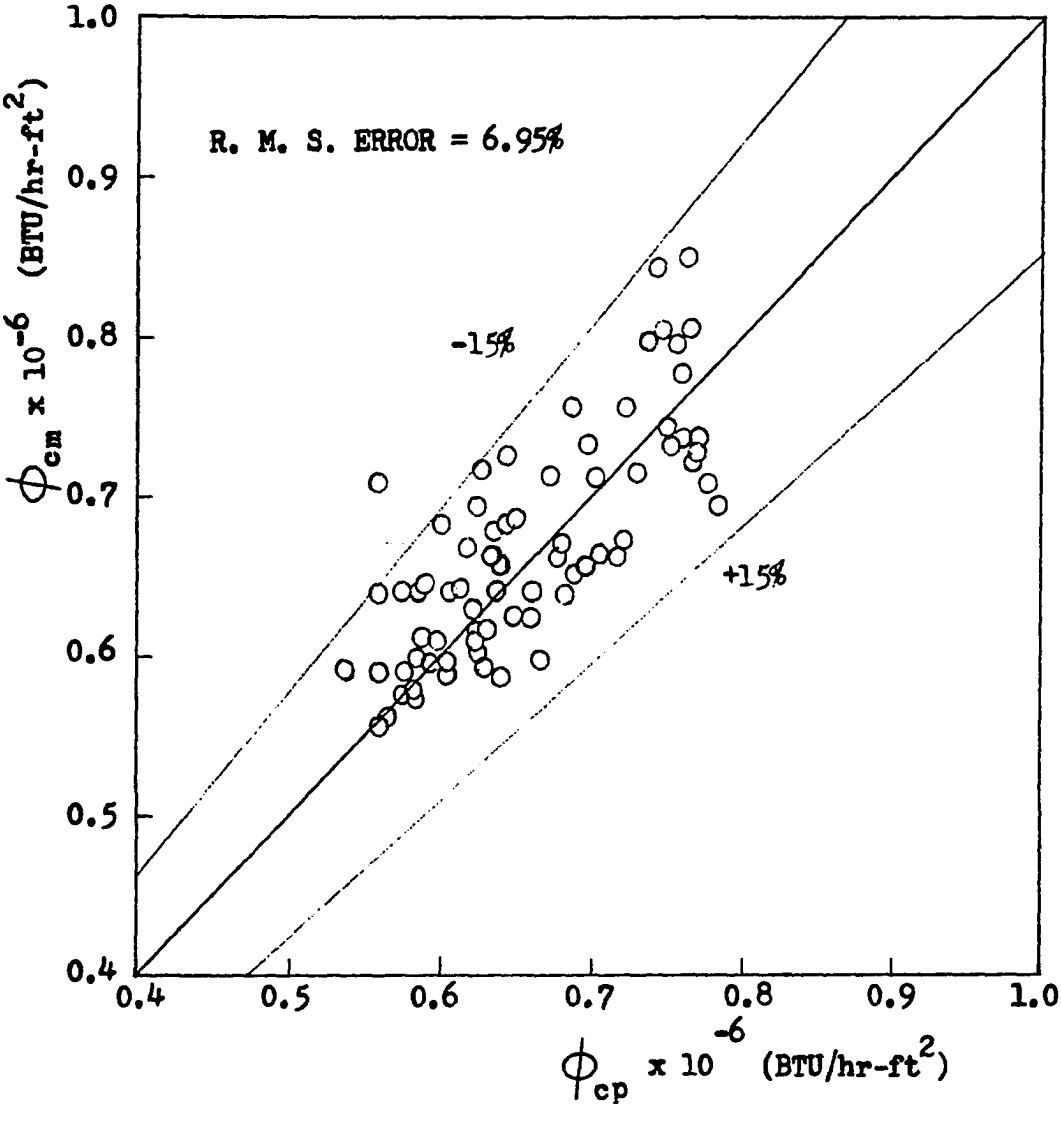

Figure 17. Comparison between prediction of Freon data and Equation 13 with distorted π_5

than 1/120 sec and 1/100 sec, respectively. The average time lag of the thermocouple from the heater surface was measured experimentally to be 0.014 $\pm$ 0.004 sec. The response time of CIC model 6100 pressure transducer is 0.017 sec. The Kistler Model 601A quartz pressure transducer has 3 microsecond rise time, and the frequency response of the associated Kistler Model 568 charge amplifier is up to 150,000 cps. The surface heat flux response to the change of input power, as indicated in reference 20, is in the order of milliseconds.

Traces of all signals recorded during transient tests were enlarged from the strip chart papers by an accurate metal arm pantograph manufactured by Charles Bruning Co., Inc. For the convenience of displaying, all signals in the same run were overlapped in the same figure. These are presented in Figures 18 through 46.

The onset time of CHF is defined to be the time between the beginning of transient and the point where the temperature trace from either one of the two thermocouples indicated a rapid increase. The results from each run were corrected for time lags and resolved into discrete numerical data in British units and the data were scaled up to equivalent water conditions by the scales listed in Table 2 as well as shown in Figures 14 and 15. The equivalent system pressure was calculated from Equation 5. These scaled

values were used as input data for MAYU-2 calculations which represented the prototype system and computed CHFR under the equivalent transient.

1. Flow transient

In this type of transient the system pressures were held nearly constant, and in all except the last few runs, power levels were held constant. Test conditions are tabulated in Table 4 and the results are shown in Figures 18 through 35.

In addition to the predictions of the onset time of CHF, the results also reveal interesting trends of transient effects, which are consistent with the experimental results in water system presented by references 20 and 28 and are described as follows.

Figures 18 and 19 are simple flow decays with different decay rates. Slower flow decay rates delayed the onset of CHF as in the case shown in Figure 18. Power was held constant within the transient period. From the safety point of view, this is a conservative assumption since actual reactor transients of this nature will have a reduction of heat flux due to generation of additional steam in the core causing a power reduction.

Figure 20 is a flow ON/OFF/ON test. CHF occurred at the time flow began to recover from its minimum value.

Table 4. List of flow transient runs

Run No.	Initial Conditions				
	P psia	ΔH Btu/lb	G x 10^{-6} lb/hr-ft^2	ϕ x 10^{-4} Btu/hr-ft^2	χ %
G1	164	7.16	0.554	3.895	16.31
G2	163	7.17	0.558	3.854	15.79
G3	164	7.17	0.488	3.721	18.68
G4	128	2.27	0.376	3.012	27.16
G5	128	2.28	0.370	2.983	27.35
G6	129	2.31	0.464	3.015	21.28
G7	144	4.78	0.445	3.253	20.94
G8	143	4.75	0.447	3.256	20.89
G9	143	4.75	0.447	3.160	20.04
G10[a]	146	4.76	0.461	3.934	25.79
G11[b]	146	4.76	0.591	3.110	12.91
G12	145	4.75	0.521	4.113	23.29
G13[b]	137	3.48	0.279	3.184	38.76
G14[b]	135	3.46	0.335	3.124	30.67
G15	135	3.46	0.469	3.602	24.27
G16	137	3.47	0.467	3.600	24.37

[a]Power decay.

[b]Power ramp up.

$G_{min} \times 10^{-6}$ lb/hr-ft^2	Time to $G_{min} \times 10^{-6}$ sec	Onset Time of CHF	
		Measured Time sec	MAYU-2 Predicted Time, sec
0.305	2.59	3.12	2.92
0.307	0.64	1.16	1.11
0.281	0.80	1.42	1.50
0.245	1.71	3.29	3.06
0.243	1.50	No CHF	
0.240	1.54	No CHF	
0.239	1.62	2.32	2.01
0.240	1.65	1.53	1.50
0.236	1.64	2.11	2.20
0.222	1.20	1.37	1.20
0.284	0.81	2.50	2.72
0.423	0.60	0.68	0.79
0.301	0.82	2.40	2.31
0.335	--	2.29	2.21
0.339	1.04	3.38	3.41
0.320	1.01	No CHF	1.12

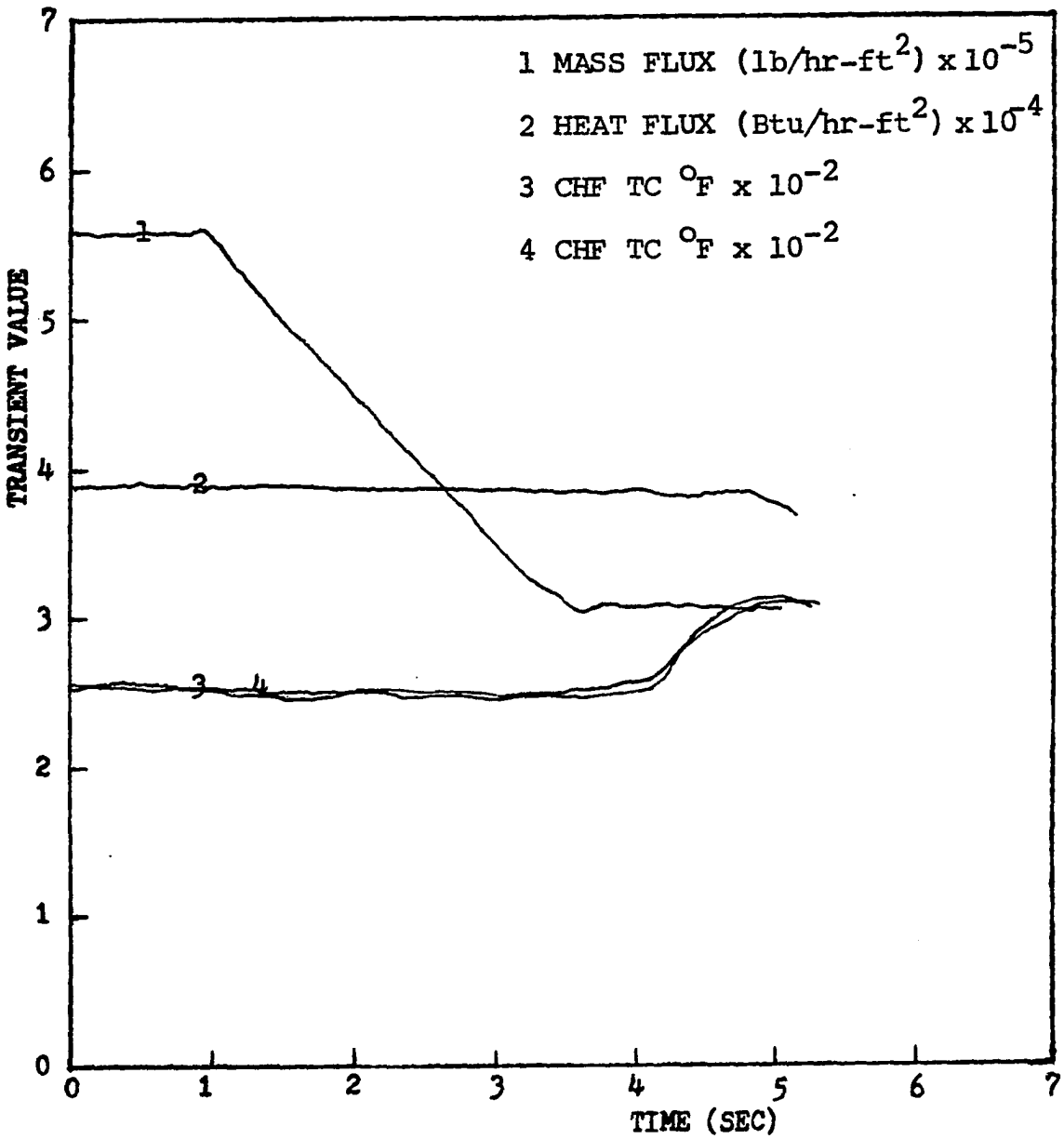

Figure 18. Flow transient run No. G1

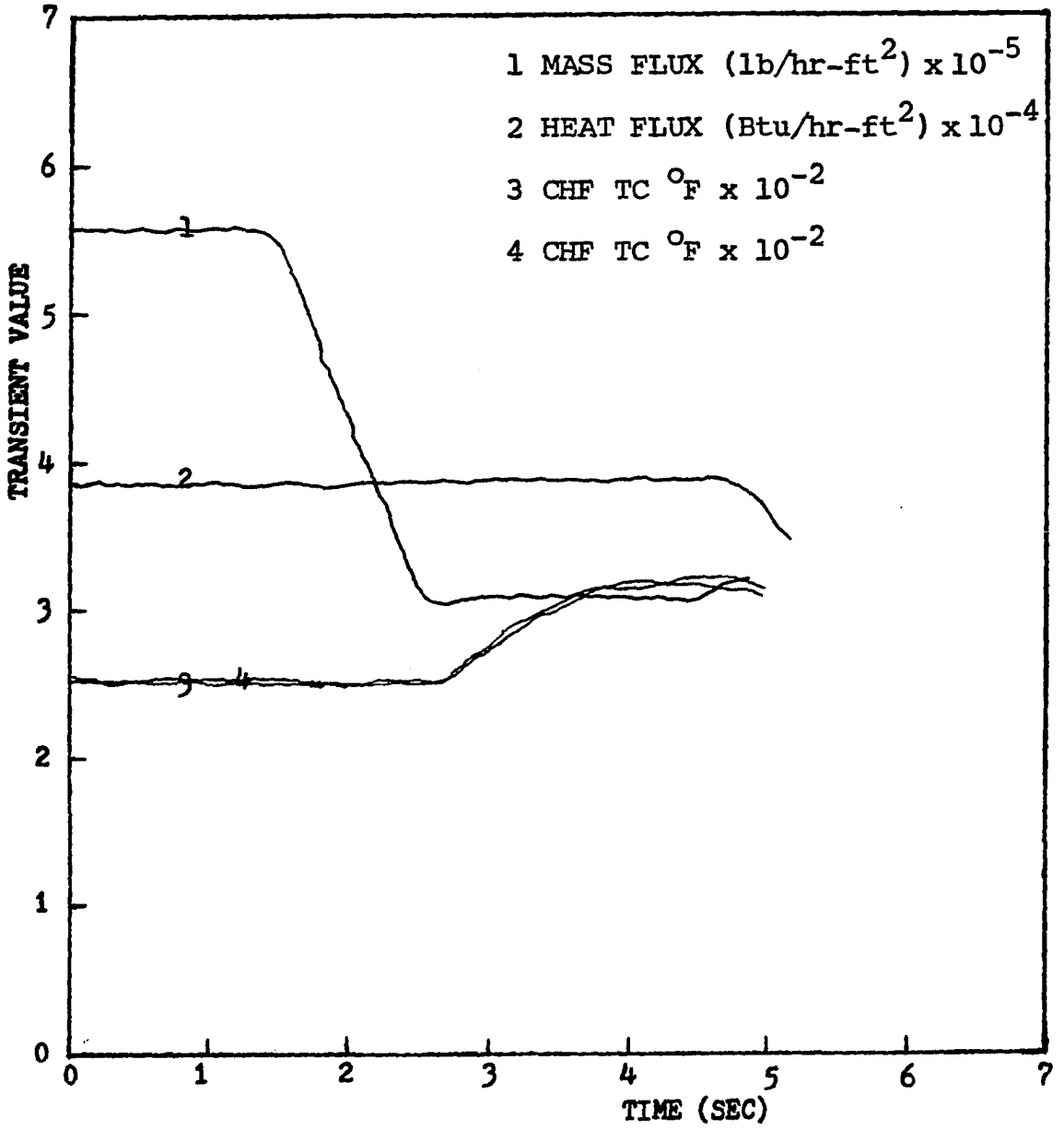

Figure 19. Flow transient run No. G2

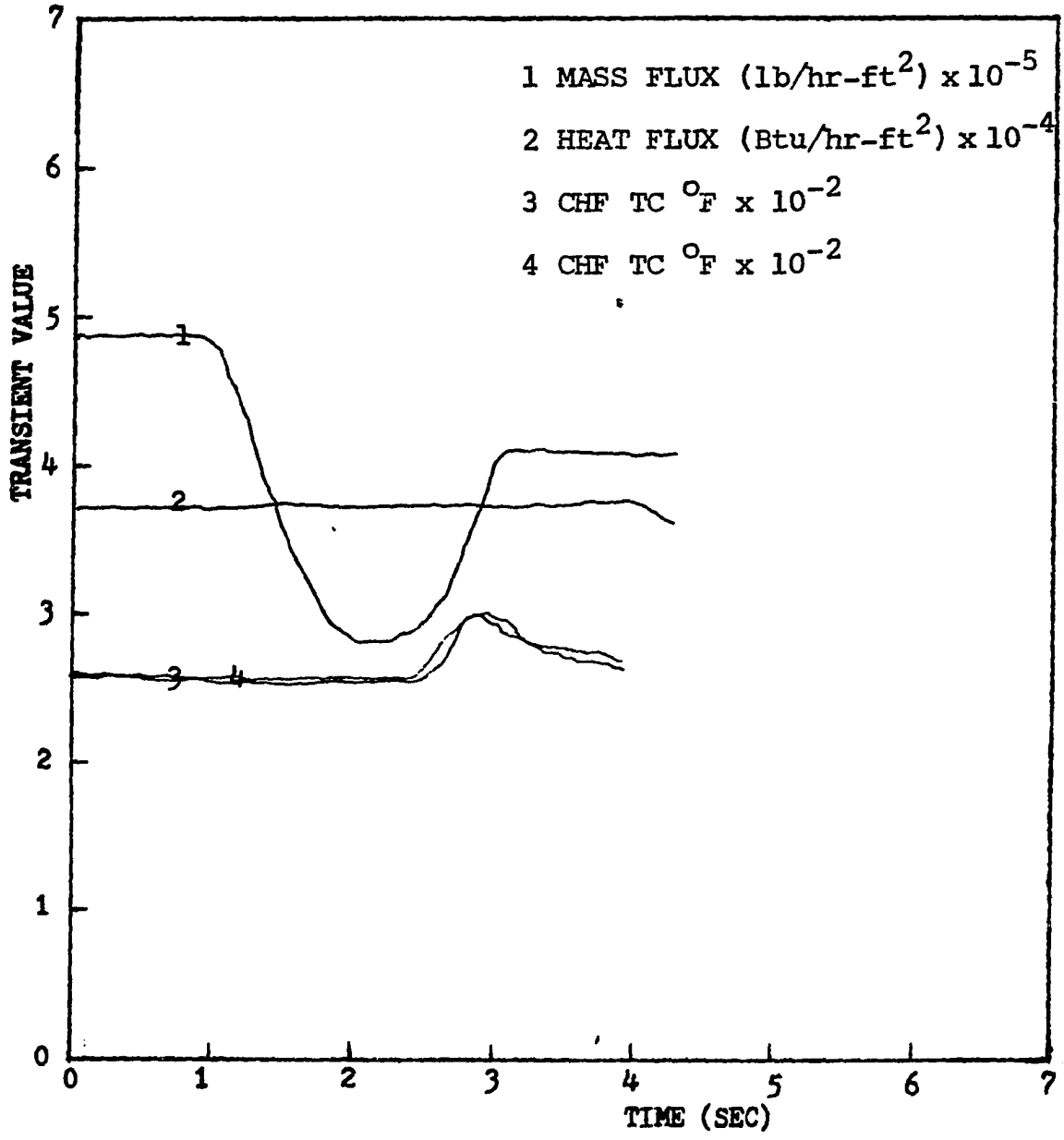

Figure 20. Flow transient run No. G3

Figure 21 through Figure 23 show three similar runs of flow ON/OFF/ON type. Figure 21 has "flow off" time about 1.7 sec and experiences CHF at 3.29 sec whereas a shorter "flow off" time is shown in Figure 22. No indication of the occurrence of CHF is shown. With a slight decrease in heat flux, no sign of CHF is shown in Figure 23 either. Loci of CHFRs in run G5 and G6 computed from MAYU-2 are shown in Figure 24. The results are consistent with model predictions.

The runs shown in Figures 25 through 31 are at the same system pressure. Figures 25 and 26 are two similar transients except flow decay patterns. CHF appears earlier in Figure 26. Figure 27 is almost identical to Figure 26 except that it is at a lower power level. Figure 28 is a run of flow decay associated with power decay. Figure 29 simulates power ramp up transient associated with flow decay. MAYU-2 calculations of the two equivalent runs of Figures 28 and 29 are shown in Figure 30. Figure 31 is the result of high heat flux and high minimum flow rate.

Two power ramp up runs are shown in Figures 32 and 33. Another two flow ON/OFF/ON type runs are shown in Figures 34 and 35. With shorter "flow off" time no sign of CHF is shown in Figure 35, though MAYU-2 indicates the onset of CHF at 1.12 sec.

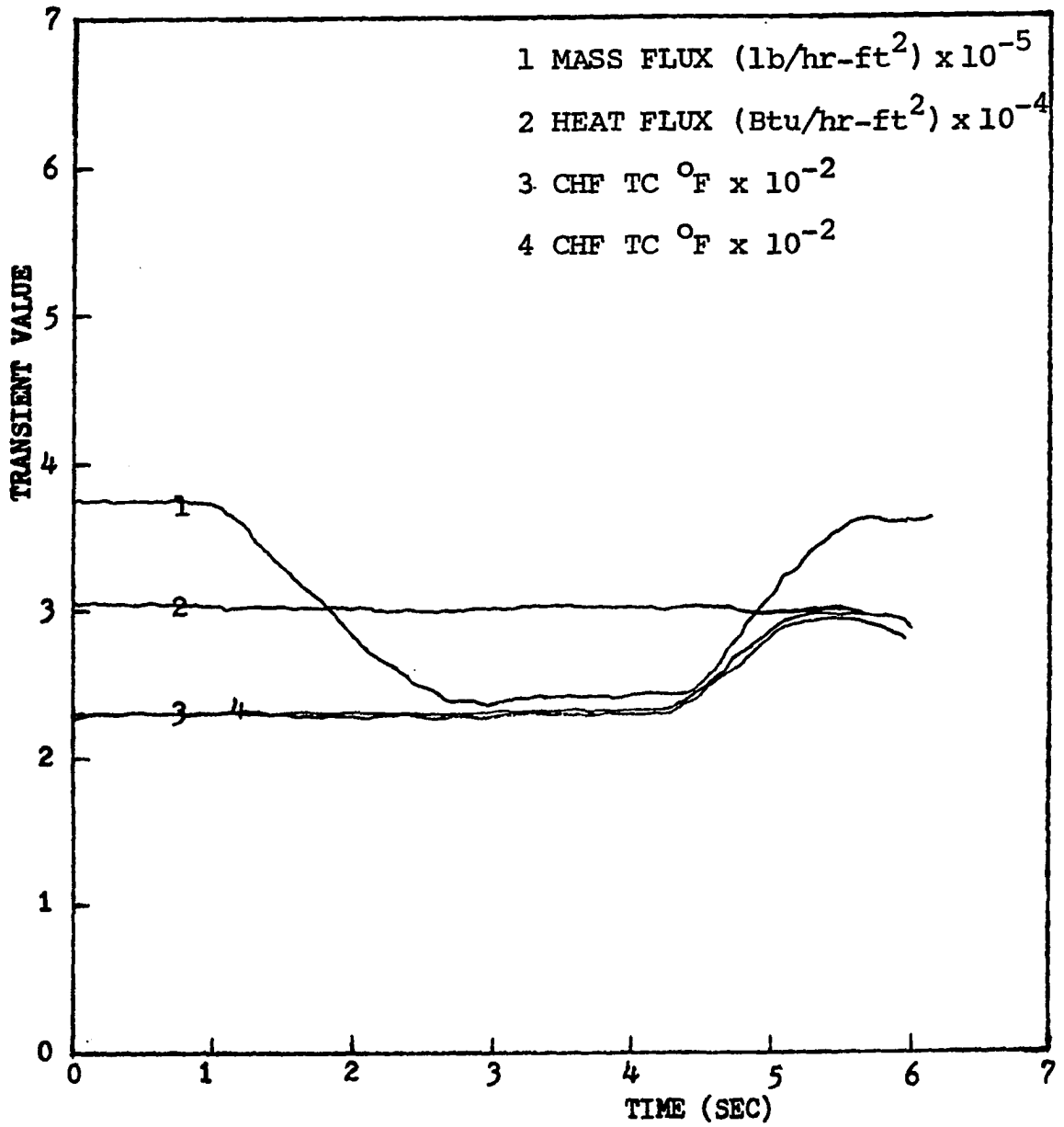

Figure 21. Flow transient run No. G4

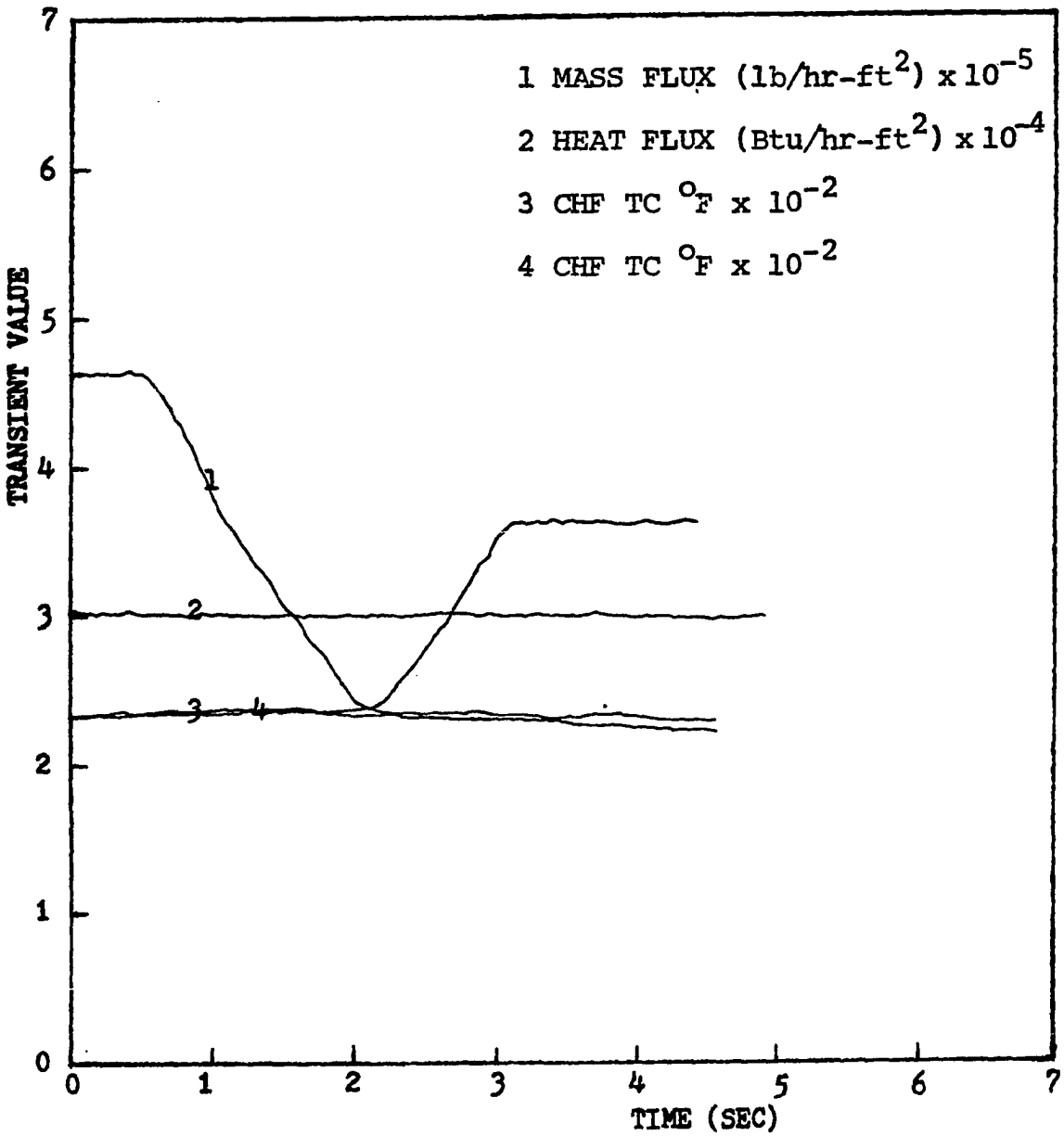

Figure 22. Flow transient run No. G5

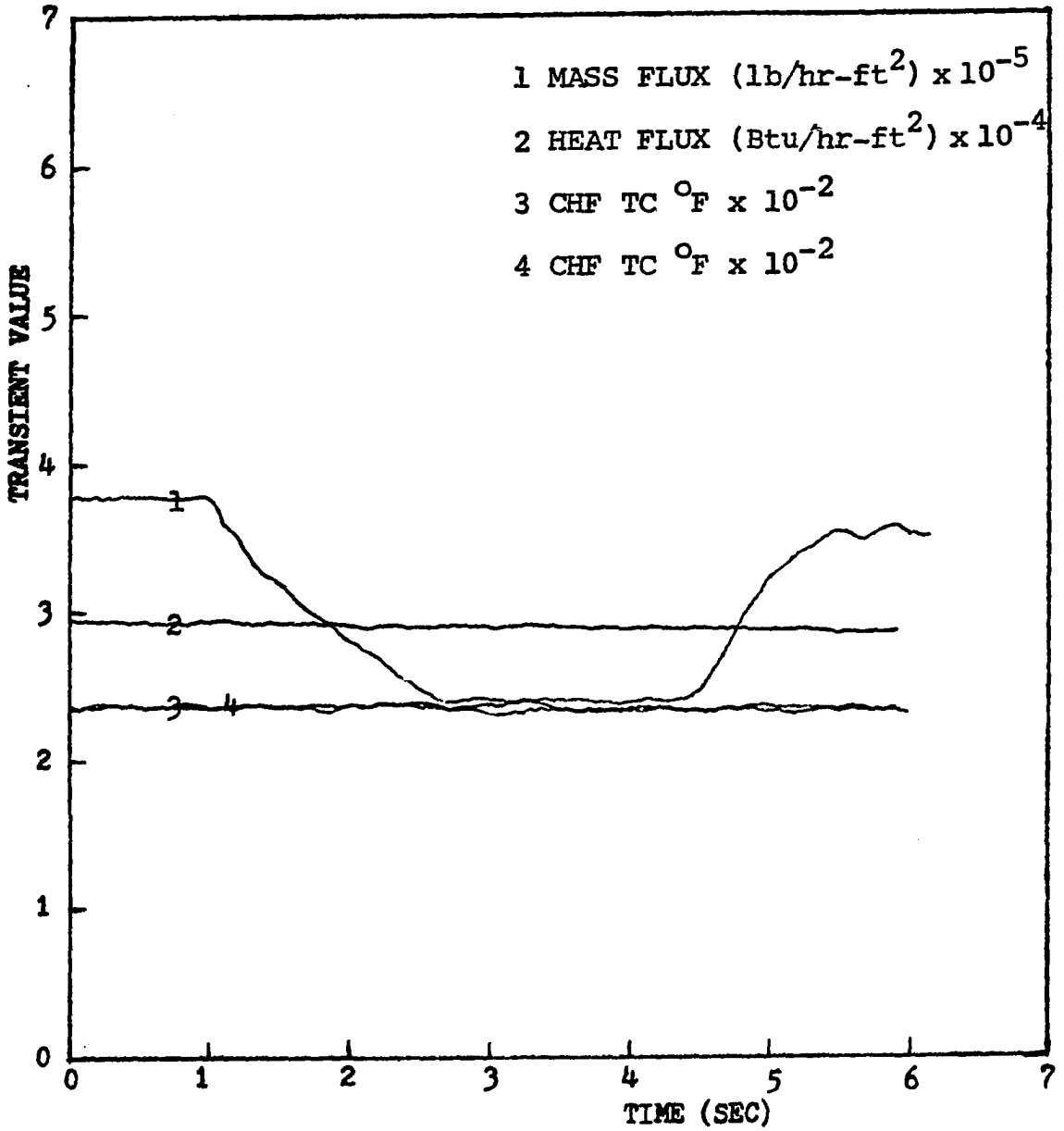

Figure 23. Flow transient run No. G6

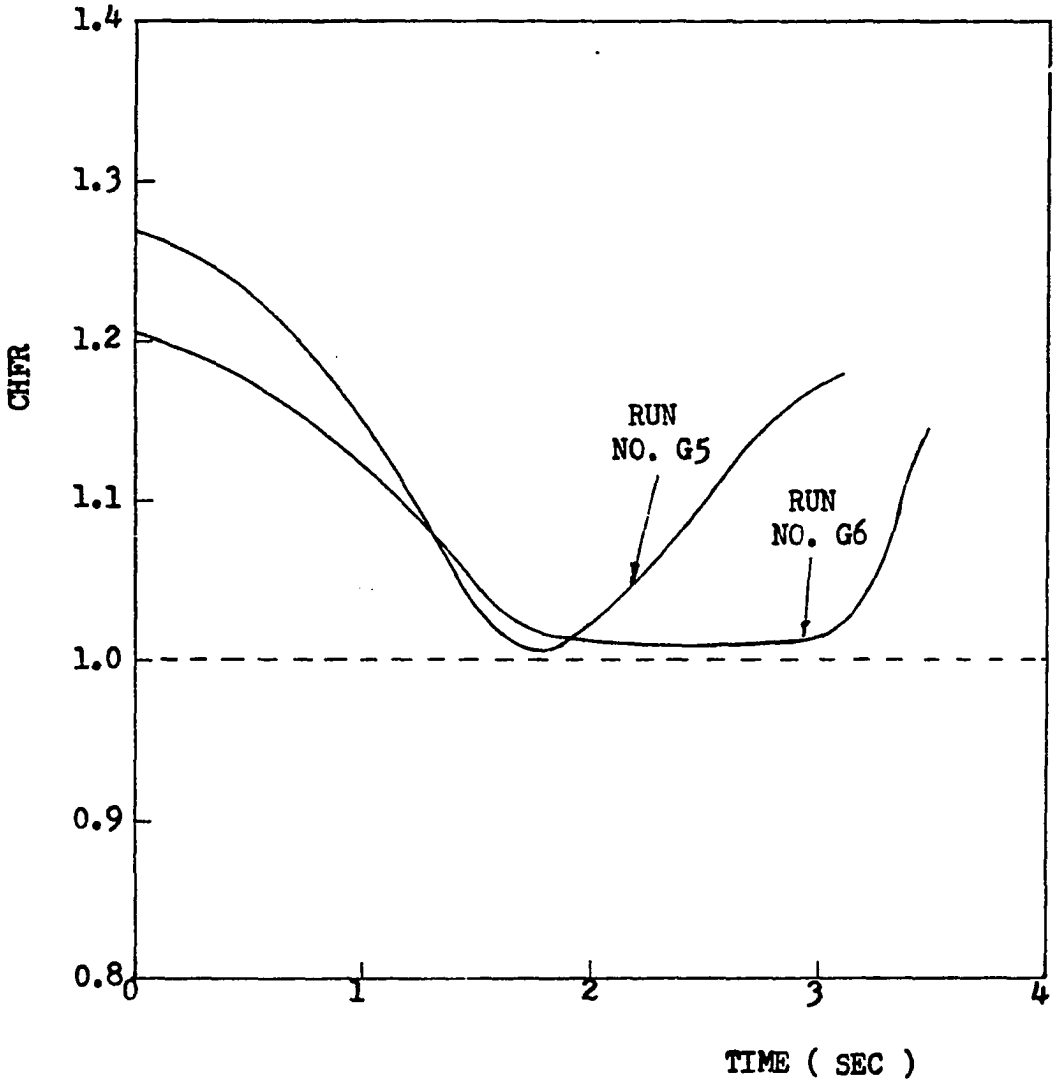

Figure 24. Variations of CHFRs after transient for the equivalent runs No. G5 and G6 by MAYU-2 prediction

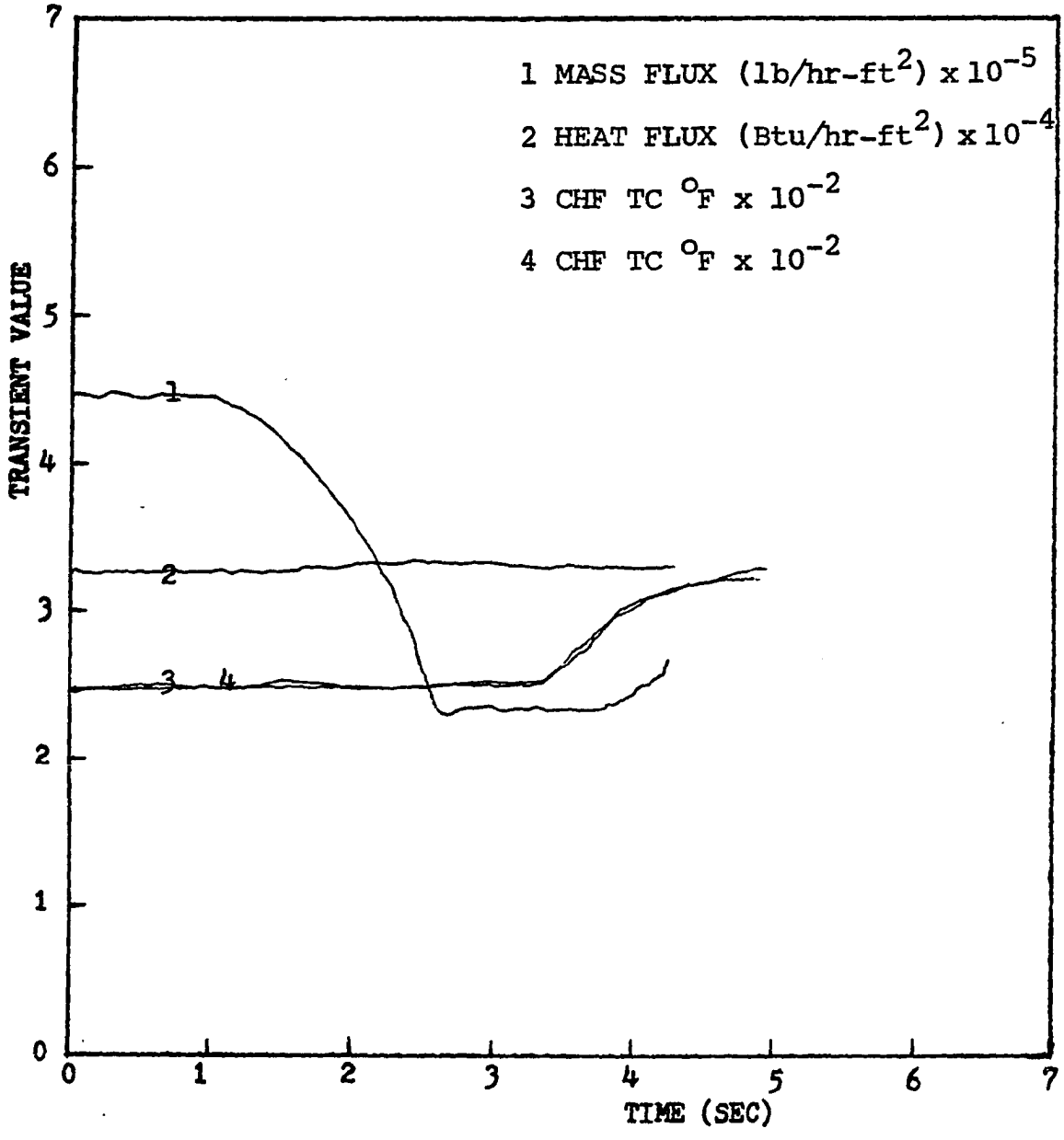

Figure 25. Flow transient run No. G7

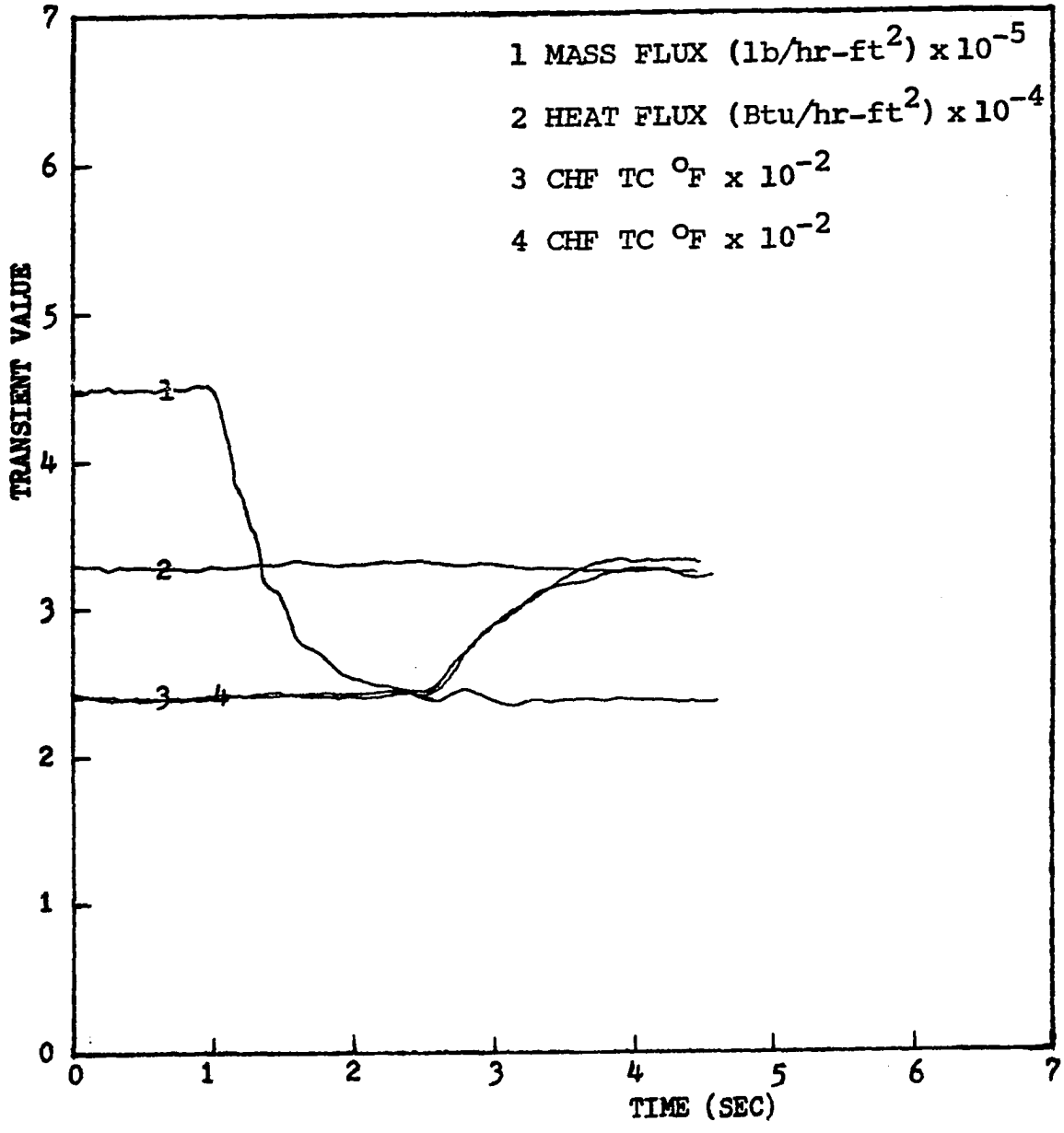

Figure 26. Flow transient run No. G8

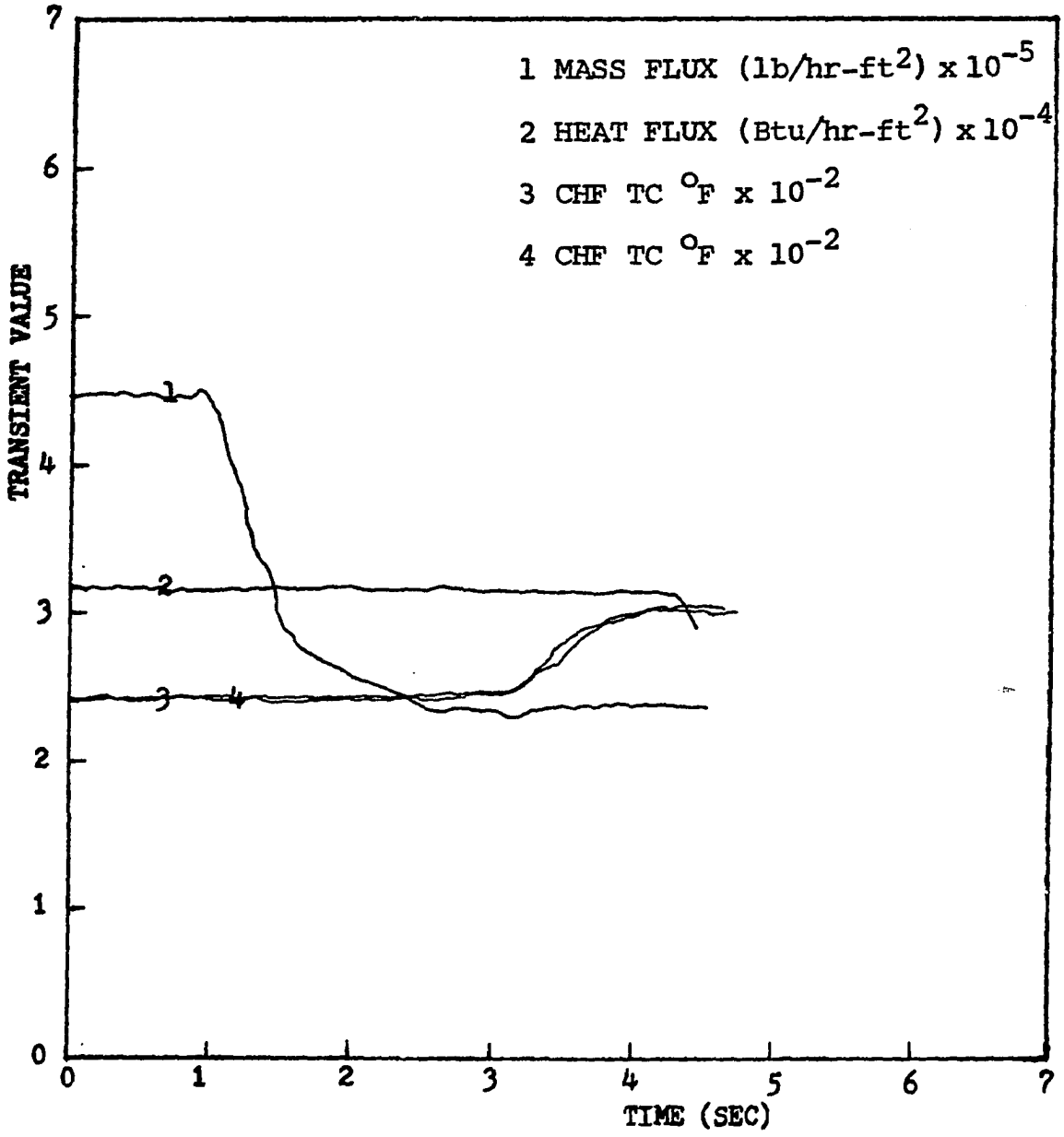

Figure 27. Flow transient run No. G9

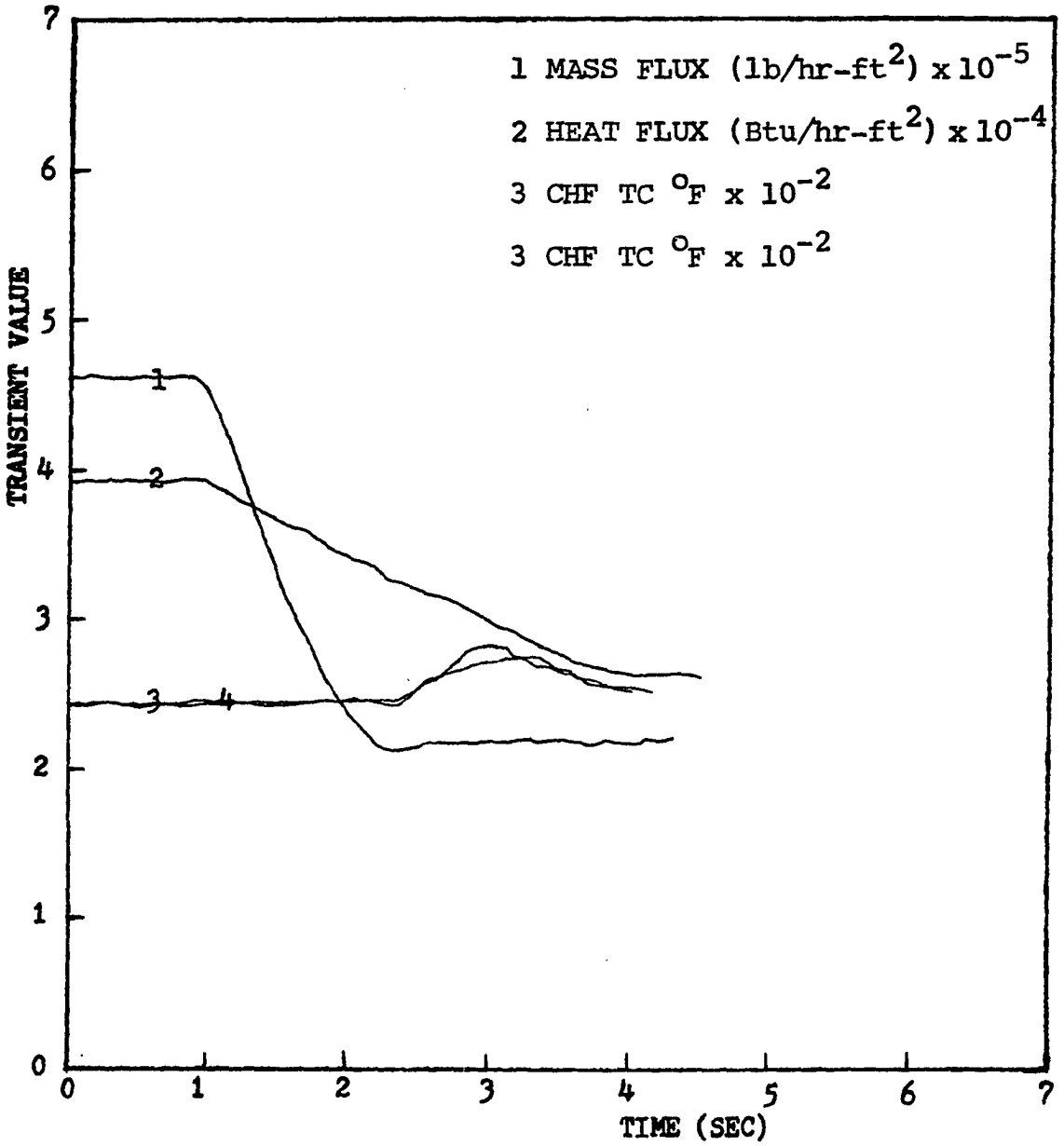

Figure 28. Flow transient run No. G10

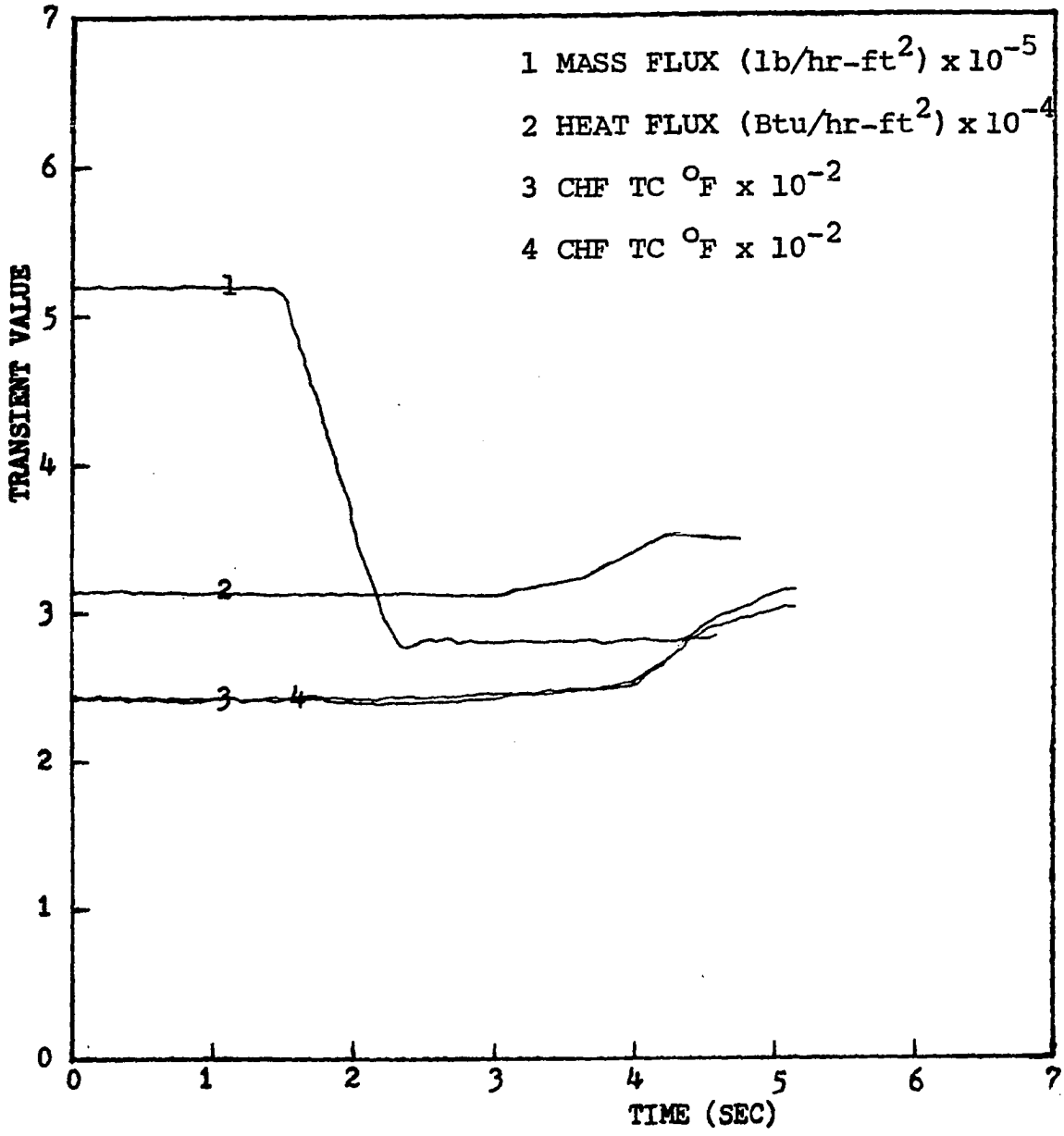

Figure 29. Flow transient run No. G11

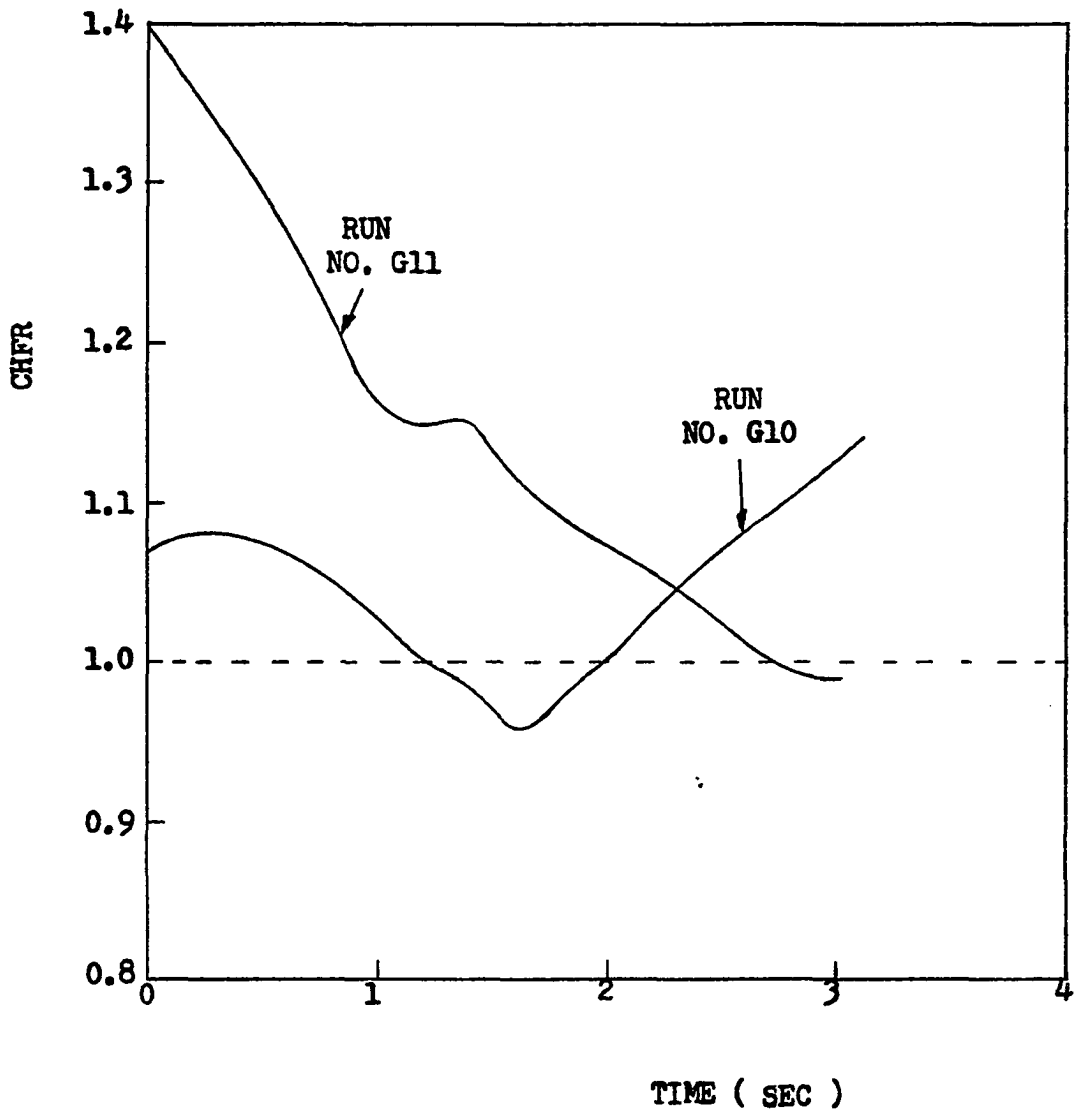

Figure 30. Variation of CHFRs after transient for the equivalent runs No. G10 and G11 by MAYU-2 prediction

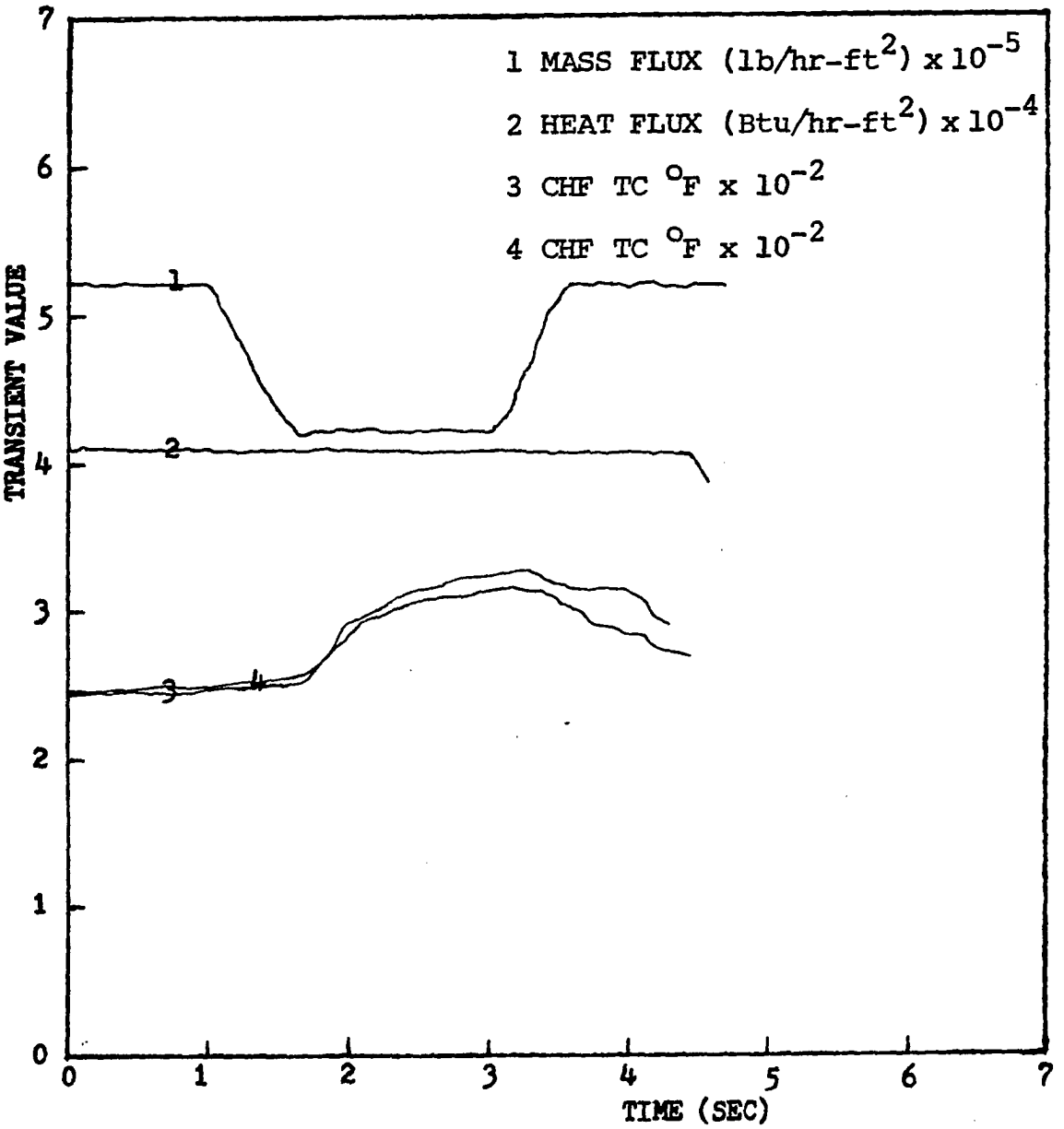

Figure 31. Flow transient run No. G12

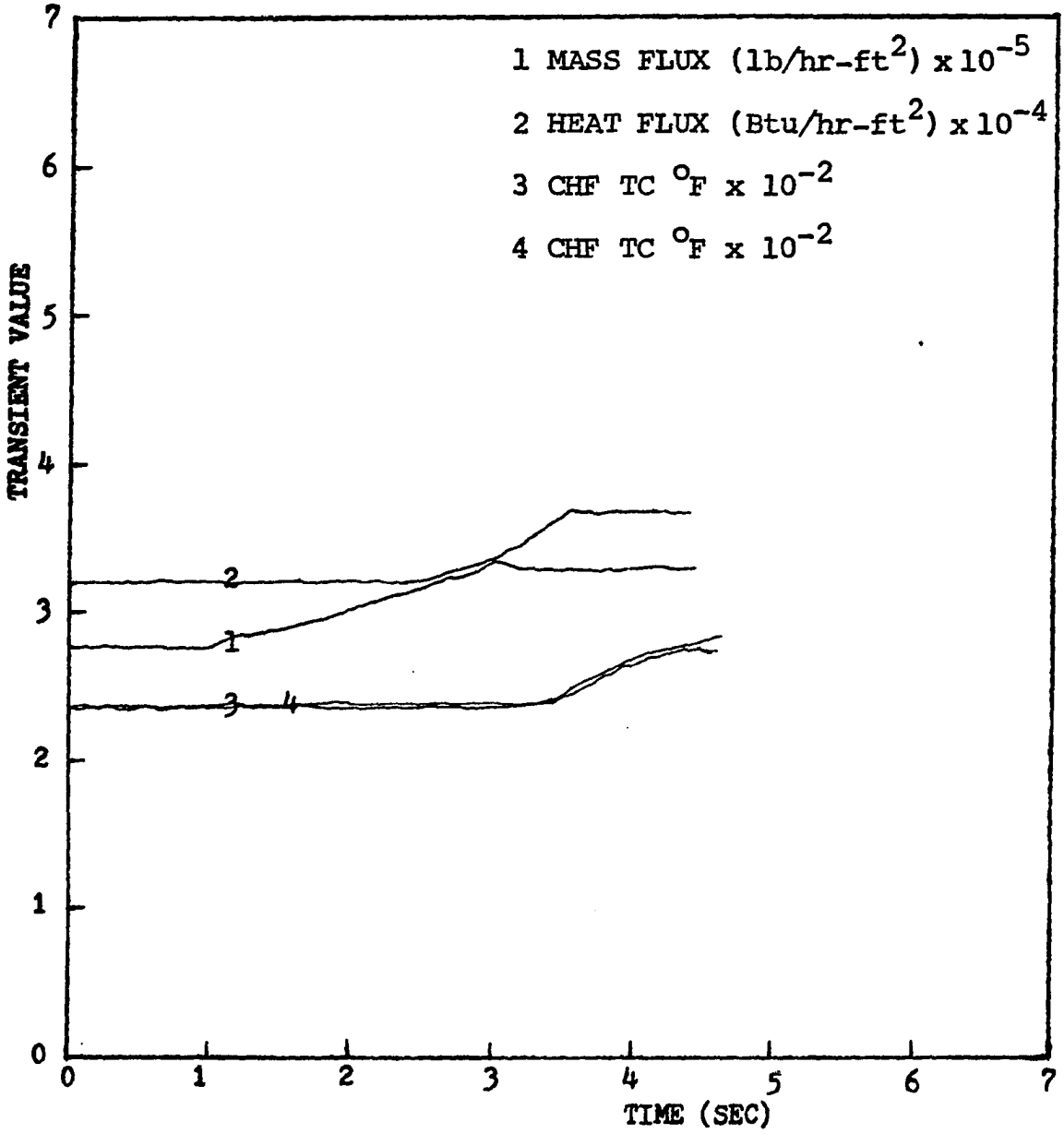

Figure 32. Flow transient run No. G13

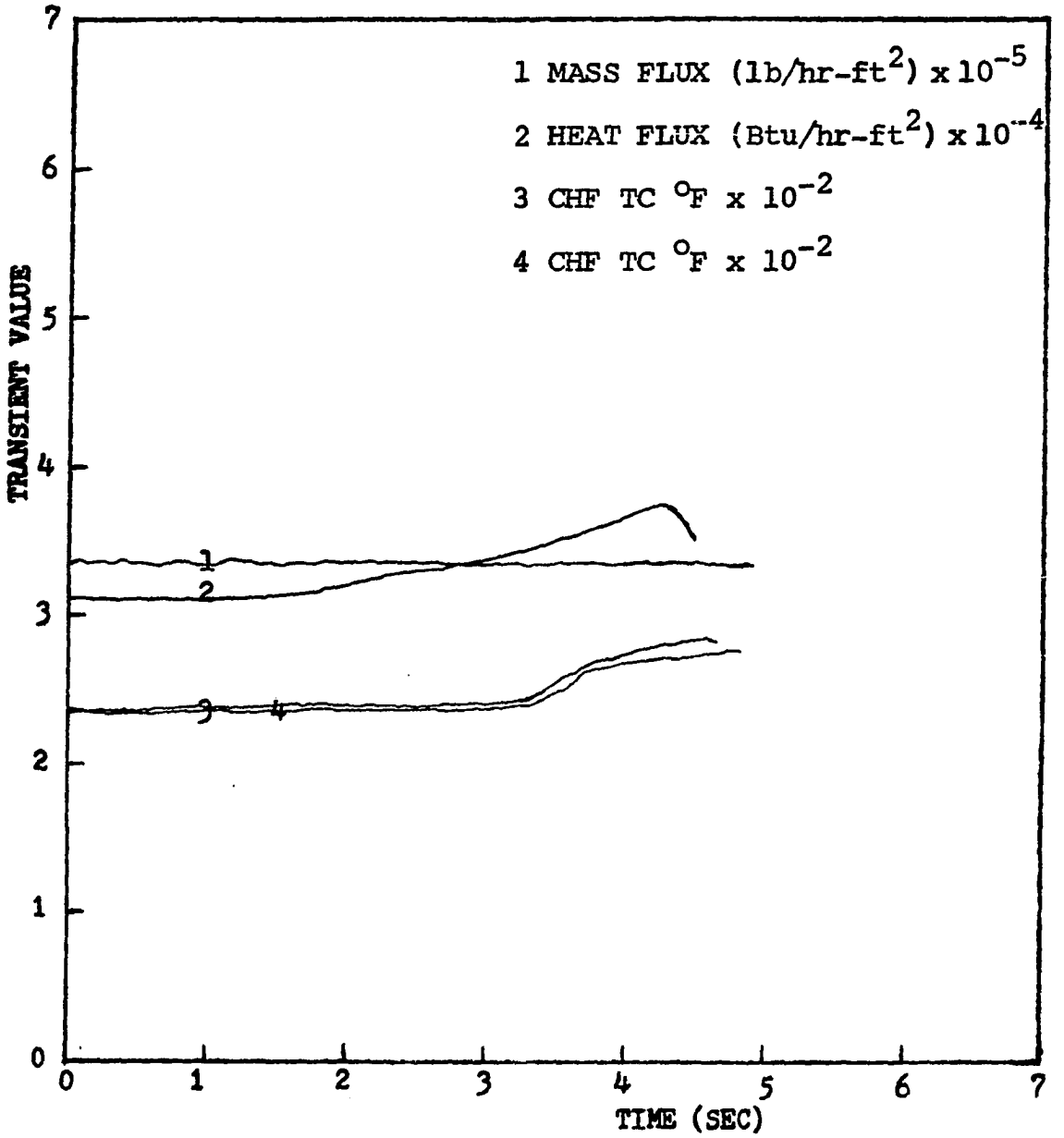

Figure 33. Flow transient run No. G14

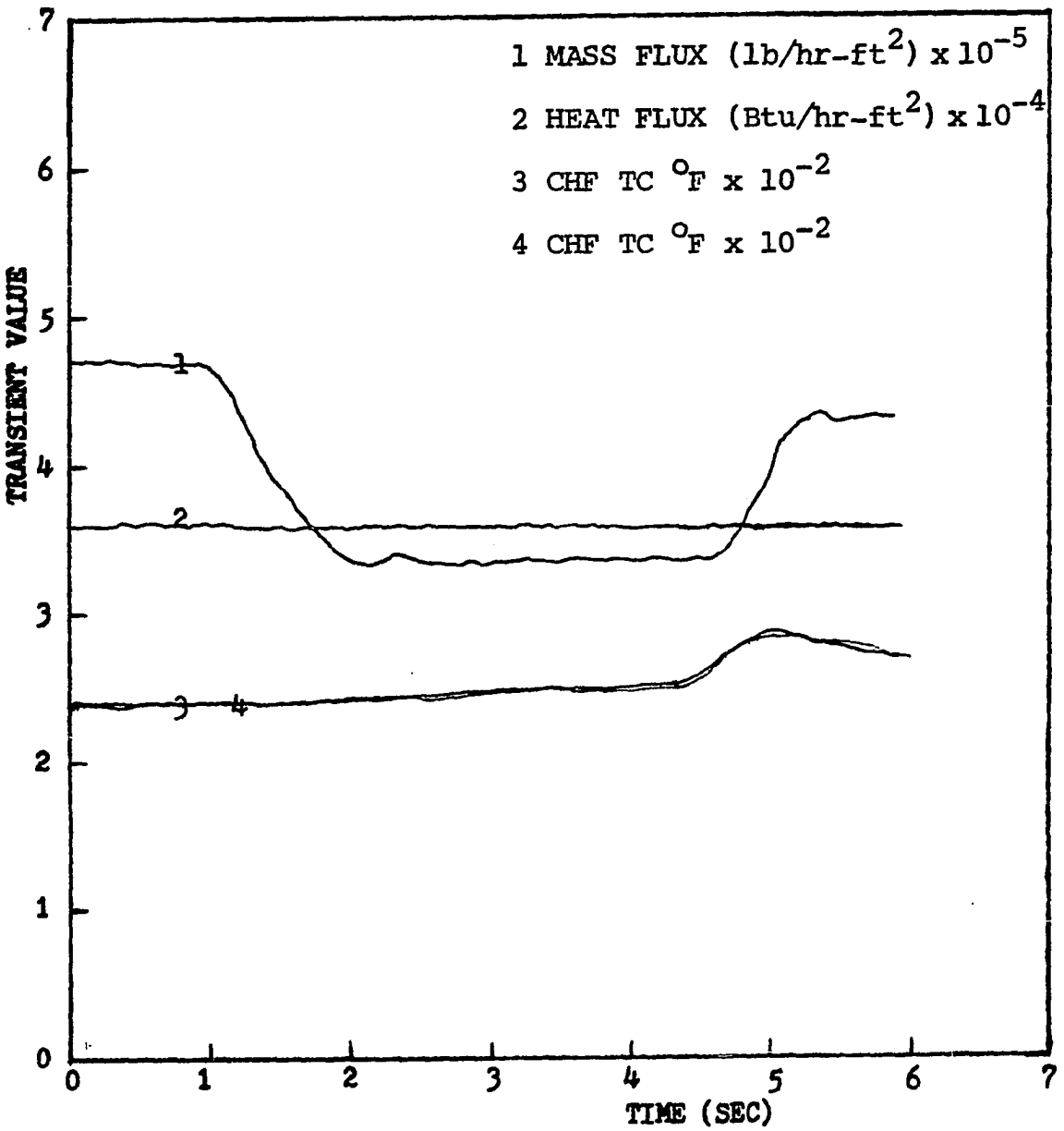

Figure 34. Flow transient run No. G15

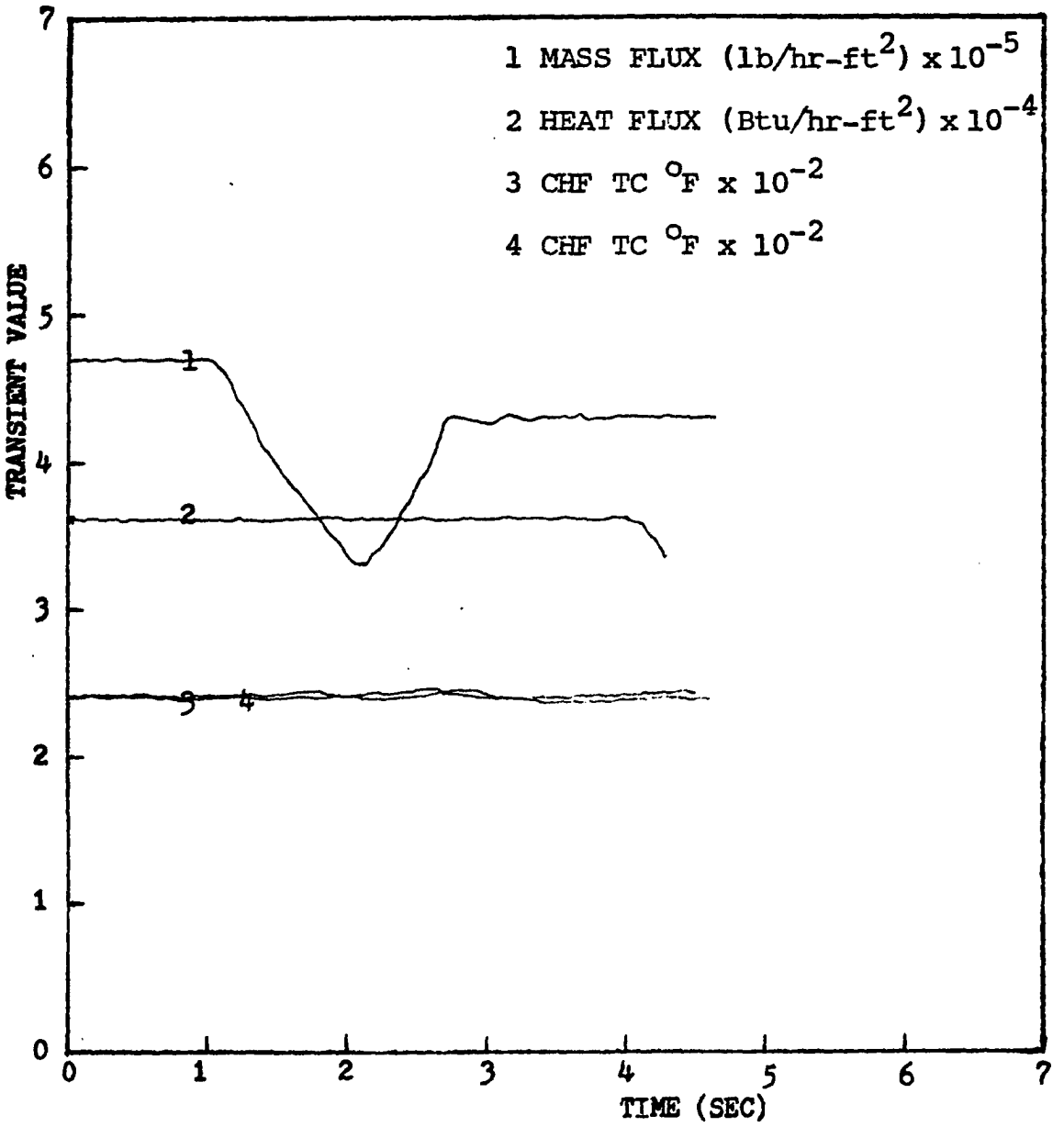

Figure 35. Flow transient run No. G16

2. Depressurization transient

In this type of transient the system pressures decayed at different rates in the range from 163 psia to 129 psia equivalent to the pressure range from 1000 psia to 800 psia in water system. Test conditions are tabulated in Table 5 and the results are shown in Figures 36 through 47. Similar trends to that observed in water system presented in reference 28 were also observed.

In Figure 36 pressure reduced from 162 psia to 146 psia within 1.8 sec and CHF occurs during depressurizing. Faster depressurization takes place in Figure 37 and it experiences earlier CHF. The sign of CHF does not appear in Figure 38 until further reduction in pressure at about 2 sec after the transient. A similar case is shown in Figure 39. Figure 40 shows a case of slow depressurization and unstable flow rate.

Figures 41 and 42 show similar runs except for pressure decay rates. Figure 43 has the same depressurization range but lower heat flux.

Figures 44, 45 and 46 are three runs with pressure and power decays associated with flow coastdown. For run P11 in Figure 46, MAYU-2 indicates an early CHF appeared at 2.47 sec after transient and reappeared at 3.40 sec. In the test result, however, only the latter CHF has occurred. Results from MAYU-2 of the three equivalent runs are shown in Figure 47.

The error distribution in predicting onset times of CHF is shown in Figure 48. Most of the data points are within $\pm$ 10% of those predicted by MAYU-2. Predictions in flow transient runs is better than that in depressurization transient runs, since in the former cases $\pi_5(t)$ was matched in both systems while in the latter cases it was not. If $\pi_{5m}(t)$ can be adjusted to match $\pi_{5p}(t)$ during depressurization transient by installing a device which can control the flow inlet temperature the results of depressurization tests may be improved.

Table 5. List of depressurization runs

Run No.	Initial Conditions P psia	ΔH Btu/lb	G x 10^{-6} lb/hr-ft^2	ø x 10^{-4} Btu/hr-ft^2	χ %
P1	162	7.15	0.309	3.282	30.79
P2	163	7.16	0.306	3.410	32.88
P3	162	7.16	0.292	3.538	36.80
P4	154	5.92	0.327	3.600	34.05
P5	162	7.14	0.317	3.486	32.32
P6	145	4.75	0.389	3.725	29.91
P7	145	4.75	0.409	3.720	28.02
P8	146	4.76	0.360	3.593	31.49
P9	153	5.94	0.440	4.130	27.56
P10	153	5.92	0.488	4.321	25.46
P11[a]	154	5.96	0.468	4.372	27.33

[a]MAYU-2 indicates an early CHF at 2.47 sec after transient and reoccurs at 3.40 sec.

P_{min} psia	Time to P_{min} sec	Onset Time of CHF	
		Measured Time sec	MAYU-2 Predicted Time, sec
146	1.61	1.66	1.47
130	1.25	1.27	1.17
153	0.22	3.28	3.24
135	0.83	3.94	3.62
132	3.10	2.73	2.62
129	1.11	1.03	0.84
130	1.62	1.02	1.10
128	1.65	1.78	1.96
127	3.42	4.25	4.00
132	3.96	3.63	3.80
131	3.03	3.56	3.40

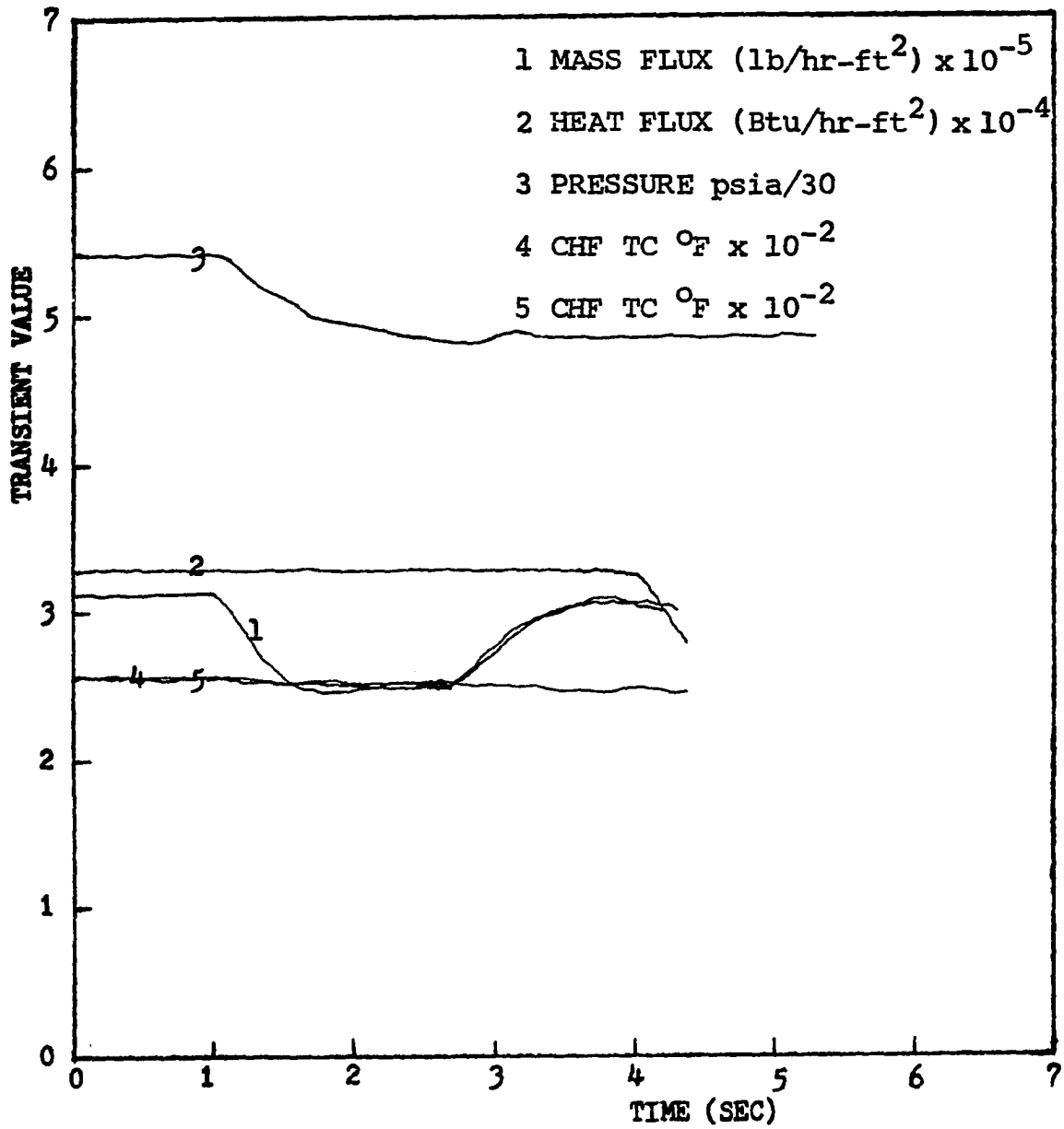

Figure 36. Depressurization transient run No. P1

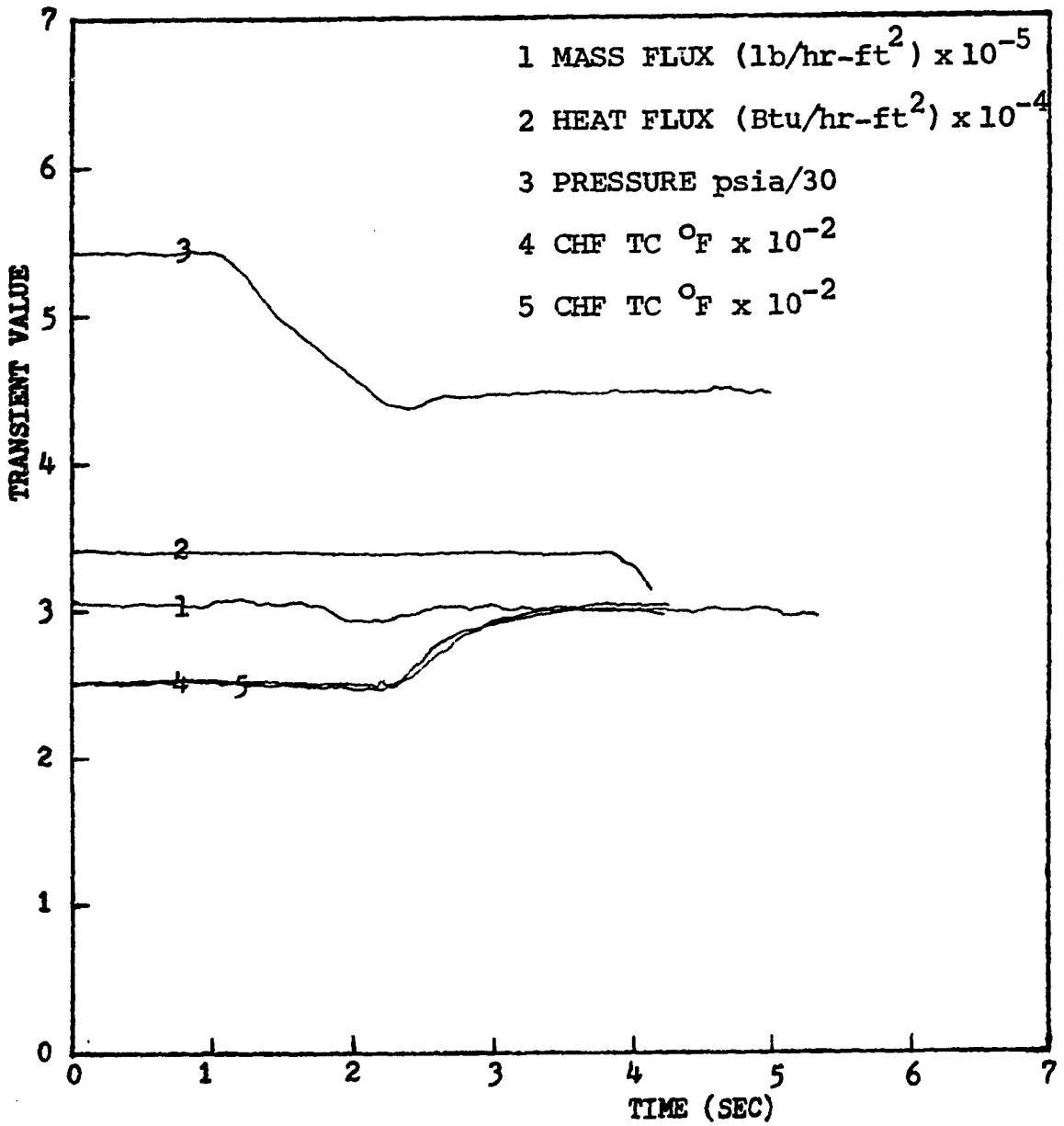

Figure 37. Depressurization transient run No. P2

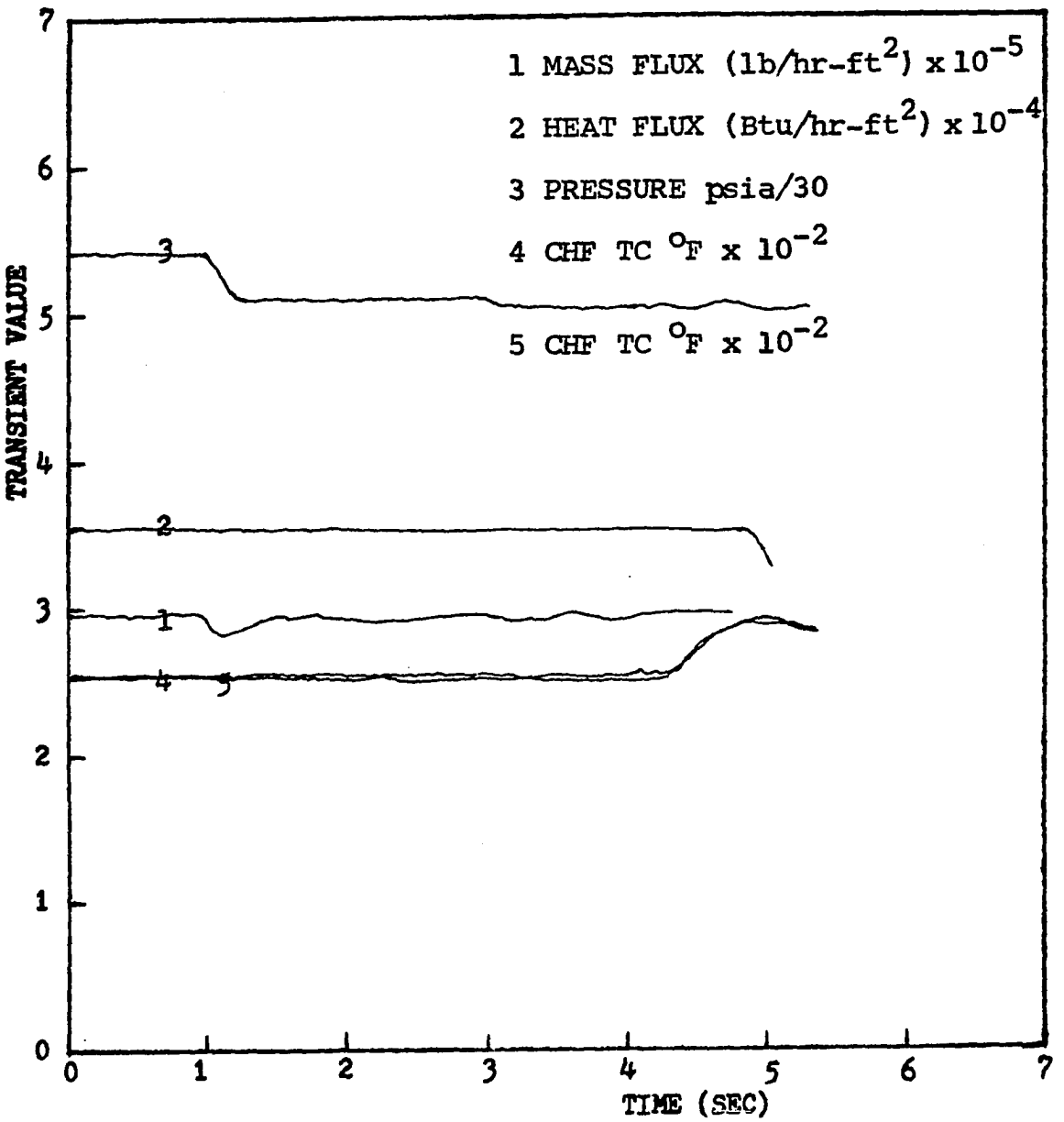

Figure 38. Depressurization transient run No. P3

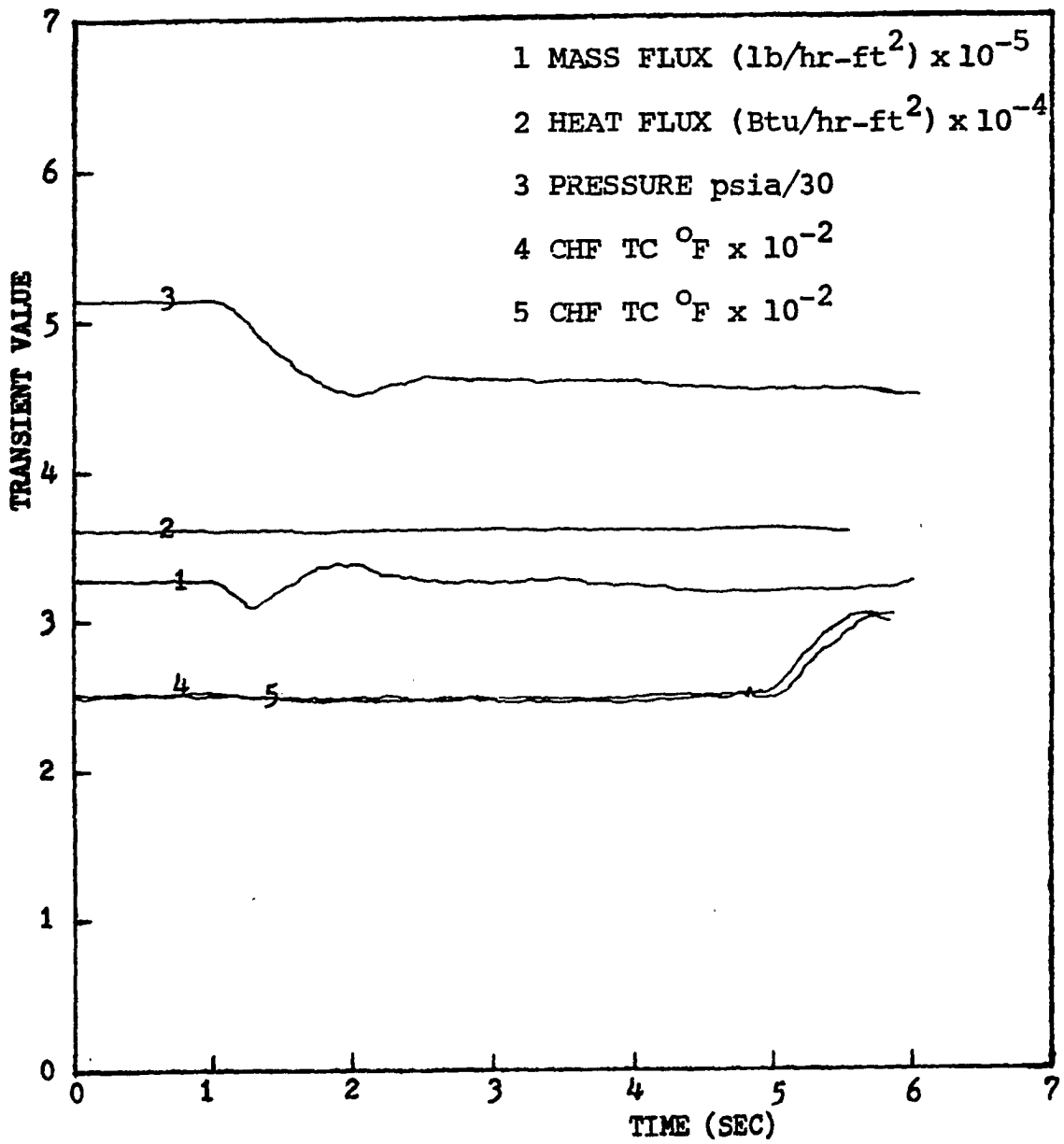

Figure 39. Depressurization transient run No. P4

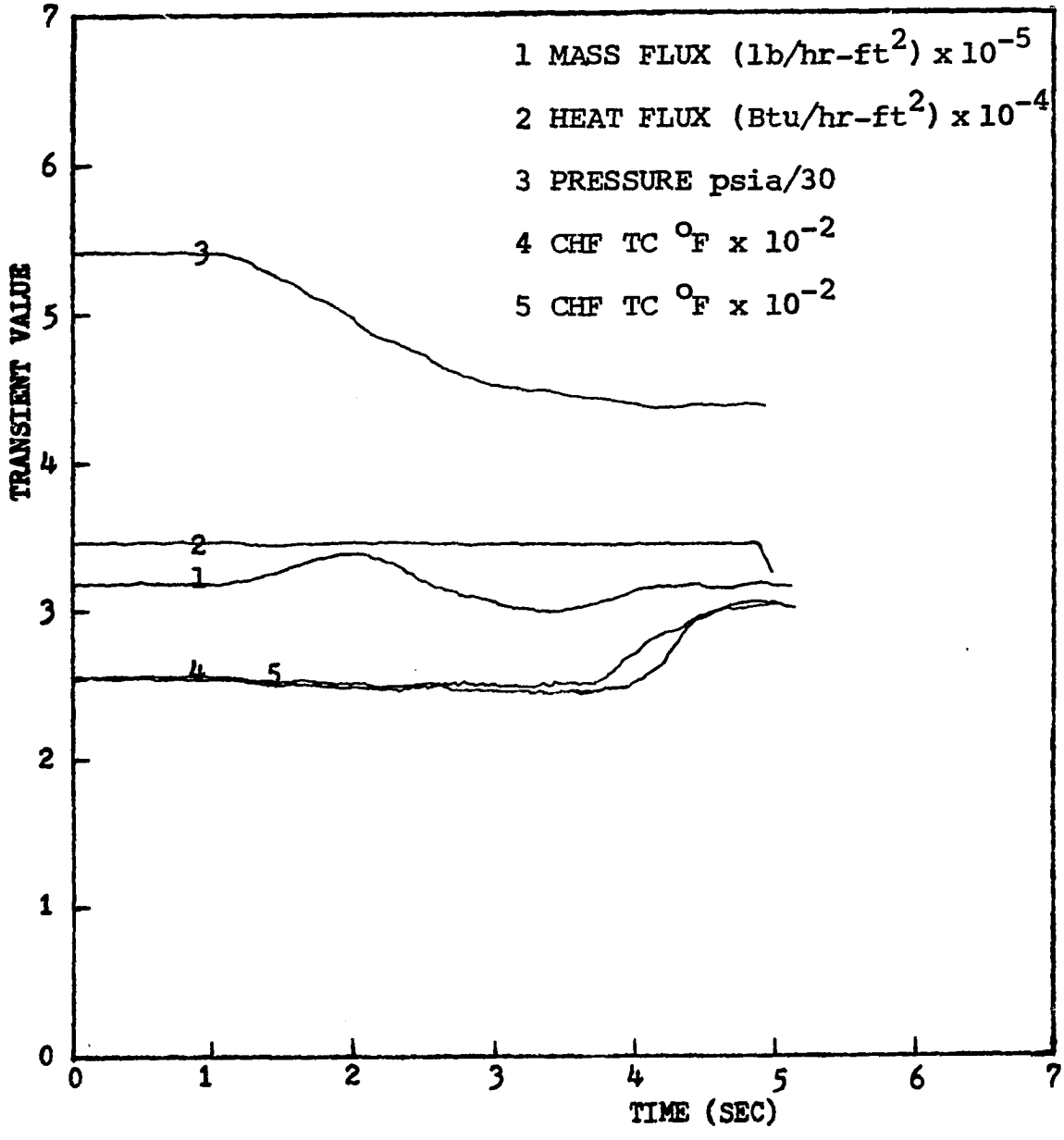

Figure 40. Depressurization transient run No. P5

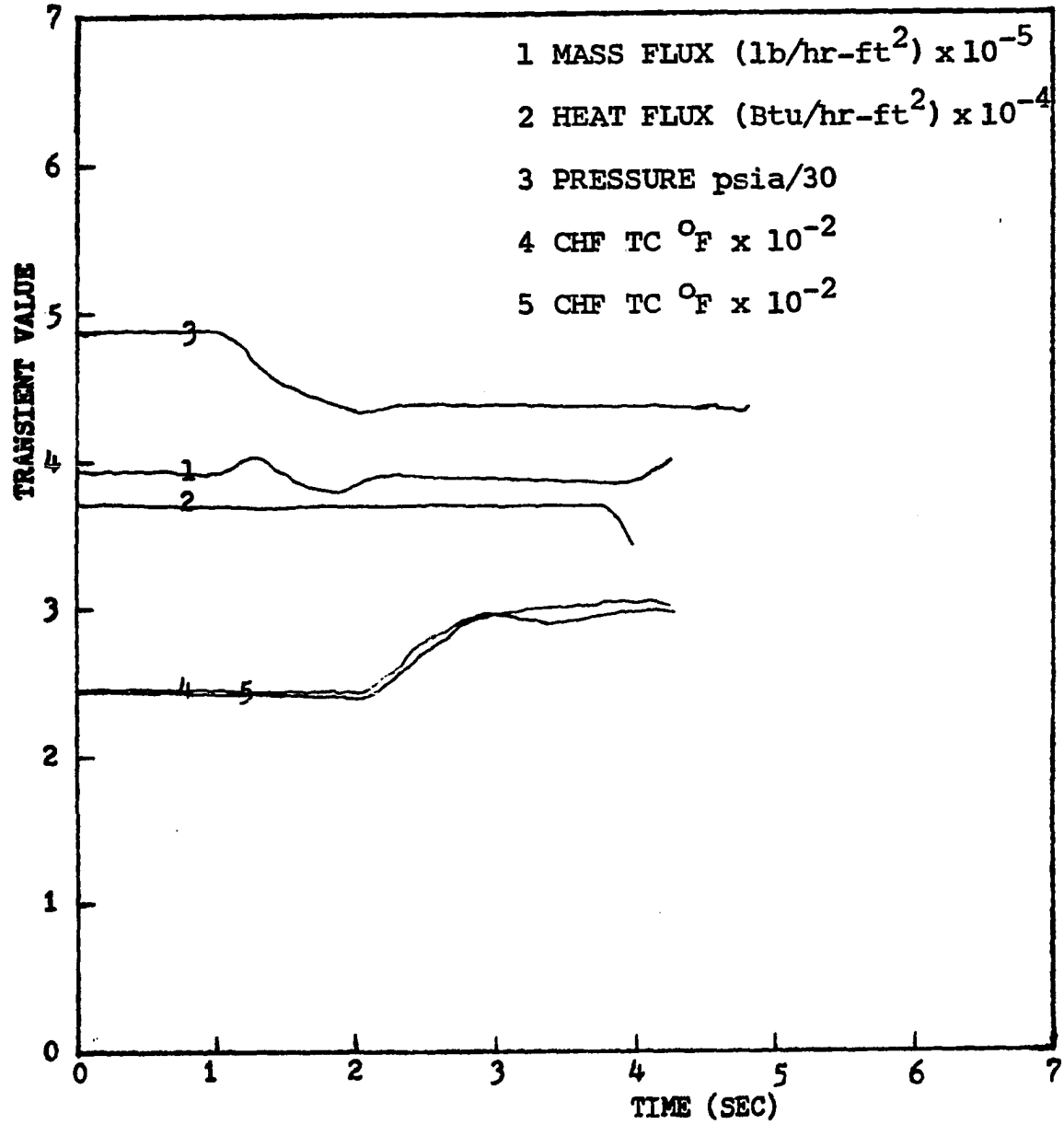

Figure 41. Depressurization transient run No. P6

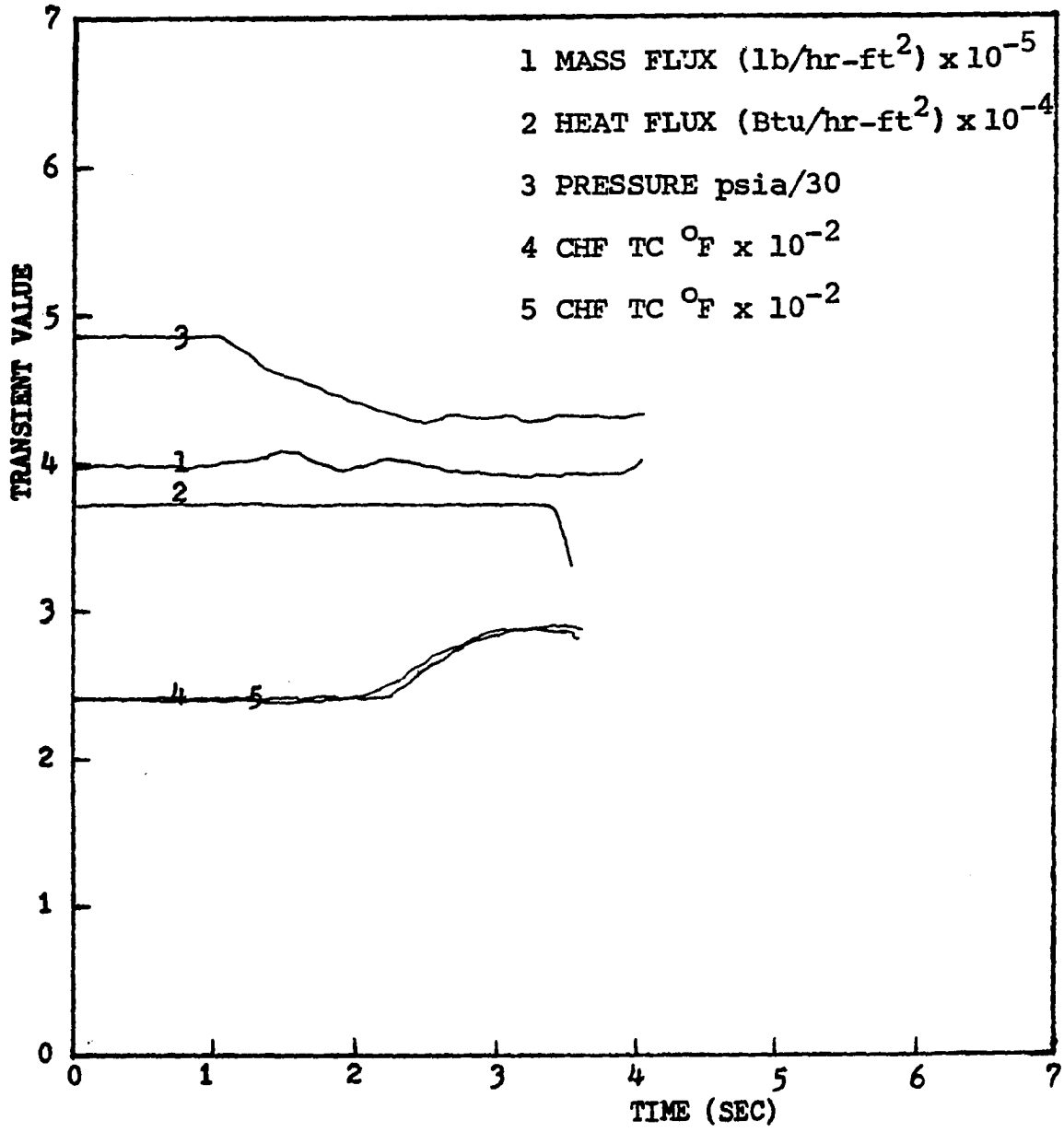

Figure 42. Depressurization transient run No. P7

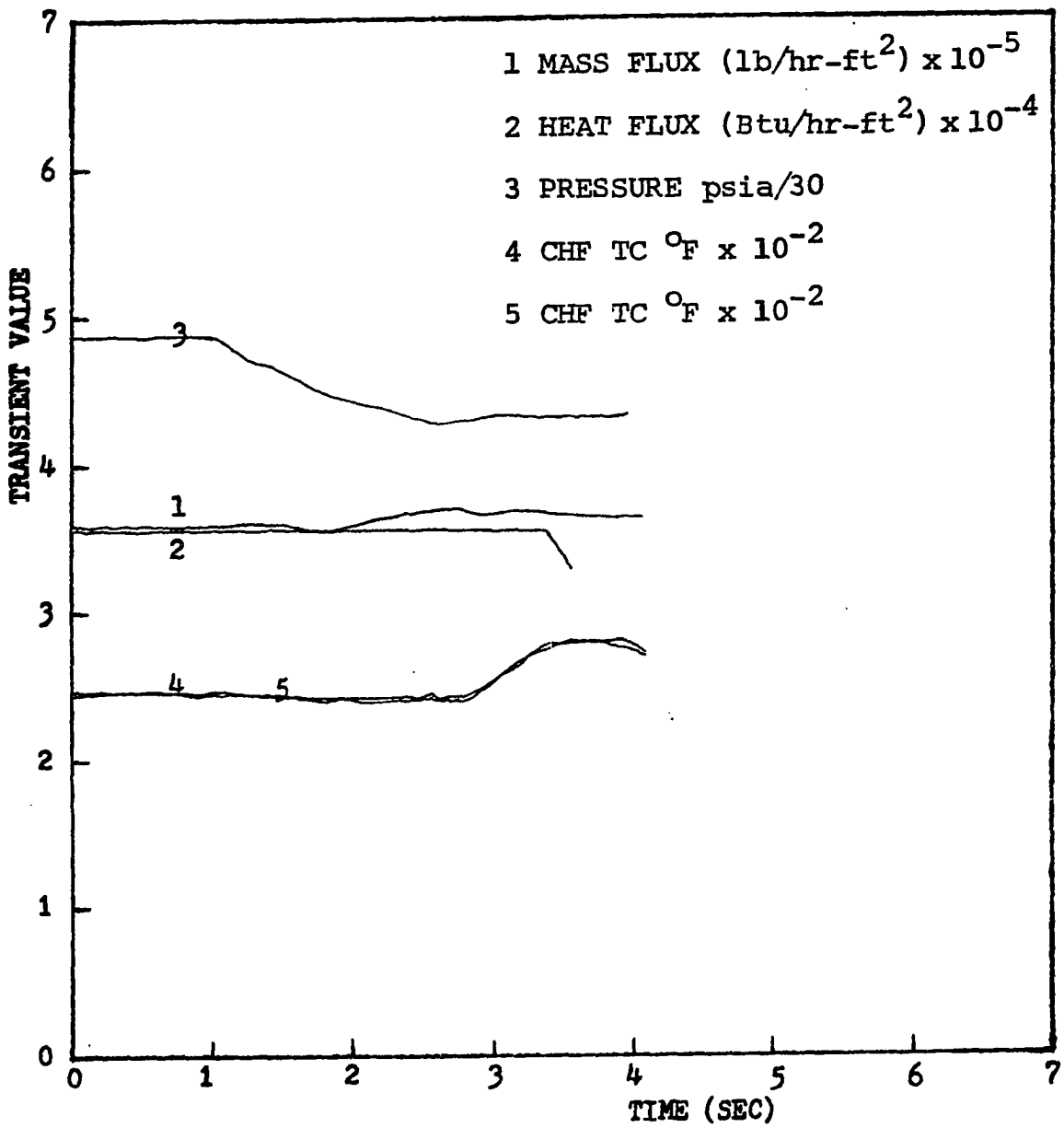

Figure 43. Depressurization transient run No. P8

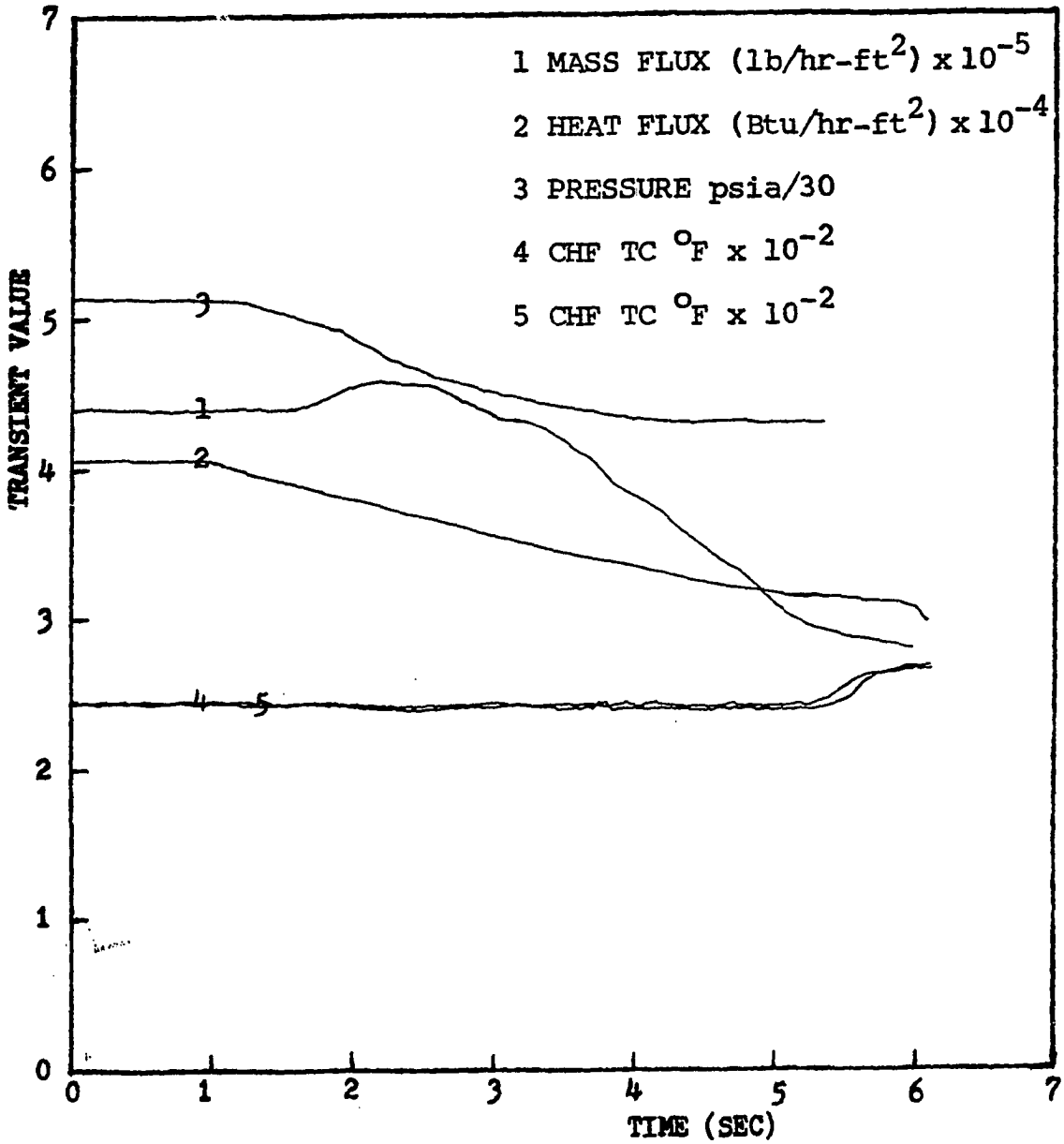

Figure 44. Depressurization transient run No. P9

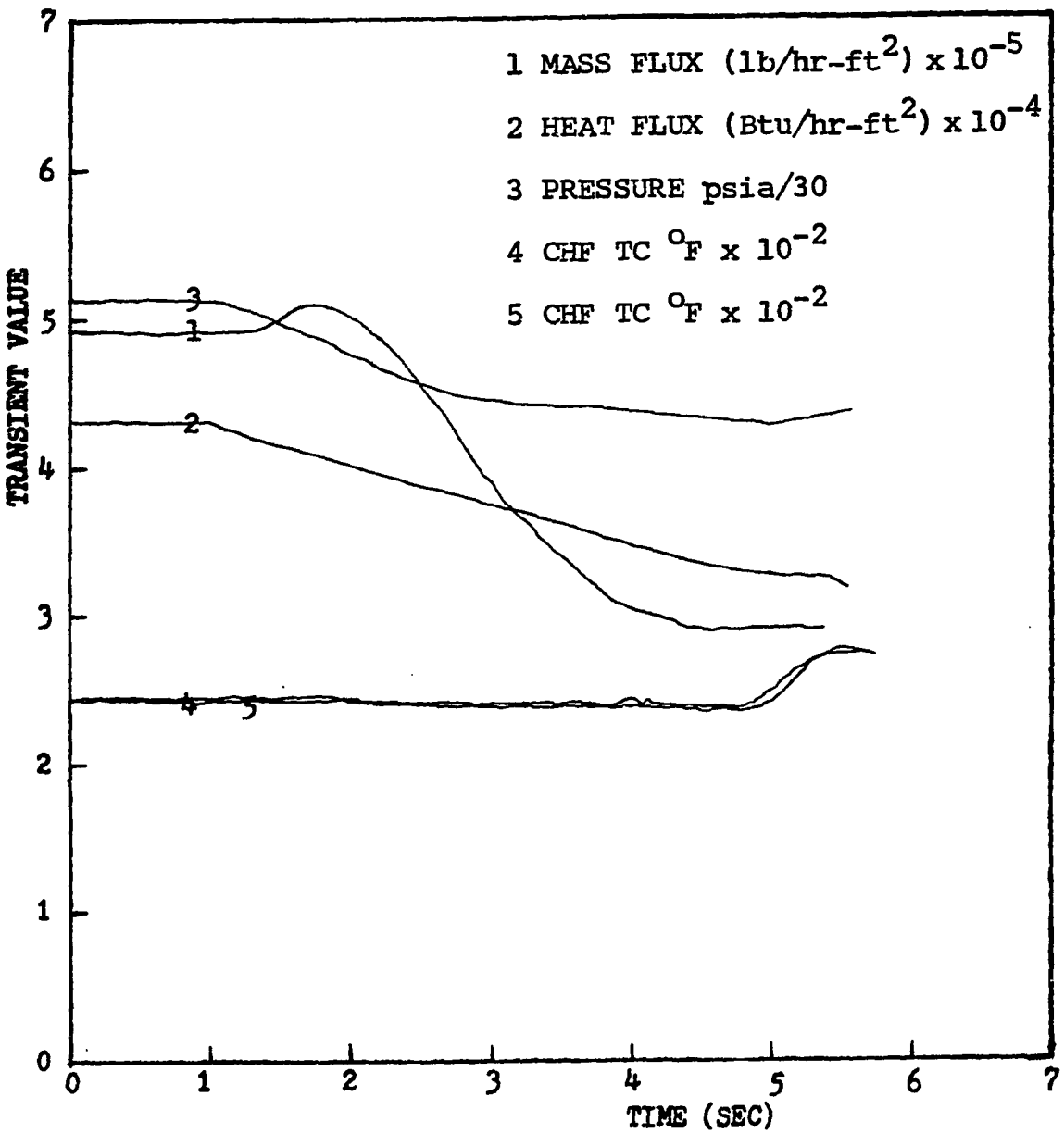

Figure 45. Depressurization transient run No. P10

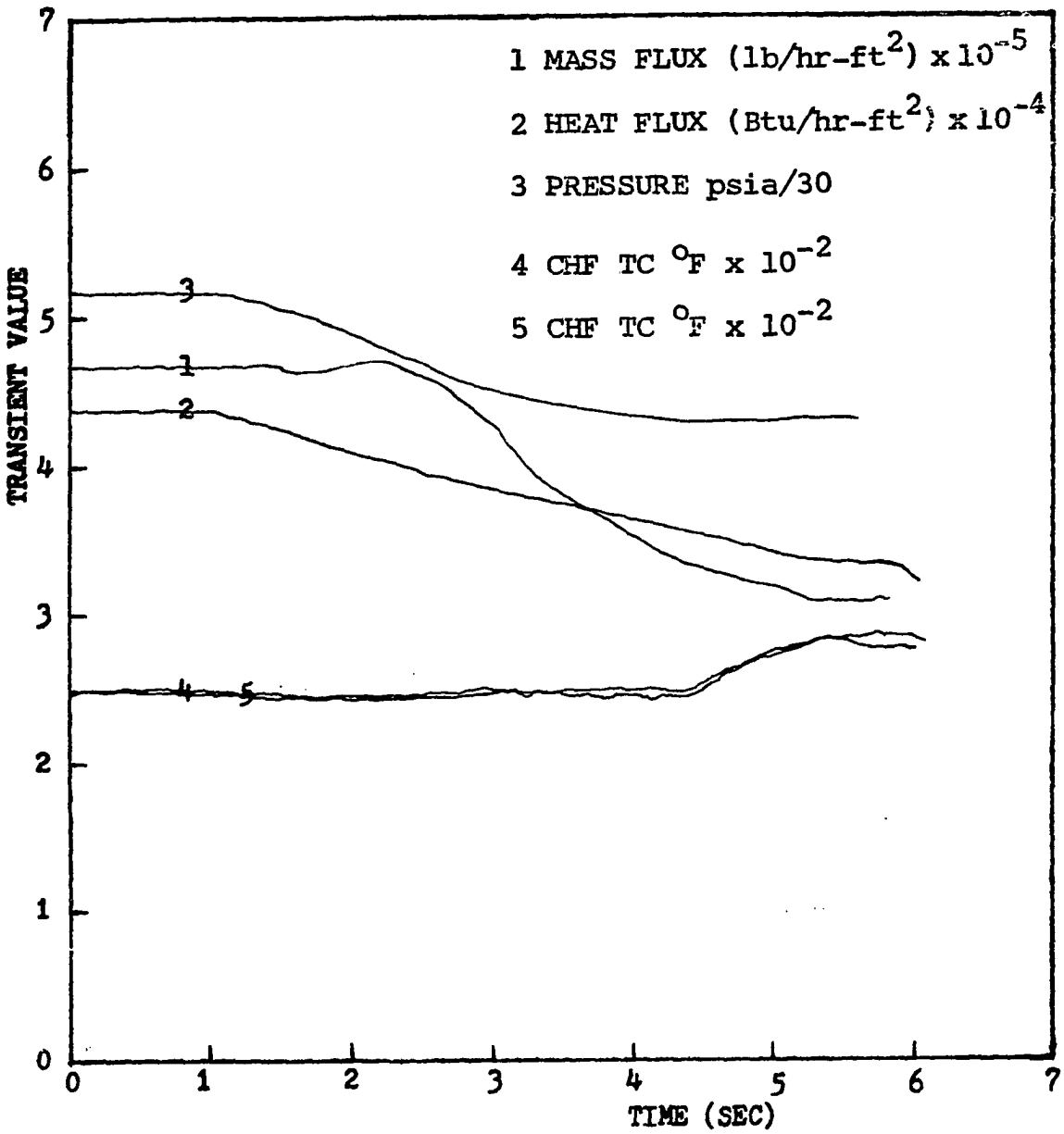

Figure 46. Depressurization transient run No. P11

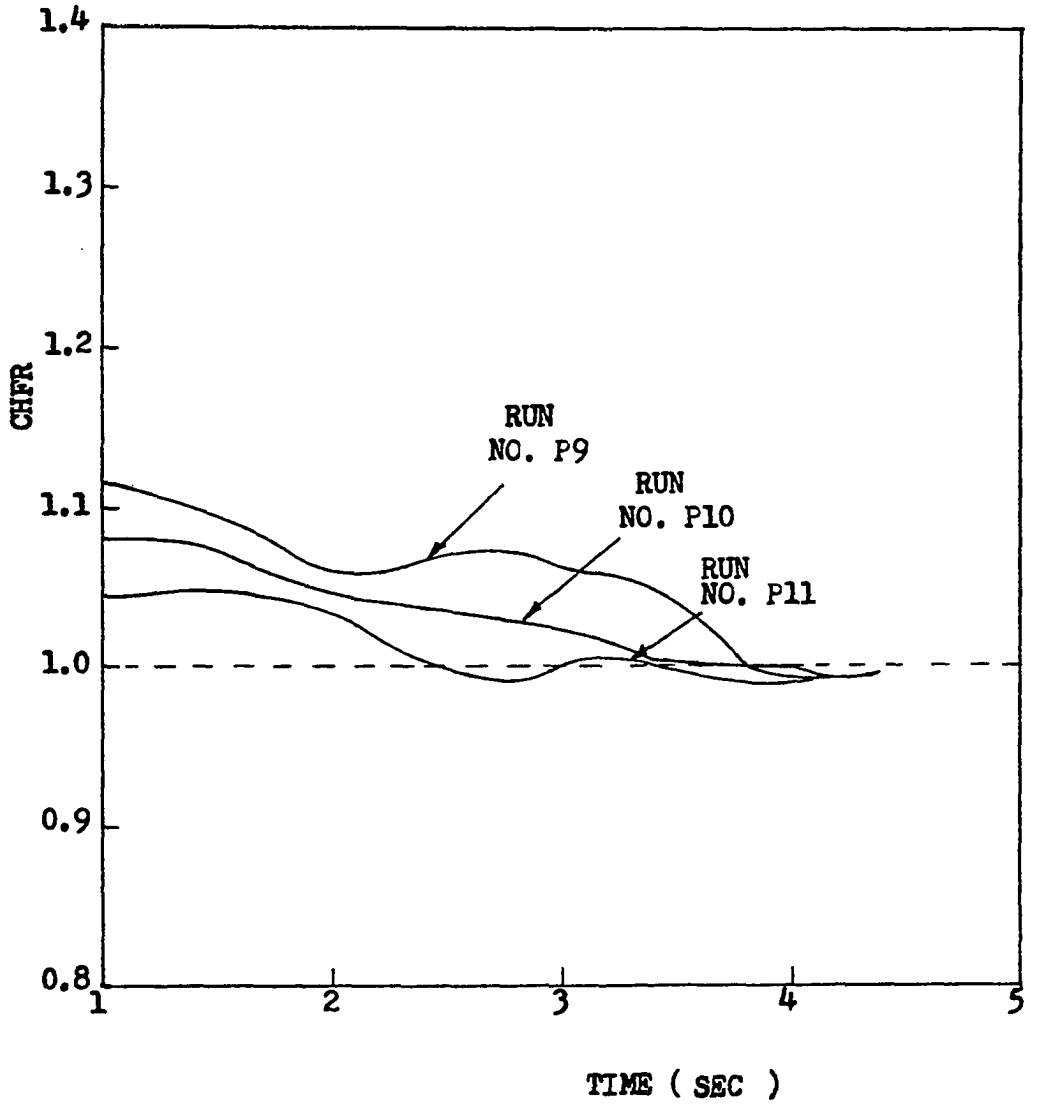

Figure 47. Variation of CHFRs after transient for the equivalent runs No. P9, P10 and P11 by MAYU-2 prediction

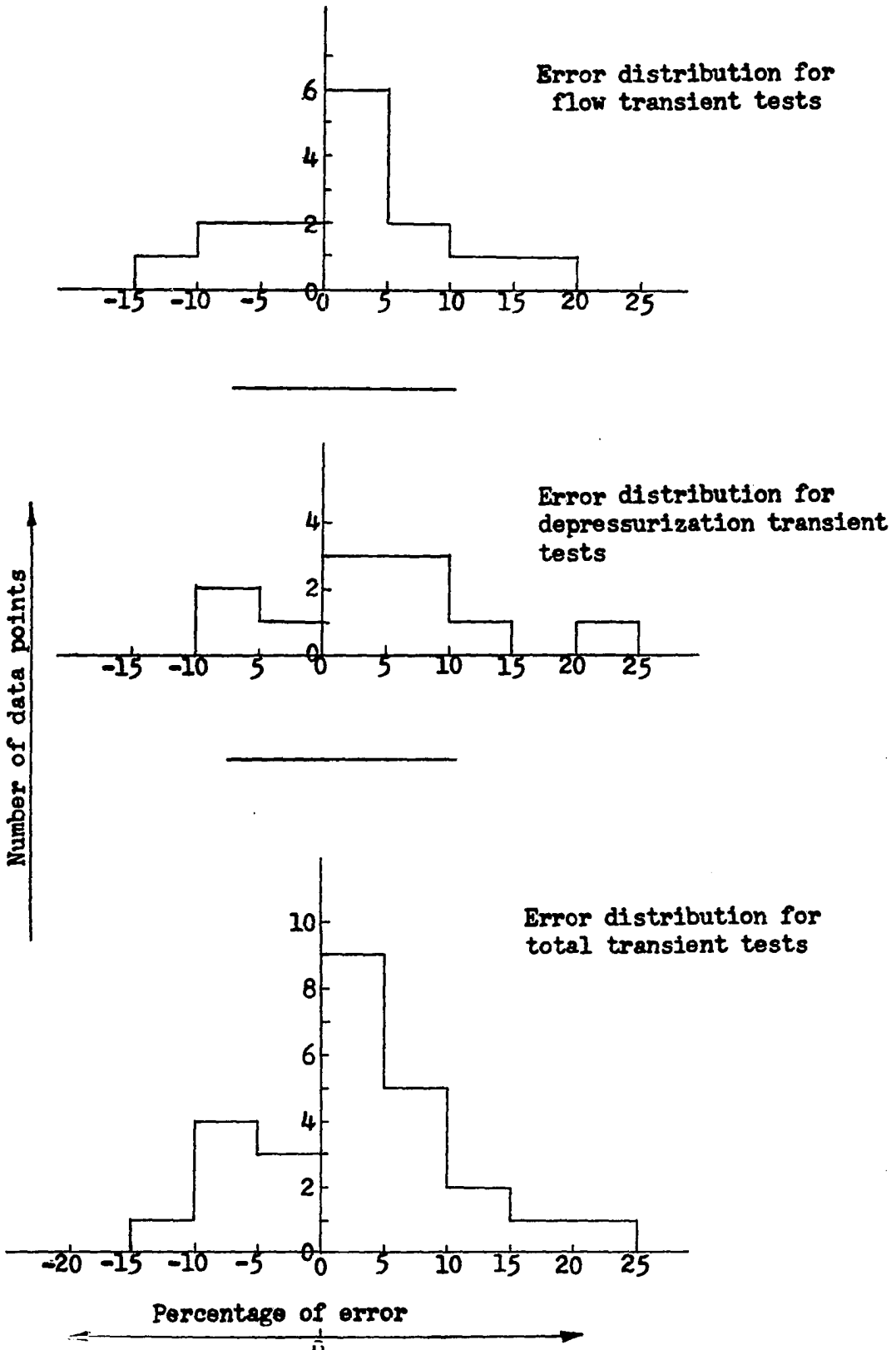

Figure 48. Distribution of error for the predictions of the onset times of CHF

VII. CONCLUSIONS

1. Seventy-two data points of steady state CHF were obtained from a compensated distortion model of Freon-11 system. By the proper distortion of Reynolds number the model can satisfactorily predict CHF for the prototype. More than 97 percent of the total data are within ± 15 percent deviation of the calculated water data.

2. The variations of the mass flux scales and CHF scales with pressur were obtained from the test data and calculated water da... It was found that the values of the parameter scales increased with decreasing pressures. This trend of pressure effect is consistent with the observations of Coffield (12), Dix (13) and Motley et al. (23).

3. The onset time of transient CHF can be predicted through the fluid modeling technique in which the operation of compensated distortion model has been extended to transient conditions. Twenty-seven transient tests were conducted and compared with the tests in a prototype based on the pressure dependent parameter scales established from the steady state CHF tests. Results show that most of the measured onset times of transient CHF are within ± 10 percent deviation of the times computed by MAYU-2.

4. By comparing with tests reported from water systems, the model tests also exhibit the capability of

providing useful qualitative predictions on the trend of CHF when the system undergoes certain types of transients.

VIII. SUGGESTIONS FOR FUTURE STUDY

More investigations on the transient CHF by fluid modeling technique would be worthwhile to extend to wider parameter ranges, especially in the subcooled region.

In order to have more realistic comparisons between model and prototype systems it would be desirable to run both water and Freon CHF tests independently under equivalent conditions. Installation of automatic control devices and curve-follower programmers would be recommended for following the trajectories of transient parameters in the prototype.

Model study on the transient CHF in more complex geometries such as rod bundles would be valuable since it would have better simulation to a real nuclear reactor fuel assembly.

IX. LITERATURE CITED

1. S. Y. Ahmad, "Fluid to Fluid Modeling of Critical Heat Flux: A Compensated Distortion Model," AECL-3663, Atomic Energy of Canada Limited (1971).

2. S. Y. Ahmad and D. C. Groeneveld, "Fluid Modeling of Critical Heat Flux in Uniformly Heated Annuli," AECL-4070, Atomic Energy of Canada Limited (1972).

3. ASME Steam Table, The American Society of Mechanical Engineers, (1967).

4. Babcock and Wilcox Company, "Multinode Computer Code Analysis of Loss-of-Coolant Accident," BAW-10015 (1971).

5. P. G. Barnett, "The Scalling of Forced Convection Boiling Heat Transfer," AEEW-R134, United Kingdom Atomic Energy Authority (1963).

6. P. B. Barnett, "An Experimental Investigation to Determine the Scaling Laws of Forced Convection Boiling Heat Transfer, Part I: The Preliminary Examination of Burnout Data for Water and Arcton 12," AEEW-R363, United Kingdom Atomic Energy Authority (1964).

7. P. G. Barnett and R. W. Wood, "An Experimental Investigation to Determine the Scaling Laws of Forced Convection Boiling Heat Transfer, Part II: An Examination of Burnout Data for Water, Freon 12 and Freon 21 in Uniformly Heated Round Tubes," AEEW-R443, United Kingdom Atomic Energy Authority (1965).

8. J. A. Bouré, "A Method to Develop Similarity Laws for Two-Phase Flows," Paper 70-HT-25, American Society of Mechanical Engineers (1970).

9. E. Buckingham, Phys. Rev., 4, 345 (1914).

10. F. F. Cadek, D. P. Dominicis and R. H. Leyse, "Full Length Emergency Cooling Heat Transfer-Final Report," WCAP-7665, Westinghouse Electric Corporation (1971).

11. J. O. Cermak, R. F. Farman, L. S. Tong, J. E. Casterline, S. Kokolis and B. Matzner, "The Departure from Boiling in Rod Bundles During Pressure Blowdown," 70-HT-12, American Society of Mechanical Engineers (1970).

12. R. D. Coffield, Jr., "A Subcooled DNB Investigation of Freon 113 and Its Similarity to Subcooled Water DNB Data," WCAP-7284, Westinghouse Electric Corporation (1969).

13. G. E. Dix, "Freon-Water Modeling of CHF in Round Tubes," 70-HT-26, American Society of Mechanical Engineers (1970).

14. Driver-Harris Company, "Designing Heating Elements," NCR-70 (1970).

15. Du Pont, de Nemours and Company, Technical Bulletin C-30 (1967).

16. Du Pont, de Nemours and Company, Technical Bulletin T-11 (1965).

17. P. R. Garabedian, Partial Differential Equations, John Wiley and Sons, Inc., New York (1964).

18. D. C. Groeneveld, "The Thermal Behavior of a Heated Surface At and Beyond Dryout," AECL-4309, Atomic Energy of Canada Limited (1972).

19. E. Janssen and J. A. Kervinen, "Burnout Conditions for Single Rod in Annular Geometry, Water at 600 to 1400 PSIA," GEAP-3899, General Electric Company (1963).

20. J. A. Kervinen, Y. H. Kong, D. W. Radcliffe and G. D. Clay, "Deficient Cooling," GEAP-10221-12, General Electric Company (1972).

21. R. T. Lahey, Jr., B. S. Shiralkar, J. M. Gonzalez and L. E. Schnebley, "The Analysis of Transient Critical Heat Flux," GEAP-13249, General Electric Company (1972).

22. G. D. McPherson and S. Y. Ahmad, Nuclear Engineering and Design, 17, 409 (1971).

23. F. E. Motley, F. F. Cadek, J. O. Cermak and L. S. Tong, S. W. Gouse, Jr., F. Paul and J. C. Purcupile, "CHF Data from Freon-11 Flow for Scaling CHF in Water," Int. Symp. Two-Phase System, Haifa (1971).

24. G. Murphy, Similitude in Engineering, The Ronald Press Co., New York (1950).

25. R. W. Murphy and A. E. Bergles, "Subcooled Flow Boiling of Fluorocarbons," Report No. DSR 71903-72, Massachusetts Institute of Technology (1971).

26. W. M. Rohsenow and H. Y. Choi, Heat, Mass and Momentum Transfer, Prentice Hall Inc., Englewood Cliffs, New Jersey (1961).

27. J. E. Shigley, Mechanical Engineering Design, 2nd ed., McGraw-Hill Company, New York (1972).

28. B. S. Shiralkar, E. E. Polomik, R. T. Lahey, Jr., J. M. Gangalez, D. W. Radcliffe and L. E. Schnebly, "Transient Critical Heat Flux-Experimental Results," GEAP-13295, General Electric Company (1972).

29. Societé Nationale d'Etude et de Construction de Moteurs d'Aviation, "Influence of Centrifugal Twisted Tapes in Freon Burn-out Flux," Special Report No. 4, EURAEC-145, European Atomic Energy Commission (1961).

30. F. W. Staub, Nucl. Sci. Eng., 35, 190 (1969).

31. G. F. Stevens and G. J. Kirby, "A Quantitative Comparison Between Burnout Data for Water at 1000 lb/in^2 and Freon-12 at 155 lb/in^2 (abs) Uniformly Heated Round Tubes, Vertical Upflow," AEEW-R327, United Kingdom Atomic Energy Authority (1964).

32. G. F. Stevens and R. V. Macbeth, J. Brit. Nucl. Eng. Soc., 9, 249 (1970).

33. Tennessee Valley Authority, "Browns Ferry Nuclear Power Station," Design and Analysis Report (1968).

34. L. S. Tong, Boiling Heat Transfer and Two-Phase Flow, John Wiley and Sons, Inc., New York (1965).

35. L. S. Tong, Journal of Nuclear Energy, 21, 241 (1967).

36. L. S. Tong, A. A. Bishop, J. E. Casterline and B. Matzner, "Transient DNB Test on CVTR Fuel Assembly," Paper 65-WA/NE-3, American Society of Mechanical Engineers (1965).

37. Watlow Electric Manufacturing Company, Bulletin No. 100 (1970).

38. Wisconsin Electric Power Company and Wisconsin-Michigan Power Company Point Beach Nuclear Plant, Unit No. 1 and 2, "Fluid Facility Description and Safety Analysis Report," (1969).

X. ACKNOWLEDGMENTS

The author wishes to express his sincere appreciation to Professor Glenn Murphy for his guidance and encouragement throughout his graduate college career. Gratitude is expressed to the Engineering Research Institute of Iowa State University for funding this study.

The author also wishes to express special thanks to his wife, Susan, for her work in data recording and typing.

XI. APPENDIX A. TABLE OF STEADY STATE CHF DATA

Run No.	Absolute Pressure P, psia	Mass Flux $G \times 10^{-6}$ lb/hr-ft^2	Inlet Subcooling ΔH, Btu/lb	Critical Heat Flux $\phi_c \times 10^{-4}$ Btu/hr-ft^2	Exit Quality χ %
1	163	0.272	7.16	4.506	47.70
2	163	0.274	7.15	3.713	42.41
3	164	0.296	7.17	3.800	39.64
4	165	0.335	7.17	4.251	38.92
5	163	0.371	7.15	4.580	37.62
6	162	0.381	7.15	4.000	30.31
7	162	0.416	7.15	4.705	33.45
8	163	0.426	7.14	4.140	27.17
9	163	0.496	7.16	4.810	27.43
10	164	0.507	7.16	4.540	23.97
11	163	0.547	7.16	5.100	25.61
12	163	0.571	7.14	4.678	21.02
13	164	0.284	7.15	3.755	41.28
14	162	0.297	7.15	4.040	42.52
15	162	0.353	7.15	4.082	34.61
16	156	0.252	5.95	3.560	44.72
17	155	0.267	5.95	3.968	47.26
18	154	0.283	5.94	3.622	39.56
19	154	0.286	5.94	3.955	43.40
20	154	0.293	5.94	3.780	39.80

Run No.	Absolute Pressure P, psia	Mass Flux $G \times 10^{-6}$ lb/hr-ft^2	Inlet Subcooling ΔH, Btu/lb	Critical Heat Flux $\phi_c \times 10^{-4}$ Btu/hr-ft^2	Exit Quality χ %
21	155	0.305	5.94	3.781	37.83
22	155	0.350	5.95	4.180	36.27
23	155	0.351	5.95	4.060	34.76
24	154	0.411	5.94	4.150	30.09
25	154	0.528	5.95	4.940	26.19
26	155	0.555	5.94	4.562	21.92
27	154	0.560	5.94	5.247	26.19
28	156	0.568	5.94	4.516	20.79
29	155	0.268	5.95	3.472	41.73
30	145	0.259	4.73	3.290	42.09
31	145	0.268	4.76	3.430	42.55
32	146	0.284	4.76	3.708	43.58
33	146	0.292	4.78	3.425	38.35
34	145	0.322	4.77	3.613	36.38
35	143	0.338	4.78	3.960	38.25
36	143	0.412	4.75	3.946	29.85
37	142	0.428	4.76	4.160	30.38
38	143	0.436	4.76	3.896	27.31
39	145	0.457	4.75	3.920	25.87
40	146	0.489	4.77	4.620	29.35
41	147	0.526	4.78	4.275	24.12

Run No.	Absolute Pressure P, psia	Mass Flux $G \times 10^{-6}$ lb/hr-ft^2	Inlet Subcooling ΔH, Btu/lb	Critical Heat Flux $\phi_c \times 10^{-4}$ Btu/hr-ft^2	Exit Quality χ %
42	147	0.550	4.78	4.524	24.55
43	146	0.556	4.77	4.324	22.75
44	136	0.263	3.48	3.215	42.06
45	136	0.275	3.48	3.460	43.36
46	138	0.284	3.49	3.470	41.92
47	138	0.285	3.48	3.290	39.33
48	138	0.290	3.49	3.258	38.10
49	137	0.302	3.48	3.760	42.90
50	137	0.319	3.46	3.385	35.73
51	137	0.322	3.46	3.700	39.16
52	138	0.334	3.47	3.260	32.42
53	137	0.369	3.49	3.844	34.96
54	136	0.389	3.50	3.530	29.73
55	135	0.398	3.50	4.075	34.14
56	137	0.421	3.48	3.580	27.52
57	138	0.546	3.48	3.758	21.20
58	137	0.558	3.46	4.596	26.44
59	128	0.252	2.29	3.070	43.25
60	129	0.271	2.30	3.167	41.18
61	129	0.273	2.25	3.595	46.94
62	128	0.291	2.27	3.356	40.70

Run No.	Absolute Pressure P, psia	Mass Flux $G \times 10^{-6}$ lb/hr-ft^2	Inlet Subcooling ΔH, Btu/lb	Critical Heat Flux $\phi_c \times 10^{-4}$ Btu/hr-ft^2	Exit Quality χ %
63	129	0.298	2.27	3.168	37.27
64	129	0.309	2.29	3.140	35.49
65	130	0.308	2.29	3.520	40.22
66	130	0.339	2.28	3.861	40.10
67	128	0.340	2.27	3.392	34.53
68	130	0.363	2.29	3.538	33.76
69	129	0.415	2.29	3.888	32.45
70	129	0.495	2.27	3.961	27.04
71	136	0.539	2.29	3.770	23.20
72	128	0.546	2.30	4.260	26.40

XII. APPENDIX B. ERROR ANALYSIS

A. Measurement of Heat Loss

The heat loss for single-phase liquid flowing through the test section was measured and checked by using the heat balance equation,

$$q = W C_{pl}(T_{out} - T_{in}) \qquad \text{(B-1)}$$

The experiment was run without preheater power and the system pressure was held at 162 psia.

Data measured from the test were plotted with $\frac{q}{W}$ against $(T_{out} - T_{in})$ in Figure B-1. The slope of the fitted straight line was 0.216.

The value of C_{pl} taken from reference 15 was 0.209 at $90^{o}F$. The heat loss was thus calculated as follows:

$$\frac{\Delta q}{q} = \frac{\Delta C_{pl}}{C_{pl}} = \frac{0.007}{0.209} = 3.35\%$$

B. Error Analysis

Data measured from the CHF tests are subjected to a number of uncertainties such as instrument error, error in Freon property evaluation, power fluctuation, pressure and flow fluctuations. The quantities of critical heat flux and mass flux were calculated from the measured data and so were also subjected to some uncertainties related to

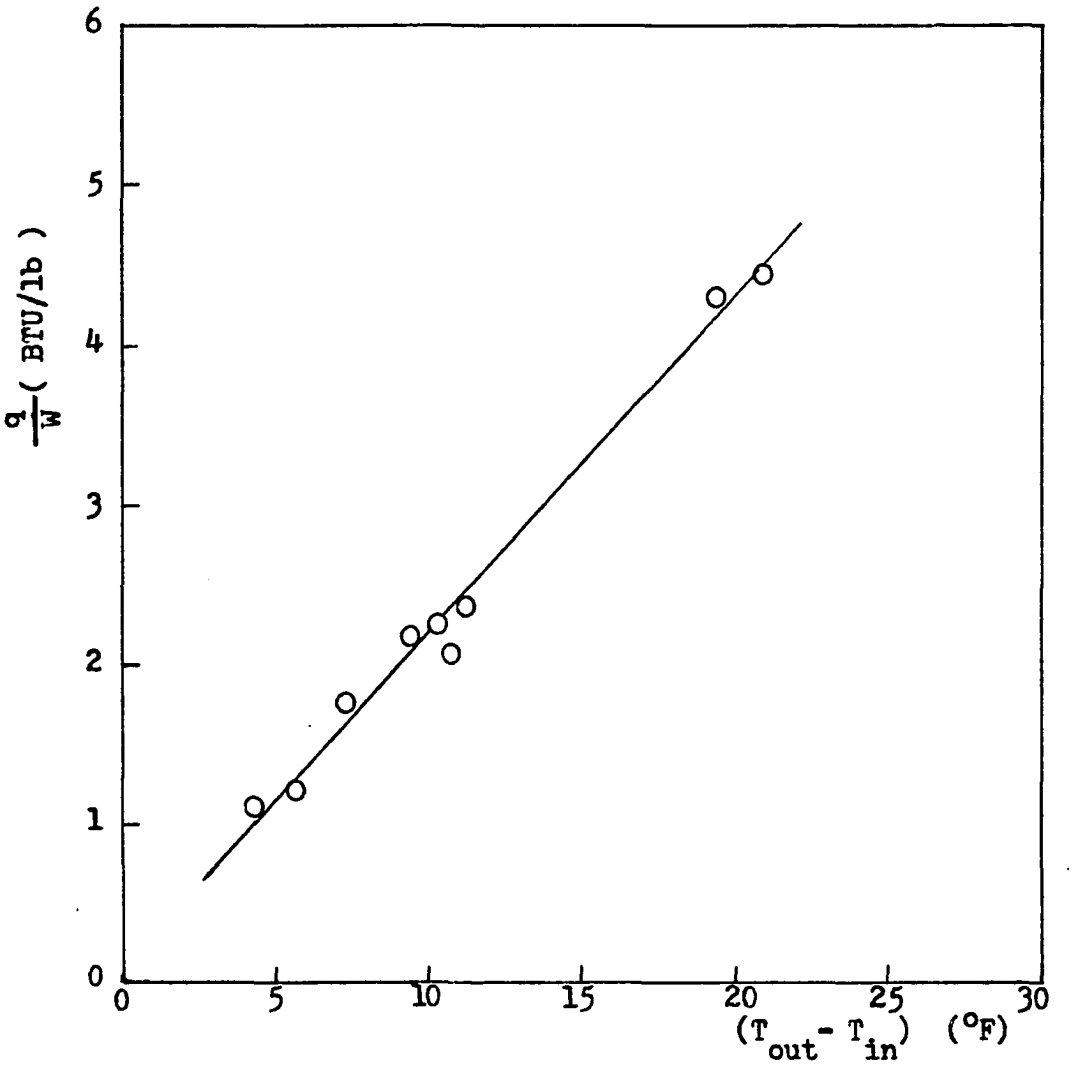

Figure B-1. Heat balance test for test section

those from the data. Their maximum possible uncertainties can be found from the principle of superposition of errors. Consider the general case of a result R, which is measured by X, Y and Z

$$R = f(X, Y, Z)$$

then

$$\Delta R = \left|\frac{\partial R}{\partial X}\Delta X\right| + \left|\frac{\partial R}{\partial Y}\Delta Y\right| + \left|\frac{\partial R}{\partial Z}\Delta Z\right|$$

Following this principle the uncertainties in ϕ_c and G of run 24 were calculated below. Error of the components were obtained from manufacturer's specifications or technical bulletins and were listed in Table B-1.

Since

$$\phi_c = C_1 \frac{\bar{V}I}{DL}, \quad C_1 \text{ is a constant}$$

$$\therefore \quad \Delta\phi_c = \frac{\partial\phi_c}{\partial\bar{V}}\Delta\bar{V} + \frac{\partial\phi_c}{\partial I}\Delta I + \frac{\partial\phi_c}{\partial D}\Delta D + \frac{\partial\phi_c}{\partial L}\Delta L$$

$$\text{or} \quad \frac{\Delta\phi_c}{\phi_c} = \frac{\Delta\bar{V}}{\bar{V}} + \frac{\Delta I}{I} + \frac{\Delta D}{D} + \frac{\Delta L}{L} = 1.7\%$$

Since

$$G_F = C_2 \frac{Q_F \rho_1}{D^2}$$

$$\text{and} \quad Q_F = Q_W \sqrt{\frac{C_3 - C_4 \rho_1}{C_5 \times \rho_1}}, \quad C_2, C_3, C_4 \text{ and } C_5 \text{ are constants}$$

Table B-1. Components of errors

Quantity	Symbol	Instrument Error	Property Error
Pressure	P	1 psia or 1%	
Flow	Q	1.5%	
Temperature	T	0.8%	
Voltage	V	0.5%	
Current	I	1 %	
Length	L	0.1%	
Diameter	D	0.1%	
Liquid density	ρ_1		1%
Vapor density	ρ_v		1%
Latent heat	λ		1%
Saturated enthalpy of liquid	h_f		1%

$$\therefore \quad \frac{\Delta Q_F}{Q_F} = \left|\frac{\Delta Q_W}{Q_W}\right| + \left|\frac{\Delta \rho_1}{2\rho_1}\right| + \left|\frac{\Delta \rho_1}{2\rho_1}\right| = 2.5\%$$

$$\therefore \quad \frac{\Delta G_F}{G_F} = \left|\frac{\Delta Q_F}{Q_F}\right| + \left|\frac{\Delta \rho_1}{\rho_1}\right| + \left|\frac{\Delta D}{2D}\right| = 3.6\%$$

If maximum heat loss was taken as 4%, the uncertainty of ϕ_c should be 5.7%.

Hence the CHF and mass flux in run 24 are

$$\phi_c = (4.130 \pm 0.235) \times 10^4 \text{ Btu/hr-ft}^2$$

$$G = (0.412 \pm 0.0148) \times 10^6 \text{ lb/hr-ft}^2$$

XIII. APPENDIX C. SAMPLE CALCULATIONS

Sample calculation for run 24 will be presented. Physical properties of Freon-11 were taken from references 15 and 16.

Data measured directly from the experiment were:

Pressure	139 psig
Flow rate	1.46 GPM
Flow inlet temperature	208.5^{o}F
Flow temperature before the rotameter	125.4^{o}F
Voltage to the heater	403.5 volts
Current throughout the heater	14.72 Amps

These were converted into the values listed in Table A-1 in British units by the following procedure.

Absolute pressure was calculated as

$$P = 139 + 14.7 = 153.7 \text{ psia}$$

Flow rate was read from the rotameter, which was calibrated for measuring water flow rate, and mass flux of Freon was calculated as follows:

At flow temperature = 125.4^{o}F, the liquid density was found

$$\rho_1 = 88.17 \text{ lb/ft}^3$$

Hence the flow rate for Freon-11 was evaluated by the formula provided from the manufacturer as

$$\text{GPM of Freon} = \text{GPM of water} \times \sqrt{\frac{\rho_{float} - \frac{\rho_F}{\rho_W}}{7.02 \times \frac{\rho_F}{\rho_W}}}$$

$$= 1.46 \times \sqrt{\frac{8.02 - \frac{88.17}{62.42}}{7.02 \times \frac{88.17}{62.42}}}$$

$$= 1.19$$

$$\therefore \quad \text{Mass flux } G = 1.19\left(\frac{gal}{min}\right) \times 0.1337\left(\frac{ft^3}{gal}\right) \times 88.17\left(\frac{lb}{ft^3}\right)$$

$$\times 60\left(\frac{min}{hr}\right) \times \frac{1}{2.045 \times 10^{-3}} \left(\frac{1}{ft^2}\right)$$

$$= 0.412 \times 10^6 \text{ lb/hr-ft}^2$$

The inlet subcooling was calculated using the relation

$$\Delta H = h_f - h_{in}$$

h_{in} is the liquid enthalpy at temperature = 208.5°F

$$\therefore \quad \Delta H = 58.05 - 52.11 = 5.94 \text{ Btu/lb}$$

The critical heat flux was calculated from the total power input:

$$\phi_c = 3.413 \times \frac{\bar{V} \cdot I}{\text{heated surface area}}$$

$$= 3.413 \times \frac{403.5 \times 14.72}{0.49087}$$

$$= 4.130 \times 10^4 \text{ Btu/hr-ft}^2$$

The exit quality was calculated from the relation

$$\chi = \frac{4\ \phi_c\ L}{G\ \lambda\ D_{he}} - \frac{\Delta H}{\lambda}$$

$$= \frac{4 \times 4.13 \times 10^4 \times 3}{0.412 \times 10^6 \times 60.22 \times \frac{0.6}{12}} - \frac{5.94}{60.22} = 30.09\%$$

For transient tests all values in Tables 4 and 5 were calculated by the same way as that for the steady state data. For MAYU-2 calculations, the input data were those which were scaled up from the data measured from the Freon system. Physical properties of water were taken from reference 3. Sample calculation for run G10 is presented.

From the design condition

$$\left(\frac{\rho_l}{\rho_v}\right)_F = \left(\frac{\rho_l}{\rho_v}\right)_W$$

the pressure in water system was obtained from Figure 2.

P_W = 897 psia for P_F = 145 psia

From the condition

$$\left(\frac{\Delta H}{\lambda}\right)_F = \left(\frac{\Delta H}{\lambda}\right)_W = 0.0785$$

h_{in} for water at pressure equal to 897 spia is 473.5 Btu/lb. At the same pressure it was also found from Table 2

$$F_G = \frac{G_W}{G_F} = 1.58$$

$$F_\phi = \frac{\phi_W}{\phi_F} = 17.36$$

Since the tabular data input option was chosen, all transient values of flow rate and heat flux in Freon system were read discretely from strip chart papers. These values were then scaled up point by point into water data as listed in Table C-1.

Table C-1. Input data calculation

Time (sec)	$G_W \times 10^{-6}$ (lb/hr-ft^2)	$\phi_W \times 10^{-6}$ (Btu/hr-ft^2)	$G_F \times 10^{-6}$ (lb/hr-ft^2)	$\phi_F \times 10^{-4}$ (Btu/hr-ft^2)
0.0	0.728	0.6829	0.461	3.934
0.2	0.654	0.6670	0.414	3.842
0.4	0.573	0.6434	0.363	3.706
0.6	0.514	0.6317	0.325	3.639
0.8	0.447	0.6111	0.283	3.520
1.0	0.392	0.5911	0.248	3.405
1.2	0.351	0.5729	0.222	3.300
1.4	0.350	0.5486	0.221	3.160
1.6	0.351	0.5303	0.222	3.055
1.8	0.350	0.5123	0.221	2.951
2.0	0.350	0.5000	0.221	2.880
2.2	0.351	0.4892	0.222	2.818
2.4	0.351	0.4809	0.222	2.770
2.6	0.350	0.4753	0.221	2.738
2.8	0.351	0.4687	0.222	2.700
3.0	0.351	0.4618	0.222	2.660

XVI. APPENDIX D. CALCULATION METHOD IN MAYU-2 CODE

(From GEAP-13249)

MAYU-2 is an extension of MAYU which allows for non-uniform axial heat flux and power transients. Calculations are performed separately in the subcooled and boiling regions. The main steps in the calculations are described below.

A. Calculation of Initial Quality

$$\chi(Z) = \frac{P_H}{G_0 \lambda A_{x-s}} \int_0^Z \phi(Z)\, dZ - \frac{\Delta H}{\lambda} \qquad \text{(D-1)}$$

where

G_0 = initial mass flux

B. Calculation of the Boiling Boundary Position Versus Time

The effect of pressure change in subcooled region is considered to be small and negligible. The one dimensional continuity equation is written as

$$V = \frac{dZ}{dt} = \frac{G(t)}{\rho_1} \qquad \text{(D-2)}$$

$$\therefore \quad \Delta Z = \int_t^{t+\Delta t} \frac{G(t')}{\rho_1}\, dt' \qquad \text{(D-3)}$$

Equation D-3 is integrated numerically using Simpson's Rule as

$$\Delta Z_1 = \frac{1}{\rho_1}\left[G(t_0) + 4G\left(t_0 + \frac{\Delta t}{4}\right) + G\left(t_0 + \frac{\Delta t}{2}\right)\right] \frac{\Delta t}{12} \qquad \text{(D-4)}$$

$$\Delta Z_2 = \frac{1}{\rho_1}\left[G(t_0) + 4G\left(t_0 + \frac{\Delta t}{2}\right) + G(t_0 + \Delta t)\right] \frac{\Delta t}{6} \qquad \text{(D-5)}$$

In the Lagrangian framework, the energy equation is

$$\frac{A_{x-s}\ \rho_1}{P_H} \frac{Dh}{Dt} = \phi(Z,t) \qquad \text{(D-6)}$$

$$\therefore \quad \frac{A_{x-s}}{P_H} \int_h^{h+\Delta h} \rho_1\, dh = \int_t^{t+\Delta t} \phi\, dt \qquad \text{(D-7)}$$

Equation D-7 is evaluated by Simpson's rule as

$$\Delta h = \frac{P_H}{A_{x-s}\ \rho_1} (\phi + 4\,\phi_1 + \phi_2) \frac{\Delta t}{6} \qquad \text{(D-8)}$$

where ϕ, ϕ_1, and ϕ_2 are computed at (t,z), $(t + \frac{\Delta t}{2}, Z)$ and $(t + \Delta t, Z)$ respectively.

A new value of ρ_1 is obtained at the new enthalpy and the process repeated until

$$h \geq h_f \quad \text{at} \quad P(t)$$

The boiling boundary and the time at which the characteristic intersects it are then obtained by interpolation

between the last two values of Z and t.

C. Two-Phase Region

Two equations of characteristics derived from one-dimensional two-phase continuity equation and energy equation are used to compute the mass flux and qualities as functions of space and time. The two equations are

$$\frac{\partial V}{\partial Z} = C_1 + C_2 \rho \qquad \text{(D-9)}$$

and

$$\frac{D\chi}{Dt} = A_1 \chi + B_1 \qquad \text{(D-10)}$$

where

$$\rho = \frac{1}{v_f + \chi v_{fg}}$$

$$C_1 = \frac{1}{v_{fg}} \frac{Dv_{fg}}{Dt} + \frac{1}{h_{fg}} \left[\left(\frac{\phi(Z,t) P_H}{A_{x-s}} + \frac{144}{J} \frac{DP}{Dt} \right) v_{fg} - \frac{Dh_{fg}}{Dt} \right]$$

$$C_2 = \frac{Dv_f}{Dt} - \frac{v_f}{v_{fg}} \frac{Dv_{fg}}{Dt} + \frac{v_f}{h_{fg}} \frac{Dh_{fg}}{Dt} - \frac{v_{fg}}{h_{fg}} \frac{Dh_f}{Dt}$$

$$A_1 = \left[\left(\frac{\phi(Z,t) P_H}{A_{x-s}} + \frac{144}{J} \frac{DP}{Dt} \right) v_{fg} - \frac{Dh_{fg}}{Dt} \right] / h_{fg}$$

$$B_1 = \left[\left(\frac{\phi(Z,t) P_H}{A_{x-s}} + \frac{144}{J} \frac{DP}{Dt} \right) v_f - \frac{Dh_f}{Dt} \right] / h_{fg}$$

The detail derivation is shown in reference 21.

D. Method of Solution

The problem is treated as an initial value problem so that for each time step the qualities and velocities at nodes along the whole length are known at the start of the step. Two step sizes, Δt and $\Delta t/2$, are used in the calculational procedure to achieve second order accuracy. The velocity variation along the characteristic is assumed to be linear. The following operations are performed:

1. $(\frac{\partial V}{\partial Z})_B$ is computed from Equation D-9, knowing χ_B from previous calculation.

2. $V_A \cong V_B + (\frac{\partial V}{\partial Z})_B \cdot \Delta Z$, where V_B is known from previous calculation.

3. The location of point R, at distant Z_R from heater inlet, is determined in three steps.

a. $$Z_{R_1} = Z_A - V_A \cdot \Delta t$$

b. $$V_{R_1} = V_Q + (\frac{Z_{R_1} - Z_Q}{\Delta Z}) \cdot (V_P - V_Q)$$

c. $$Z_R = Z_{R_1} - [Z_{R_1} - Z_A + (V_A + V_{R_1})/2 \cdot \Delta t] / [1 + (V_P - V_Q) \frac{\Delta t}{2 \cdot \Delta Z}]$$

where the Newton-Raphson method of successive approximations has been used in c.

4. $\chi_R = \chi_Q + (\frac{Z_R - Z_Q}{\Delta Z})(\chi_P - \chi_Q)$ by linear interpolation between known quantities χ_P and χ_Q at the previous time step t.

5. The quantities A_1 and B_1 in Equation D-10 are evaluated at the middle of the time step.

6. $(\frac{D\chi}{Dt})_R$ is computed from Equation D-10.

7. $\chi_A = \chi_R + (\frac{D\chi}{Dt})_R \cdot \Delta t$

8. $G_A = V_A/(v_f + \chi_A v_{fg})$

The calculation starts at t=0 at the axial node immediately following the position of the boiling boundary. At the boiling boundary

$$\chi = 0 \quad , \qquad V = G(t)v_f$$

Once the solution has been obtained at $t + \Delta t$, the procedure is repeated twice, starting at t with half length and time step, so that a solution is again obtained at $t + \Delta t$ with two steps of $\Delta t/2$. The best estimates of χ_A and V_A are given by

$$\chi_A = 2\,\chi_{A_{1/2}} - \chi_{A_1}$$

$$V_A = 2\,V_{A_{1/2}} - V_{A_1}$$

where the subscript 1/2 denotes values obtained using two steps of $\Delta t/2$ and 1 denotes the values obtained with one step of Δt.

The solution proceeds in this manner until the total time is equal to or slightly greater than the specified run time. A simplified flow chart is shown in Figure D-1.

E. Subroutines

The following functions are included in MAYU-2:

1. RLIN (t, NOPT)

This calculates the inlet mass flux, pressure, power decay factor, dP/dt at a given time "t" and for the input option used.

2. HEAT (Z, NOPT)

This calculates the axial peaking factor for a given distant "Z" and input option used.

3. PROP (P)

This calculates thermodynamic properties versus pressure.

h_f, v_h, h_{fg}, v_{fg}, $\frac{dh_{fg}}{dP}$, and $\frac{dh_f}{dP}$ are calculated.

4. BB (t)

This interpolates for the boiling boundary position at any given time "t".

5. VSUB (h)

This calculates the liquid specific volume versus enthalpy.

Figure D-1. Simplified flow chart of MAYU-2 code (from GEAP-13249)

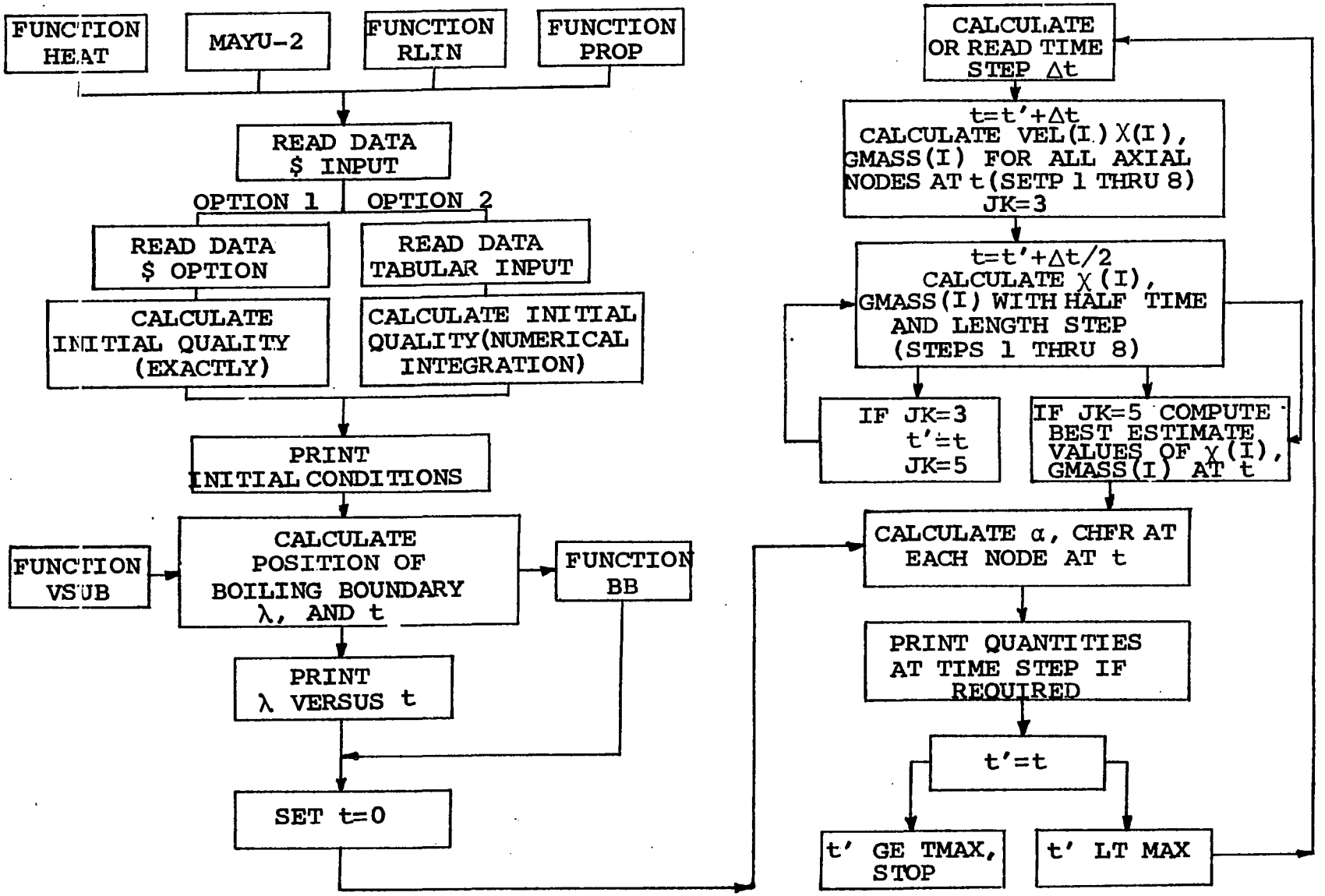
FUNCTION HEAT
MAYU-2
FUNCTION RLIN
FUNCTION PROP
READ DATA $ INPUT
OPTION 1
OPTION 2
READ DATA $ OPTION
READ DATA TABULAR INPUT
CALCULATE INITIAL QUALITY (EXACTLY)
CALCULATE INITIAL QUALITY(NUMERICAL INTEGRATION)
PRINT INITIAL CONDITIONS
FUNCTION VSUB
CALCULATE POSITION OF BOILING BOUNDARY λ, AND t
FUNCTION BB
PRINT λ VERSUS t
SET t=0
CALCULATE OR READ TIME STEP Δt
t=t'+Δt CALCULATE VEL(I) χ(I), GMASS(I) FOR ALL AXIAL NODES AT t(SETP 1 THRU 8) JK=3
t=t'+Δt/2 CALCULATE χ(I), GMASS(I) WITH HALF TIME AND LENGTH STEP (STEPS 1 THRU 8)
IF JK=3 t'=t JK=5
IF JK=5 COMPUTE BEST ESTIMATE VALUES OF χ(I), GMASS(I) AT t
CALCULATE α, CHFR AT EACH NODE AT t
PRINT QUANTITIES AT TIME STEP IF REQUIRED
t'=t
t' GE TMAX, STOP
t' LT MAX